Liquefaction Susceptibility in the San Bernardino Valley and Vicinity, Southern California—A Regional Evaluation

U.S. GEOLOGICAL SURVEY BULLETIN 1898

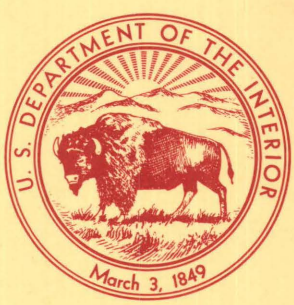

SELECTED SERIES OF U.S. GEOLOGICAL SURVEY PUBLICATIONS

Periodicals

Earthquakes & Volcanoes (issued bimonthly).
Preliminary Determination of Epicenters (issued monthly).

Technical Books and Reports

Professional Papers are mainly comprehensive scientific reports of wide and lasting interest and importance to professional scientists and engineers. Included are reports on the results of resource studies and of topographic, hydrologic, and geologic investigations. They also include collections of related papers addressing different aspects of a single scientific topic.

Bulletins contain significant data and interpretations that are of lasting scientific interest but are generally more limited in scope or geographic coverage than Professional Papers. They include the results of resource studies and of geologic and topographic investigations, as well as collections of short papers related to a specific topic.

Water-Supply Papers are comprehensive reports that present significant interpretive results of hydrologic investigations of wide interest to professional geologists, hydrologists, and engineers. The series covers investigations in all phases of hydrology, including hydrogeology, availability of water, quality of water, and use of water.

Circulars present administrative information or important scientific information of wide popular interest in a format designed for distribution at no cost to the public. Information is usually of short-term interest.

Water-Resources Investigations Reports are papers of an interpretive nature made available to the public outside the formal USGS publications series. Copies are reproduced on request unlike formal USGS publications, and they are also available for public inspection at depositories indicated in USGS catalogs.

Open-File Reports include unpublished manuscript reports, maps, and other material that are made available for public consultation at depositories. They are a nonpermanent form of publication that may be cited in other publications as sources of information.

Maps

Geologic Quadrangle Maps are multicolor geologic maps on topographic bases in 7.5- or 15-minute quadrangle formats (scales mainly 1:24,000 or 1:62,500) showing bedrock, surficial, or engineering geology. Maps generally include brief texts; some maps include structure and columnar sections only.

Geophysical Investigations Maps are on topographic or planimetric bases at various scales; they show results of surveys using geophysical techniques, such as gravity, magnetic, seismic, or radioactivity, which reflect subsurface structures that are of economic or geologic significance. Many maps include correlations with the geology.

Miscellaneous Investigations Series Maps are on planimetric or topographic bases of regular and irregular areas at various scales; they present a wide variety of format and subject matter. The series also includes 7.5-minute quadrangle photogeologic maps on planimetric bases that show geology as interpreted from aerial photographs. Series also includes maps of Mars and the Moon.

Coal Investigations Maps are geologic maps on topographic or planimetric bases at various scales showing bedrock or surficial geology, stratigraphy, and structural relations in certain coal-resource areas.

Oil and Gas Investigations Charts show stratigraphic information for certain oil and gas fields and other areas having petroleum potential.

Miscellaneous Field Studies Maps are multicolor or black-and-white maps on topographic or planimetric bases on quadrangle or irregular areas at various scales. Pre-1971 maps show bedrock geology in relation to specific mining or mineral-deposit problems; post-1971 maps are primarily black-and-white maps on various subjects such as environmental studies or wilderness mineral investigations.

Hydrologic Investigations Atlases are multicolored or black-and-white maps on topographic or planimetric bases presenting a wide range of geohydrologic data of both regular and irregular areas; principal scale is 1:24,000, and regional studies are at 1:250,000 scale or smaller.

Catalogs

Permanent catalogs, as well as some others, giving comprehensive listings of U.S. Geological Survey publications are available under the conditions indicated below from the U.S. Geological Survey, Books and Open-File Reports Section, Federal Center, Box 25425, Denver, CO 80225. (See latest Price and Availability List.)

"Publications of the Geological Survey, 1879–1961" may be purchased by mail and over the counter in paperback book form and as a set of microfiche.

"Publications of the Geological Survey, 1962–1970" may be purchased by mail and over the counter in paperback book form and as a set of microfiche.

"Publications of the U.S. Geological Survey, 1971-1981" may be purchased by mail and over the counter in paperback book form (two volumes, publications listing and index) and as a set of microfiche.

Supplements for 1982, 1983, 1984, 1985, 1986, and for subsequent years since the last permanent catalog may be purchased by mail and over the counter in paperback book form.

State catalogs, "List of U.S. Geological Survey Geologic and Water-Supply Reports and Maps For (State)," may be purchased by mail and over the counter in paperback booklet form only.

"Price and Availability List of U.S. Geological Survey Publications," issued annually, is available free of charge in paperback booklet form only.

Selected copies of a monthly catalog "New Publications of the U.S. Geological Survey" are available free of charge by mail or may be obtained over the counter in paperback booklet form only. Those wishing a free subscription to the monthly catalog "New Publications of the U.S. Geological Survey" should write to the U.S. Geological Survey, 582 National Center, Reston, VA 22092.

Note.—Prices of Government publications listed in older catalogs, announcements, and publications may be incorrect. Therefore, the prices charged may differ from the prices in catalogs, announcements, and publications.

Liquefaction Susceptibility in the San Bernardino Valley and Vicinity, Southern California—A Regional Evaluation

By JONATHAN C. MATTI and SCOTT E. CARSON

A study of seismically induced liquefaction susceptibility under strong ground-shaking conditions generated by scenario earthquakes on the San Andreas, San Jacinto, and Cucamonga faults

U.S. GEOLOGICAL SURVEY BULLETIN 1898

U.S. DEPARTMENT OF THE INTERIOR
MANUEL LUJAN, JR., Secretary

U.S. GEOLOGICAL SURVEY
Dallas L. Peck, Director

UNITED STATES GOVERNMENT PRINTING OFFICE: 1991

For sale by the
Books and Open-File Reports Section,
U.S. Geological Survey,
Federal Center, Box 25425,
Denver, CO 80225

Library of Congress Cataloging in Publication Data

Matti, Jonathan C.
Liquefaction susceptibility in the San Bernardino Valley and vicinity, southern California : a regional evaluation / by Jonathan C. Matti and Scott E. Carson.
p. cm. — (U.S. Geological Survey bulletin ; 1898)
Includes bibliographical references.
Supt. of Docs. no.: I 10.3:1898
1. Soil liquefaction—California, southern. 2. Earthquakes—California.
I. Carson, Scott E. II. Title. III. Series.
QE75.B9 no. 1898
[TA710.3.C2]
557.3 s—dc20
[624.1'5136]

89-600228
CIP

CONTENTS

PLATES

[Plates are in pocket]

FIGURES

TABLES

Liquefaction Susceptibility in the San Bernardino Valley and Vicinity, Southern California—A Regional Evaluation

By Jonathan C. Matti *and* Scott E. Carson

Abstract

This report discusses earthquake-induced liquefaction susceptibility of alluvial sediments of the San Bernardino Valley and vicinity, southern California. The study includes maps that zone the region into areas having high to low susceptibility for each of three scenario earthquakes: an M_s=8.0 earthquake on the San Andreas fault, an M_s=7.0 earthquake on the San Jacinto fault, and an M_s=6.75 earthquake on the Cucamonga fault.

The evaluation was conducted by using a combination of site-specific and regional techniques. For the site-specific phase, penetration-resistance data from representative locations throughout the study area were analyzed to determine local susceptibility to liquefaction for each of the scenario earthquakes. For the regional phase, susceptible conditions at local sites were linked to particular geologic and hydrologic conditions, which then were mapped throughout the San Bernardino Valley region. This process yielded groupings of site-specific susceptibility results where the group boundaries are defined by different combinations of geologic unit, ground-water interval, and distance to causative fault. Each regional grouping was evaluated statistically to determine its overall susceptibility to liquefaction, and for each scenario earthquake, high, moderately high, moderate, or low susceptibility was assigned depending on the percentage of site-specific liquefaction analyses that indicated susceptible conditions. These ratings form the basis for compiling liquefaction-susceptibility maps that yield the following results.

An M_s=8.0 earthquake on the San Andreas fault is accompanied by elevated (high, moderately high) susceptibilities wherever ground water is shallow. Within 0 to 4 miles of the fault, the overall susceptibility of sands and silty sands is high, even where ground water is as deep as 30 to 50 feet subsurface. For areas 4 to 8 miles from the fault, overall susceptibilities remain high where ground water is shallower than 10 feet subsurface but decline to moderate where ground water is deeper. At all distances from the fault, silty sediments have lower susceptibility than sandy sediments, but the numerical abundance of sandy sediments at most locations tends to increase the overall susceptibility rating even at deeper ground-water intervals.

An M_s=7.0 earthquake on the San Jacinto fault is accompanied by susceptibilities whose intensities vary with fault distance and ground-water conditions. Elevated susceptibilities (high, moderately high) occur within 0 to 4 miles of the fault wherever ground water is shallower than 20 feet and within 4 to 8 miles of the fault wherever ground water is shallower than 10 feet. Within 0 to 4 miles of the fault, susceptibilities decline to moderate wherever ground water is between 20 and 50 feet subsurface; within 4 to 8 miles of the fault, susceptibilities decline to moderate and low where ground water is between 30 and 50 feet subsurface. In general, silty sediments appear to be less susceptible than sandy samples, especially at ground-water levels below 30 feet subsurface.

Elevated susceptibilities accompanying an M_s=6.75 earthquake on the Cucamonga fault are not as widespread as those for larger earthquakes on the San Andreas and San Jacinto faults. Within 0 to 4 miles of the fault, susceptibilities probably are high and moderately high where ground water is shallow, but because penetration data from this fault-distance interval were not available for our investigation, the ratings are inferred on the basis of their comparison with susceptibility results from equivalent ground-water intervals at greater distances from the fault. At all distances between 4 and 15 miles of the fault, high or moderately high susceptibility occurs wherever ground water is shallower than 10 feet, but susceptibilities decline to moderate and low where ground water is deeper than 10 feet subsurface.

The shape and size of the susceptibility zones largely are controlled by depth to ground water and distance to the causative fault, although the age and type of sediment also influence its susceptibility. The main zones of elevated susceptibility are associated with shallow ground-water zones that occur under the modern flood plains of Cajon Creek, Warm Creek, and the Santa Ana River. These areas are underlain

Manuscript approved for publication June 7, 1989.

by recently deposited Holocene sediments that would be expected to have lower penetration resistance and higher susceptibility than older sediments. However, even the older Holocene and uppermost Pleistocene sediments have elevated susceptibilities comparable to those in the younger deposits, and this fact accounts for zones of high and moderately high susceptibility that extend away from the modern flood plains and into adjacent areas underlain by older deposits. Additional areas of elevated susceptibility occur in isolated zones downstream from the mouths of canyons along the base of the San Bernardino Mountains.

Our interpretation that alluvial sediments of the San Bernardino Valley region are widely susceptible to earthquake-induced liquefaction in part can be attributed to the strong ground-shaking conditions required by the M_s=8.0, 7.0, and 6.75 earthquakes specified in our analysis. The peak-acceleration values generated by these large-magnitude earthquakes are greater than those that would apply if probabilistic methods were used to estimate the anticipated ground-shaking conditions. Probabilistic or statistical estimates of seismic potential use peak-acceleration values that are likely to be exceeded by earthquakes within a specified return period (such as 50 years). Probabilistic methods in effect scale down ground-motion parameters because, for a given 50-year or 100-year period, small- to moderate-size earthquakes statistically are more likely to occur than are large to great earthquakes. If a large earthquake occurs in the San Bernardino Valley region in the next few decades, as many workers have proposed, then a large-magnitude scenario-earthquake approach to regional hazard analysis is appropriate for evaluating liquefaction susceptibility in the San Bernardino Valley region.

The susceptibility maps can be used in conjunction with what is known about the geomorphic setting and layering characteristics of sedimentary materials underlying the San Bernardino Valley region to estimate where liquefaction-induced ground failures are most and least likely to occur, at least on a regional basis. Where ground water is shallower than 10 feet subsurface, the possibility of ground failure is consistent with the high to moderately high susceptibility of sediments within this ground-water interval. These areas require special attention during future land-use planning and development, and mitigation of existing hazards may be advisable. In areas of deeper ground water—where liquefaction susceptibility is moderate to low—liquefaction-induced ground failures are less likely but cannot be ruled out.

INTRODUCTION

This report presents a regional evaluation of susceptibility to earthquake-induced sediment liquefaction in the San Bernardino Valley and vicinity, southern California (fig. 1). Liquefaction is a process whereby strong earthquake shaking causes sediment layers saturated with ground water to lose their strength and behave as a fluid; this subsurface process can lead to near-surface ground failures that result in property damage and loss of life. Several general factors indicate that parts of the San Bernardino Valley area might be susceptible to liquefaction: (1) alluvial sediments that underlie the valley region generally are similar to those that have undergone liquefaction elsewhere (Carson and others, 1986); (2) ground-water conditions in some parts of the valley are conducive to liquefaction (Carson and Matti, 1985, 1986); and (3) the tectonic setting and seismic history of the region (Matti and others, 1985) suggest that earthquakes strong enough to generate liquefaction in susceptible materials have occurred in the past and are likely to occur in the future.

Purpose, Scope, and Limitations

This report identifies areas within the San Bernardino Valley region that are susceptible to earthquake-induced liquefaction given the ground-shaking conditions specified in our analysis. The evaluation is generalized and regional in scope—that is, our analytical approach does not identify the exact locations where liquefaction will or will not occur but instead outlines broad areas that have high to low liquefaction susceptibility based on the typical hydrologic and geologic characteristics of each area.

By targeting areas of greater or lesser susceptibility, this report can (1) assist building and public-safety officials who wish to identify areas where site-specific liquefaction evaluations are necessary and (2) assist planners who wish to consider liquefaction hazards in land-use planning and zoning. The report is directed toward persons concerned about liquefaction but unfamiliar with technical aspects of its causes, consequences, and methods of evaluation. Accordingly, the body of the report is as technically simple as the subject allows; procedural documentation is reserved for the appendixes. Thus, the basic points of our methodology and results can be determined by reviewing the text and can be elaborated as needed by referring to the appendixes.

The susceptibility maps that accompany this report are designed to reveal areas where liquefaction has any significant possibility of occurring and to distinguish these areas from those where susceptibility to liquefaction unequivocally is minimal. To achieve this goal, our evaluation incorporated two conservative procedures: (1) we assumed geologic and hydrologic conditions (large local earthquakes and shallowest ground-water levels) that would identify the maximum extent of susceptible conditions and (2) our site-specific evaluations included some analytical procedures whose cumulative effect tended to increase liquefaction susceptibility slightly. We adopted this conservative approach to ensure that no areas having significant liquefaction susceptibility escaped recognition and to ensure that zones of significant susceptibility could be emphasized and targeted for further planning and evaluation.

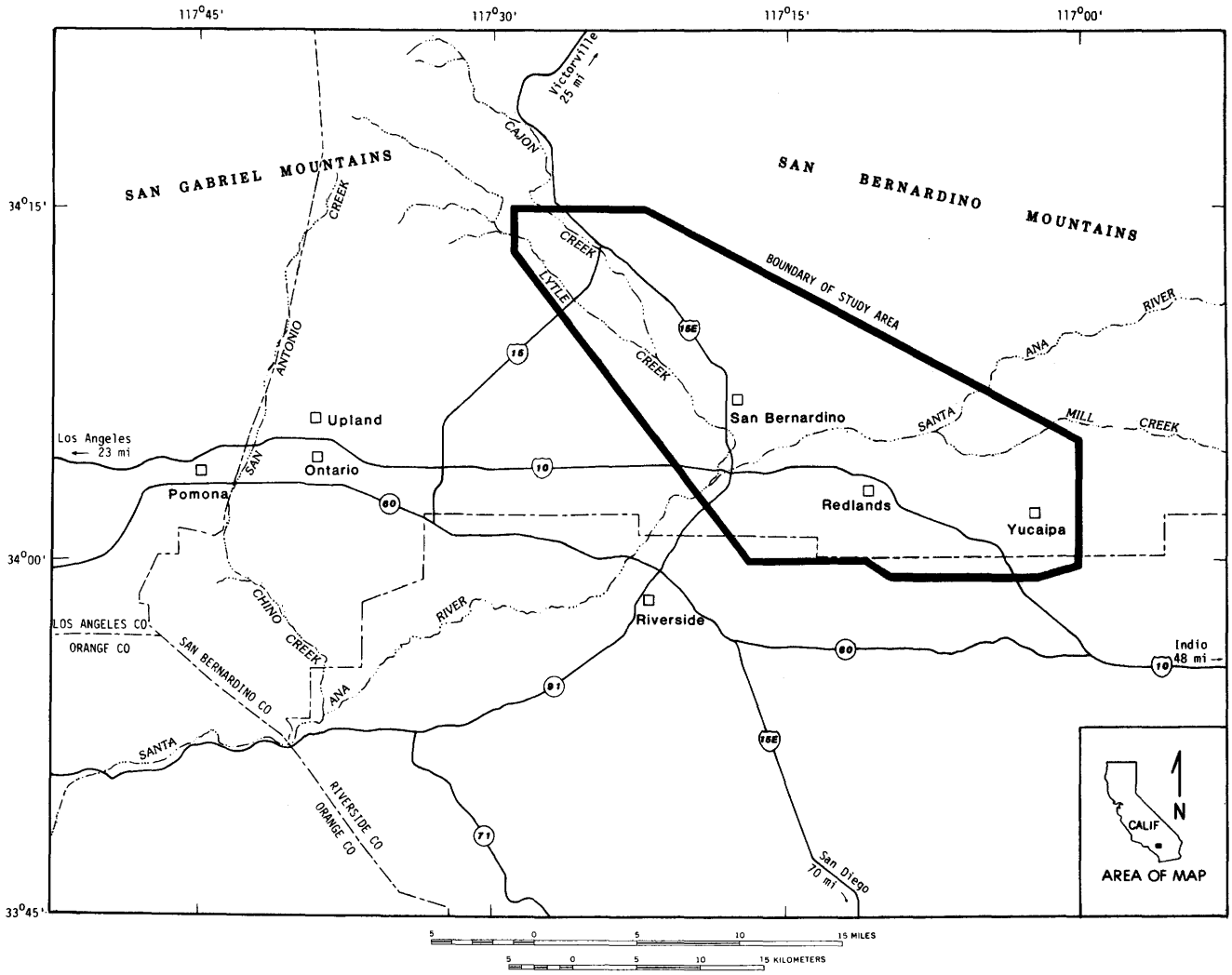

Figure 1. Location of the study area, San Bernardino Valley and vicinity, southern California.

Liquefaction of subsurface sediment does not in itself pose a hazard or risk to structures or life; the hazard is posed by ground failures that can be induced by liquefaction. Ground failures do not always accompany subsurface liquefaction, however, and many susceptible areas may experience no ground failure at all if the physical effects of liquefaction do not propagate to near-surface zones. Although we use the susceptibility results of this investigation to estimate the potential for liquefaction-induced ground failure, we do not document the character or distribution of ground failures stemming from liquefaction in the San Bernardino Valley region nor do we evaluate the level of hazard or risk resulting from such ground failures. The prediction and evaluation of liquefaction-induced ground failures and their attendant risks are beyond the scope of this investigation.

Previous Investigations

Previous investigations of liquefaction susceptibility in the San Bernardino Valley region include both unpublished and published studies. The unpublished studies include site-specific liquefaction evaluations performed by private geotechnical firms and filed with municipal and county regulatory agencies in compliance with permitting requirements. These site investigations incorporate various kinds of procedural approaches, earthquake-risk analyses, and ground-shaking conditions. In the public domain, Fife and others (1976) noted that liquefaction was a possible hazard in the San Bernardino Valley region, and they made general comments about the distribution of susceptible zones by integrating generalized ground-water conditions and marshland patterns (Fife, 1974) with generalized grain-

size patterns for alluvial sediments occurring within the valley. The firm of John R. Byerly, Inc. (1982), was commissioned by the City of San Bernardino Water Department to evaluate liquefaction susceptibility on the basis of geotechnical data from seven sites located around the periphery of the shallow ground-water zone in the metropolitan area. Tinsley and others (1985) discussed liquefaction potential in the San Bernardino Valley area as part of a larger evaluation of liquefaction conditions in southern California. Their analysis in the San Bernardino area utilizes our map of ground-water conditions for the 1973–79 period (Carson and Matti, 1985) and a generalized map of surficial sedimentary materials in the upper Santa Ana River valley region (Cox and Morton, 1978).

LIQUEFACTION—GENERAL BACKGROUND

The Liquefaction Process

The physical process of seismically induced liquefaction is well understood (Youd, 1973; Seed and Idriss, 1982, p. 65–70; National Research Council, 1985, p. 15–70). During an earthquake, seismic waves travel through the Earth and vibrate the ground. In cohesionless granular material having low relative density (for example, loose sandy sediment), this vibration can disturb the particle framework, thus leading to increased compaction of the material and reduction of pore space between the framework grains. If the sediment is saturated, water occupying the pore spaces resists this compaction and exerts pore pressure that reduces the contact stress between the sediment grains. With continued shaking, transfer of intergranular stress to pore water can generate pore pressures great enough to cause the sediment to lose its strength and change from a solid state to a liquefied state. This mechanical transformation can cause various kinds of ground failure at or near the surface.

The liquefaction process typically occurs at depths less than 50 ft subsurface, although the most susceptible conditions occur at depths shallower than 30 ft subsurface. Diminished susceptibility as depth increases is due to the increased firmness of deeper sedimentary materials, which can be attributed mainly to two factors: (1) increased overburden pressure resulting from the load of overlying sediment layers and (2) increased geologic age. These two factors tend to create a denser packing of sediment grains in the deeper sedimentary materials, which thus are less likely to experience the additional compaction and elevated pore pressures that are necessary to induce loss of shear strength and liquefaction during an earthquake.

Liquefaction of subsurface materials can lead to several types of near-surface ground failure, depending on the slope conditions and the geologic and hydrologic setting (Seed, 1968; Youd, 1973; Tinsley and others, 1985, p. 266–267; National Research Council, 1985, p. 18–27). Four common types of ground failure are (1) lateral spreads (landslides having limited displacement as used by Seed, 1968), (2) flow failures (flow landslides as used by Seed, 1968), (3) ground oscillation, and (4) loss of bearing strength (quick conditions as used by Seed, 1968). Sand boils (injections of fluidized sediment) commonly accompany these different types of ground failure (Ambraseys and Sarma, 1969) and form sand volcanoes at the ground surface or convolute layering and sand dikes in subsurface sediment layers.

Damaging ground failure resulting from earthquake-induced liquefaction has occurred throughout the world. For example, during the Guatemala earthquake of February 4, 1976, differential lateral displacements and settlements resulting from lateral spreading destroyed or damaged 90 percent of the houses in the La Playa area of Lake Amatitlan (Hoose and others, 1978). The Niigata, Japan, earthquake of June 16, 1964, generated widespread damage resulting from liquefaction (Seed and Idriss, 1967). There, extensive areas were covered by water and sand that were ejected from sand boils and from cracks in the earth, and loss of bearing strength led to differential settlement that caused extensive damage. Many overlying structures settled 3 ft or more or suffered severe tilting, and buoyant subgrade structures such as sewage-treatment tanks floated to the surface. Sand boils that were generated during the Imperial Valley, California, earthquake of May 18, 1940 ejected large quantities of sand in the nearby Yuma Valley, creating extensive damage to irrigation systems by covering fields and choking canals and ditches (Richter, 1958, p. 108).

Procedures for Evaluating Liquefaction Susceptibility

The factors that determine whether sedimentary materials are susceptible to earthquake-induced liquefaction can be grouped into three categories: (1) the geotechnical properties of the sediment, (2) depth to ground water, and (3) the intensity and duration of ground shaking. By using a variety of techniques, it is possible to determine each of these factors at an individual site to evaluate whether or not liquefaction is likely to occur during an earthquake of specified magnitude. By using additional analytical methods and statistical analysis, site-specific results can be extrapolated regionally to assign generalized liquefaction-susceptibility ratings to large areas.

Site-Specific Evaluations

By performing laboratory and in-place geotechnical tests on subsurface sediments occurring at a particular site, it is possible to evaluate whether liquefaction is likely to occur there. Geotechnical engineers and engineering geologists commonly use this procedure to evaluate

liquefaction susceptibility for land parcels being considered for development. For this type of investigation, subsurface borings are made at a number of closely spaced locations, the sediments encountered are logged and sampled, tests of penetration resistance are conducted, and laboratory tests may be performed on the collected samples to obtain various kinds of geotechnical data. On the basis of these analyses, the sediments are evaluated for their susceptibility to liquefaction under specified ground-shaking conditions by comparing their geotechnical properties with those of sediments known to have liquefied under similar ground-shaking conditions. Techniques for site-specific liquefaction analysis have been described by several authors, including Seed and Idriss (1971, 1982), Seed and Peacock (1971), Castro (1969), Andersen and others (1982), Poulos and others (1985), and Seed and others (1985).

Regional Evaluations

Regional evaluations of liquefaction hazards incorporate three components: liquefaction susceptibility, liquefaction opportunity, and liquefaction potential (Youd and Perkins, 1978; Youd and others, 1978; Tinsley and others, 1985). A **liquefaction-susceptibility evaluation** uses the geotechnical properties of sedimentary materials together with depth to ground water, expected earthquake magnitude, and strength of induced ground shaking to identify those sedimentary materials that are likely to liquefy during particular seismic events. A **liquefaction-opportunity evaluation** uses the frequency, magnitude, and location of anticipated future earthquakes to estimate recurrence intervals for earthquake shaking strong enough to generate liquefaction in susceptible materials. A **liquefaction-potential evaluation** combines the results of the susceptibility and opportunity evaluations to identify areas that, on a probabilistic basis, are most and least likely to experience liquefaction during specified earthquakes having specified recurrence intervals. Our investigation incorporates these three components but combines them in a manner appropriate to the geologic setting of the San Bernardino Valley region. Our analysis of liquefaction susceptibility is modeled along the lines of Youd and Perkins (1978). However, instead of using probabilistic methods to estimate liquefaction opportunity and liquefaction potential, we use a scenario-earthquake approach that evaluates the effects of specific earthquakes occurring on specific faults in the San Bernardino Valley region.

Ideally, an investigation of liquefaction susceptibility for a large region like the San Bernardino Valley would incorporate numerous site-specific evaluations spaced closely throughout the entire region. This dense network of local evaluations would be used to determine in great detail the regional distribution of susceptible and nonsusceptible sediments. However, such an approach is not possible for the San Bernardino Valley because existing site-specific evaluations are not distributed widely throughout the region and are not uniform in technical quality and because the siting of new evaluations necessary to fill gaps in the existing data base would be too costly. Therefore, alternative approaches to regional liquefaction analysis must be employed—approaches that inevitably lead to generalizations and compromises in techniques and results.

Liquefaction evaluations for large areas like the San Bernardino Valley can be conducted successfully if the geologic and hydrologic conditions known to be conducive to liquefaction at specific sites can be extrapolated regionally. This extrapolation can be accomplished by a correlation process whereby geologic and hydrologic conditions that are found to be susceptible at local sites are linked to particular geologic units and ground-water intervals whose distribution then can be mapped throughout the region. This approach has been developed by Youd and Perkins (1978), Youd and others (1978), and Tinsley and others (1985), who used site-specific data to identify characteristic susceptibilities for different combinations of geology and hydrology, which they then mapped regionally. This extrapolation process requires certain generalizations and assumptions about geology, hydrology, and ground shaking and necessarily leads to generalized statements about liquefaction susceptibilities regionally.

Methods Used in This Study

For the site-specific phase of this investigation, we used analytical procedures described by Seed and Idriss (1982) to determine liquefaction susceptibility at representative locations throughout the San Bernardino Valley area.[1] For the regional phase, we used techniques modeled after those developed by Youd and others (1978) and Tinsley and others (1985), although we modified some aspects of their method to accommodate geologic and hydrologic conditions within the San Bernardino Valley region. Our investigation incorporated the following steps: (1) we made a geologic map of the San Bernardino Valley region, showing faults and various surficial geologic units (pl. 1); (2) we evaluated ground-water conditions (pl. 2); (3) we compiled geotechnical data from existing site investigations and screened these data for their applicability to liquefaction analysis; (4) we conducted subsurface drilling

[1] Seed and others (1985) recently introduced correction factors and refined susceptibility curves that modify the procedures described by Seed and Idriss (1982) and improve evaluations of liquefaction susceptibility at specific sites. These refinements were published too late to be incorporated into our analysis. Application of the refined techniques would improve the evaluation of susceptibility in the San Bernardino Valley region by refining susceptibility results for ground-water depths between 30 and 50 ft subsurface. However, our application of the new susceptibility curves to penetration data collected by the U.S. Geological Survey (Carson and others, 1986) indicates that the results of our investigation for ground-water depths between 0 and 30 ft subsurface would not be altered significantly.

at representative sites in the valley region to obtain additional geotechnical data (Carson and others, 1986); (5) we evaluated data from more than 800 samples at 138 sites to determine liquefaction susceptibility for ground-shaking conditions created by scenario earthquakes on the San Andreas, San Jacinto, and Cucamonga faults; (6) we extrapolated these evaluations throughout the San Bernardino Valley region by using generalizations and assumptions about the geology, hydrology, and ground-shaking conditions; and (7) we constructed maps that zone the San Bernardino Valley region into areas of high to low susceptibility for each of the three scenario earthquakes (pls. 3–5).

GEOLOGIC SETTING

Sedimentary Materials

The San Bernardino Valley region is a broad, gently sloping lowland that flanks the southwest margin of the San Bernardino Mountains. The lowland is underlain by alluvial sediments eroded from bedrock in the adjacent uplands and washed by rivers and streams into the valley region, where the sediment has accumulated in layers of gravel, sand, silt, and clay. Sediment accumulation has continued for several million years, during which time an ever-thickening blanket of sediment gradually has buried the original hill-and-valley topography of the San Bernardino Valley; Perris Hill and the Shandin Hills are vestiges of that original topography that have not yet been buried by the encroaching sediment. Deeper parts of the sedimentary fill are older and are well consolidated; near-surface sediments are younger and are only slightly consolidated. The relatively loose near-surface sediments potentially are susceptible to earthquake-induced liquefaction, and they are the focus of this report.

Near-surface alluvial sediments of the San Bernardino Valley region accumulated in two depositional regimes: (1) alluvial fans that extend downslope from the mouths of mountain canyons and (2) river flood plains of the Santa Ana River and Cajon and Lytle Creeks. Although the alluvial-fan deposits tend to be coarser grained and more poorly sorted than the flood-plain deposits, both alluvial suites show considerable range in particle size from place to place in the San Bernardino Valley. Near the mountain front, the deposits consist of sand-bearing cobble and boulder gravel interstratified with layers of sand and gravelly sand. Downstream from the mountain front, the gravelly sediment gradually becomes finer grained. Where the alluvial-fan and flood-plain regimes meet in the vicinity of metropolitan San Bernardino, sand and silt ultimately predominate over subordinate layers of clay and pebbly gravel.

Within both the alluvial-fan and flood-plain regimes, the latest cycle of river and stream development in many areas has led to channel downcutting that has left older parts of the sedimentary blanket standing above the level of the modern channels. Very young loose sediment is accumulating in the bottoms of the incised channels, while the higher standing sediments are inactive, are firmer and more compacted, and are developing pedogenic-soil profiles. This pattern of downcutting and backfilling has occurred several times in the long history of the alluviated lowland, leading to a complex pattern of surficial-geologic units—each representing a different depositional age and (or) a different sediment type.

Detailed geologic mapping of these surficial deposits has led to recognition of a large number of individual map units (Matti and others, 1985; J.C. Matti and S.E. Carson, unpub. mapping, 1980–86), but for purposes of liquefaction evaluation, we have grouped these into three major categories on the basis of depositional age. Younger Holocene deposits (Qh_2 on pl. 1) include sedimentary materials that we interpret to have accumulated within the last 500 to 1,000 yr. Older Holocene deposits (Qh_1 on pl. 1) include sedimentary materials that we interpret to have accumulated between 500 or 1,000 yr ago and 10,000 to perhaps 15,000 yr ago. Pleistocene deposits (Qp on pl. 1) include sedimentary materials that we interpret to have accumulated between 10,000 or 15,000 yr ago and about 750,000 yr ago.

Age determinations for the surficial deposits are preliminary and are based mainly on the degree of pedogenic-soil development on the upper surfaces of the units. The soil profiles are thin and slightly developed on younger alluvial deposits but are progressively thicker and better developed on progressively older deposits. The age of an alluvial deposit in relation to another deposit can be determined by comparing the development of their respective soil profiles, and the numeric age of a soil profile can be determined from radiometric analysis of organic carbon associated with the soil. We have assigned ages to surficial-geologic units in the San Bernardino Valley region by comparing their soil profiles with those under study elsewhere in the region (McFadden, 1982; Weldon and McFadden, 1987; Harden and others, 1986; J.W. Harden and J.C. Matti, unpub. data).

Disagreement exists regarding the thickness of the youngest, loosest sedimentary materials in the San Bernardino Valley region. Many published studies and unpublished geotechnical site investigations conclude that Holocene and latest Pleistocene deposits (less than about 15,000 yr old) form an extensive blanket of young loose sediment as much as a few hundred feet thick. By contrast, radiocarbon age determinations from subsurface borings (Carson and others, 1986) and penetration-resistance data from multiple sources suggest that the loose Holocene materials may be less than 50 to 75 ft thick in many areas and that they are underlain abruptly by firmer, denser sedimentary materials that have considerably higher penetration resistance.

The validity of either thickness model has direct bearing on liquefaction susceptibility throughout the San

Bernardino Valley region. (1) A thick pile of loose sediment saturated with ground water inherently would be more susceptible to liquefaction and might generate larger, more extensive liquefaction-induced ground failures than would a thin blanket of loose sediment and (2) a thick pile of loose sediment would amplify the shaking intensity of earthquake waves by comparison with a thin blanket of loose sediment, thus increasing liquefaction susceptibility by increasing the strength of ground shaking.

Alluvial Setting and Liquefaction Susceptibility

The relation between geologic setting and liquefaction susceptibility has been reviewed by several workers (Youd and Hoose, 1977; Youd and Perkins, 1978; Tinsley and others, 1985) who recognize a general correlation between the age and type of sedimentary deposit and the likelihood of liquefaction. All other factors being equal, younger sediments tend to be more susceptible than older sediments, and sands and silty sands deposited in river channels and flood plains tend to be more susceptible to liquefaction than coarser or finer grained sediments deposited in other environments. On the basis of these general guides alone, a geologic map of the San Bernardino Valley region could identify areas of greater or lesser susceptibility.

Geologic Age

Tinsley and others (1985) grouped Quaternary sedimentary deposits in southern California into three age classes according to their susceptibility to earthquake-induced liquefaction: deposits less than 1,000 yr old (latest Holocene), deposits 1,000 to 10,000 yr old (earlier Holocene), and undifferentiated older deposits between 10,000 and 500,000 yr old (late and middle Pleistocene). Tinsley and others (1985) showed that the progressively older deposits have progressively lower susceptibilities that reflect their increased compaction, relative density, and longer history of seismic shaking. This correlation between sediment age and liquefaction response led us to subdivide the sedimentary fill of the San Bernardino Valley region into three units that are modeled from those recognized by Tinsley and others (1985). From youngest to oldest, these three units (Qh_2, Qh_1, and Qp) should be increasingly resistant to earthquake-induced liquefaction.

Sediment Type and Depositional Environment

Youd and Perkins (1978) and Tinsley and others (1985) showed that sedimentary materials accumulating in certain depositional environments inherently are more susceptible to liquefaction than materials accumulating in other environments. For example, clean sands and silty sands in river channels generally are more susceptible than mixtures of coarser sand and gravel that occur on alluvial fans (Youd and Perkins, 1978, table 2). According to this generalized guideline, sedimentary materials in the San Bernardino Valley that have accumulated in channel systems of the Santa Ana River and Cajon and Lytle Creeks inherently are more susceptible than materials deposited in alluvial-fan environments, especially near the mountain fronts where the fan sediments are coarser grained and more poorly sorted than their counterparts farther away from the mountain front.

Implication for the San Bernadino Valley

Our analysis indicates that the liquefaction susceptibility of sedimentary materials in the San Bernardino Valley region generally can be correlated with their age and depositional setting, but these criteria have only general value for mapping and predicting susceptibility patterns. For example, young sediments of unit Qh_2 occurring in the flood plain of the Santa Ana River generally have lower penetration resistance than sediments of units Qh_1 and Qp elsewhere in the region. As a result, the youthful floodplain sediments are more susceptible than older deposits. However, for the strong ground-shaking conditions specified in our study, both younger Holocene sediments (unit Qh_2) and older Holocene and youngest Pleistocene sediments (unit Qh_1) generally demonstrate a similar degree of susceptibility regardless of their geologic age or depositional setting—as long as they are near surface and are saturated with ground water. This departure from the patterns observed by Tinsley and others (1985) reflects the high seismic potential of the San Bernardino Valley region by comparison with many other metropolitan areas in southern California.

Faults

The San Bernardino Valley region is the site of numerous faults, some of which are capable of generating large earthquakes. The major faults are strike-slip structures of the San Andreas family—faults that generate earthquakes when blocks on either side of the fault plane slide right-laterally past each other. These include the San Jacinto fault and the modern trace of the San Andreas fault. Many of the smaller faults are normal or reverse dip-slip faults that have evolved because of complications within the San Andreas fault system (Matti and others, 1985). Dip-slip faults generate earthquakes when blocks on either side of the fault plane slide up or down relative to each other. Reverse dip-slip faults include the Cucamonga fault along the base of the southeastern San Gabriel Mountains (Morton and Matti, 1987; Matti and others, 1982) and the San Gorgonio Pass fault zone (Matti and others, 1985). Normal dip-slip faults include the Crafton Hills fault complex (Matti and others, 1985) and other normal faults observed or inferred

to occur in and around the San Bernardino Valley and San Bernardino Mountains (Matti and others, 1985; Weldon, 1985).

Earthquake Potential

Numerous faults in the San Bernardino Valley region are actively generating small earthquakes (Green, 1983; Nicholson and others, 1986), and some of these faults have generated large earthquakes in the recent geologic past (Weldon and Sieh, 1985). Estimates of the potential for future damaging earthquakes on these faults involve three questions: (1) which fault will generate the next earthquake; (2) how large will it be; and (3) when will it occur? Answers to these questions not only are relevant to earthquake-preparedness planning but are essential for evaluating earthquake hazards such as liquefaction. Two approaches currently are available for evaluating the seismic potential of the San Bernardino Valley region: (1) probabilistic approaches that are based on the annual probability for earthquakes stemming from all available sources and (2) empirical approaches that incorporate specific scenario earthquakes on specific faults.

Probabilistic Versus Scenario Models of Earthquake Potential

Probabilistic estimates of seismic risk are based on the idea that the potential for an earthquake in a given region is equal to the annual probabilities for earthquakes on all faults capable of generating energy of a certain level in the region (Idriss, 1985). Such approaches usually are based on the statistical premise that earthquakes occur randomly in time and that the annual probability for earthquake occurrence is the same from year to year given a Poisson (random) probability distribution. Coupled with this random probability model is the observation that small and moderate earthquakes occur more frequently than large and great earthquakes. Thus, a random-probability model for earthquake risk in the San Bernardino Valley region would propose that, for a given period—for example, 50 yr, about the average usable life of noncritical structures—the probability of a small to moderate earthquake is greater than the probability of a large to great earthquake and is the same each year. Thus, the annual seismic potential for a 50-yr period would be relatively low even if it included input from all seismic sources. If nothing is known about the recurrence (repeat time) of earthquakes or if an average faulting-recurrence interval has been determined but the time of the last earthquake is not known, then it is appropriate to evaluate seismic risk by using a Poisson model where the probability of an earthquake is the same during any particular time interval.

If a faulting-recurrence interval has been established and if the time of the last earthquake is known or can be estimated, the use of random-probability models to estimate the level of seismic risk for any given year is not appropriate. Instead, information about where we are within the earthquake-recurrence cycle (Thatcher, 1984) requires conditional rather than random probabilistic analyses, where at any given time the probability of earthquake occurrence is conditional upon when the last earthquake occurred and when the next earthquake might be expected (on average). With conditional analyses, the probability of earthquake occurrence increases from year to year at a rate that depends upon how long it has been since the last earthquake occurred and upon statistical uncertainties associated with the average length of the cycle.

Investigations of earthquake history have demonstrated that earthquakes in southern California do not occur randomly in time but instead occur at faulting-recurrence intervals that are approximately constant on average (Sieh, 1978, 1984; Weldon and Sieh, 1985). This conclusion has led to the idea that particular fault segments will generate characteristic earthquakes of specified magnitude having a certain regularity (Schwartz and Coppersmith, 1984). In historic time, no large earthquakes are known to have occurred on the three faults that are capable of generating shocks whose shaking effects would be felt intensely in the San Bernardino Valley region—the San Andreas fault between Cajon Pass and San Gorgonio Pass, the San Jacinto fault between Riverside and the San Gabriel Mountains, and the Cucamonga fault. Because these three faults have not generated major earthquakes in at least 140 yr, they are closer to failure with each passing year. Accordingly, we elected to evaluate the seismic potential of the San Bernardino Valley region by considering the impact of large local earthquakes on each fault.

Scenario Earthquakes on the San Andreas, San Jacinto, and Cucamonga Faults

San Andreas fault.—Three segments of the San Andreas fault occur adjacent to the San Bernardino Valley region (Matti and others, 1985): (1) the Coachella Valley segment to the southeast, (2) the Mojave Desert segment to the northwest, and (3) the San Bernardino segment that flanks the San Bernardino Mountains and intervenes between the Mojave Desert and Coachella Valley segments. The Coachella Valley segment has not generated a major earthquake since about A.D. 1680 (National Earthquake Prediction Evaluation Council, 1988). The Mojave Desert segment ruptured during the great M=8+ earthquake of 1857, but the ground-rupture zone apparently did not extend southeastward to include the San Bernardino segment (Sieh, 1978; Weldon and Sieh, 1985).

Separately or in combination, the Mojave Desert, Coachella Valley, and San Bernardino segments of the San Andreas have potential for generating large earthquakes whose ground-shaking effects could severely affect the San Bernardino Valley region. A number of workers recently have concluded that the probability of such an event is increasing annually. For example, Raleigh and others

(1982) summarized data indicating that the San Andreas fault in southern California is a mature seismic gap that will be filled by California's next great earthquake; although their study did not assign probabilities to a specific time period, they implied that this sector of the fault is near failure. Lindh (1983) assigned annual conditional probabilities that by the year 2012 will accumulate to 40 percent for an earthquake on the Indio segment of the San Andreas fault (M=7.5 to 8) and 25 percent for the Mojave segment of the San Andreas fault (M=7.5 to 8). Lindh's preliminary forecasts were summarized by Wesson and Wallace (1985, p. 43), who also quoted a U.S. Geological Survey report to the National Security Council wherein the likelihood of an M=8.3 earthquake along the southern San Andreas "is estimated to be between 2 and 5 percent per year, or about 50 percent in the next 20 or 30 years" (Wesson and Wallace, 1985, p. 37). Sykes and Nishenko (1984) suggested that a 325-km length of the San Andreas fault spanning the Mojave Desert, San Bernardino, and Coachella Valley segments has about a 25 percent chance of generating an earthquake near magnitude 8 during the next 20 yr; shorter segments yielding an M=7.5 to 7.6 earthquake have cumulative probabilities estimated to be as great as 50 to 60 percent. Weldon and Sieh (1985, p. 811–812, fig. 15) discussed four fault-rupture scenarios for the San Andreas fault in the San Bernardino region, three of which suggest that failure is overdue "in the sense that more time than the average interval between events has passed since the last event." Most recently, the National Earthquake Evaluation Prediction Council (1988, p. 2, 30–40) estimated 10-yr to 30-yr probabilities for large (M=7.5 to 8+) earthquakes on the southern San Andreas fault that range from 0.2 in the near 10-yr timeframe to 0.6 over the 30-yr timeframe.

The magnitude of a large earthquake on the San Andreas fault in the San Bernardino Valley region depends on the fault-rupture scenario that develops, and uncertainty exists concerning the most likely pattern and scale of rupture. Sieh (1978, p. 3935–3936) and Allen (1981) speculated that a truly great earthquake could result if ground rupture on the San Andreas were to extend from the Coachella Valley segment through San Gorgonio Pass and onto the San Bernardino and Mojave Desert segments. This large-rupture scenario is advocated by Sykes and Seeber (1985) and seems to be incorporated into the seismic-potential evaluations by Raleigh and others (1982), Lindh (1983), Sykes and Nishenko (1984), and Wesson and Wallace (1985). However, the complex geologic setting of the San Andreas fault in the San Bernardino Valley region (Matti and others, 1985) may preclude throughgoing rupture on the Coachella Valley and Mojave Desert segments, and alternative fault-rupture scenarios have been proposed (Rasmussen, 1981; see the discussion by Weldon and Sieh, 1985, p. 811–812 and the National Earthquake Prediction Evaluation Council, 1988). These alternative earthquake scenarios may lead to magnitudes somewhat lower than the M=8.0+ magnitude required by long fault-rupture lengths.

The actual fault-rupture scenario for the San Andreas fault in the San Bernardino Valley region presently cannot be predicted. However, to accommodate the ground-shaking conditions accompanying a worst-case earthquake on this fault, we adopted an M_s (surface-wave magnitude) =8.0 shock in our evaluation of liquefaction susceptibility. This scenario earthquake is compatible with most fault-rupture predictions and is consistent with our goal of identifying the maximum extent of susceptible conditions throughout the San Bernardino Valley region.

San Jacinto fault.—The San Jacinto fault southeast of Riverside is thought to have generated two M=6.5 to 7.0 earthquakes in 1899 and 1918 (Sanders and Kanamori, 1984, p. 5873–5875, fig. 1). However, it is not clear that a significant earthquake has been generated in historic time by the segment of the fault between Riverside and the southeastern San Gabriel Mountains.

Some workers suggest that the northern part of the segment may have been the source for an M=5–6 earthquake in 1899 (Thatcher and others, 1975, fig. 1, p. 1145; Sykes and Nishenko, 1984, p. 5922) and that the southern part of the segment may have been the source for M=5–6 earthquakes in 1907 and 1923 (Thatcher and others, 1975, fig. 1; Sykes and Nishenko, 1984, p. 5922). However, the location and origin of the 1899 earthquake have not been documented, and the location and origin of the 1907 and 1923 shocks are disputed. Hanks and others (1975, fig. 1) position the 1907 event on or adjacent to the San Andreas fault instead of on the San Jacinto fault, and Toppozada and Parke (1982, table 1, fig. 10) position the event well north of the San Andreas fault in the San Bernardino Mountains (see the epicentral position shown by Real and others, 1978). The 1923 M=6.25 event is assigned to the San Jacinto fault by most workers (Thatcher and others, 1975; Hanks and others, 1975; Toppozada and Parke, 1982; Sanders and Kanamori, 1984), but Nicholson and others (1986, p. 4900) suggest that this earthquake may have occurred on northeast-oriented faults that they believe underlie the San Bernardino Valley. Alternatively, the extent of damage in the Loma Linda area (Laughlin and others, 1923) may reflect rupture along faults mapped by Morton (1978a,b,c) that are parallel to the San Jacinto zone but east of it. Despite these ambiguities, or perhaps because of them, Thatcher and others (1975) identified the San Bernardino segment of the San Jacinto fault as a seismic gap, and they contrasted its history with more active segments of the fault farther to the southeast.

The range of magnitudes for a large earthquake on the San Jacinto fault in the San Bernardino Valley region depends on the fault-rupture scenario that develops. Matti and others (1985) pointed out that the San Jacinto fault in the San Bernardino-Riverside area consists of at least two segments: a right-stepping segment in the San Jacinto

Valley region that is thought to be the site of earthquakes in 1899 and 1918 (Sanders and Kanamori, 1984) and a segment that extends northwestward from a distinctive left-curving bend developed in the Reche Canyon area. Both segments are less than 75 km long and may define separate fault-rupture zones. Evernden and Thomson (1985) used this concept to suggest that the San Bernardino Valley segment could generate an M_L=6.4 earthquake (M_L=local magnitude). Sykes and Nishenko (1984, fig. 2, table 2, p. 5922, 5925) indicate that the San Bernardino segment has a cumulative probability of nearly 100 percent for generating an M=6.4 to 6.7 earthquake by the year 2003, and Lindh (1983) assigned annual probabilities that by the year 2012 will accumulate to 45 percent for an M=6.75 earthquake on the segment.

The likely length of fault rupture along the San Bernardino segment is unknown because none of the earthquakes attributed to it have generated surface ruptures. A minimum rupture from the mouth of Lytle Creek to the head of Reche Canyon would be about 25 km and would lead to a magnitude range of about 6.7 to 7.0 according to the rupture-length versus magnitude curves for strike-slip faults presented by Bonilla and others (1984, fig. 1). Using the same curves, a larger 35-km rupture involving coseismic displacements on the Glen Helen and San Jacinto faults between Cajon Pass and the head of Reche Canyon would lead to magnitudes in the range of 7.0 to 7.2. Even greater magnitudes would develop if both the San Bernardino Valley and San Jacinto Valley segments were to rupture coseismically.

The actual fault-rupture scenario for the San Jacinto fault in the San Bernardino Valley region presently cannot be predicted. However, to accommodate ground-shaking conditions accompanying a worst-case earthquake on this segment, we incorporated an M_s=7.0 shock in our evaluation of liquefaction susceptibility. This scenario earthquake is compatible with upper bound earthquakes proposed for the fault by Ziony and Yerkes (1985, p. 80) and is consistent with our goal of identifying the maximum extent of susceptible conditions throughout the San Bernardino Valley region.

Cucamonga fault.—The Cucamonga fault is a north-dipping reverse- and thrust-fault zone that bounds the southern margin of the eastern San Gabriel Mountains (Morton, 1975; Matti and others, 1985; Morton and Matti, 1987). The fault zone is part of a family of reverse and thrust faults in southern California that are responsible for the Pleistocene and Holocene uplift of mountainous regions like the Santa Ynez, Santa Susana, San Gabriel, and San Bernardino Mountains. These mountains form the so-called Transverse Ranges that trend east-west across the predominantly northwest topographic and structural grain of southern and central California. The Cucamonga fault is not known to have generated a significant earthquake in historic time, but a series of fault scarps in Holocene and uppermost Pleistocene alluvial-fan deposits at the southeastern base of the San Gabriel Mountains attests to a succession of ground-rupturing earthquakes in the recent geologic past (Matti and others, 1982; Morton and Matti, 1987). Field data indicate that these paleoearthquakes were similar in origin, mechanics, and scale to the M=6.4 San Fernando earthquake in 1971. Seismic-moment considerations suggest that an earthquake generating ground-surface displacement of about 6 ft along a fault rupture extending throughout 6 to 16 mi of the Cucamonga zone might generate earthquakes in the M_s range of 6.5 to 7.2 (J.C. Matti, D.M. Morton, J.C. Tinsley, and L.D. McFadden, unpub. data, 1986; Matti and others, 1985, p. 14, 16). For our liquefaction-susceptibility analysis, we used a scenario earthquake having M_s=6.75.

GROUND WATER

Because ground-water saturation of sediment shallower than about 50 ft subsurface is required for earthquake-induced liquefaction to occur, our evaluation of liquefaction susceptibility required that we identify the distribution of shallow water levels throughout the San Bernardino Valley region. Plate 2 is a contour map showing minimum depths to ground water (Carson and Matti, 1986). The map was constructed by contouring water-level measurements reported to the California Department of Water Resources for the period from 1973 through 1983, and it depicts what the regional ground-water table would look like if the shallowest water level measured in each local well during this period is used as the basis for constructing the map. Such a map differs from most hydrologic maps in that it does not show the actual shape of the water table at any particular time, nor does it show the average or typical ground-water conditions during the reporting period. Instead, the map shows a hypothetical ground-water table that is based on the shallowest water level measured in each local well during a particular period of record. Such a map is useful to an evaluation of liquefaction susceptibility because it delineates areas that at one time or another during the reporting period were underlain by shallow ground water.

Beginning in about late 1977, ground-water levels in the San Bernardino Valley and vicinity have risen, mainly because of two factors: (1) Several wetter-than-normal years since 1977 contributed increased volumes of surface runoff and natural recharge in the San Bernardino Valley area and contributed to increased water conservation stemming from accelerated water-spreading activities by local water agencies and (2) commencing in 1972, ground water in the valley region has been replenished by artificial recharge of imported water derived from the California State Water Project. Together, the accelerated natural and artificial recharge of ground-water basins since 1977 has

resulted in rising water tables that reached their shallowest levels at the end of the 1973–83 reporting period.

The distribution of shallow ground water during the shallowing period corresponds fairly well to the distribution of naturally occurring shallow ground water observed before depletion of ground-water reservoirs during the first two thirds of this century. Prior to modification of natural patterns by extensive human activities, the distribution of ground water in the San Bernardino Valley was controlled by long-term steady-state geohydrologic conditions that in places produced naturally occurring bodies of near-surface ground water (for example, the areas of marshy ground portrayed by Mendenhall, 1905, and Fife, 1976). During the first two-thirds of this century, these prevailing conditions were modified considerably due to extensive ground-water withdrawal for irrigation and for industrial, municipal, and domestic uses; as a result, regional water tables generally were considerably lower. However, since 1977 the combined increase in natural and artificial recharge has raised the water table to levels much like those in the later years of the 19th century. We conclude that whenever the regional water table shallows in the San Bernardino Valley area it will lead to ground-water patterns generally similar to the those depicted on plate 2; moreover, we suggest that these patterns provide an appropriate basis for a regional study of liquefaction susceptibility in the valley area.

The ground-water map on plate 2 is regional and cannot be used as a site-specific guide. The contours depict the general distribution of water levels occurring across the valley region, but the map is not precise enough to identify water depths at a specific site. This limitation stems from factors discussed by Carson and Matti (1985, 1986).

EVALUATION OF LIQUEFACTION SUSCEPTIBILITY IN THE SAN BERNARDINO VALLEY REGION—GEOTECHNICAL SUMMARY

In this section we summarize the analytical procedures that are used in our geotechnical evaluation of liquefaction susceptibility in the San Bernardino Valley region. Appendixes A–C elaborate on these procedures and address technical details that are not discussed in this summary.

Site-Specific Evaluation of Liquefaction Susceptibility

For the site-specific phase of this investigation, we used the technique of Seed and Idriss (1982) to determine liquefaction susceptibility for each of the scenario earthquakes on the San Andreas, San Jacinto, and Cucamonga faults. At each site where appropriate penetration-resistance data were available, we evaluated the susceptibility of a given sediment by determining or estimating values for various geotechnical parameters and for the anticipated strength of ground shaking. We then used these parameters to define threshold conditions that, if exceeded, would promote liquefaction at the site.

Standard Penetration Tests—Basis for Liquefaction Evaluations

The Seed and Idriss (1982) method depends upon penetration-resistance data obtained from the Standard Penetration Test (SPT)—a standard engineering procedure that determines the looseness or firmness of a sedimentary material by measuring its resistance to penetration by a cylindrical sampling device that is driven through the sediment by repeated blows from a mechanical hammer. Penetration resistance is measured in blow counts—the number of blows (N) required to drive the sample through a prescribed interval of sediment. The larger the blow count (N), the firmer or denser is the sediment, and the less likely it is to liquefy.

Sedimentary Materials Evaluated

Although surficial materials in the San Bernardino Valley include a variety of sediment types ranging in grain size from clay to gravel, we evaluated susceptibility only for sand and silty sand. Because of their granular cohesionless character, loose accumulations of these materials are more likely to liquefy than are clay-rich sediments, which tend to be too cohesive for compaction to occur during earthquake shaking. Although gravels have been known to liquefy, the standard penetration test is not a very effective method of evaluating their susceptibility because gravelly sediment tends to yield N values that are excessively high and are not an accurate measure of their potential susceptibility (National Research Council, 1985, p. 104). If these elevated N values are included within data populations that then are evaluated statistically for their overall susceptibility, the resulting evaluation may indicate lower susceptibilities than actually exist. To circumvent this problem, we did not incorporate penetration results from sediments described as gravel, gravelly, or with gravel, regardless of their N value.

Data Sources

Penetration data that are used in this study are derived from four sources: (1) soil and foundation investigations filed with city and county agencies in compliance with permitting procedures, (2) subsurface investigations for flood-control structures and building projects prepared by the U.S. Army Corps of Engineers, (3) logs of test borings for bridges on State and Federal highways prepared by the California Department of Transportation (CalTrans), and (4) SPT data obtained during a 27-site drilling project conducted in the San Bernardino Valley area by the U.S.

Geological Survey (Carson and others, 1986). Plate 1 shows the distribution and density of SPT data used in this study.

Screening Procedures

Penetration data from the sources described above were generated by using a variety of different field methods and equipment. Procedural differences can lead to significant differences in blow count for sedimentary materials having identical physical characteristics—a shortcoming that creates problems for liquefaction evaluations that use blow-count data to compare the relative susceptibilities of sedimentary materials. This problem can be circumvented if the penetration test is standardized to comply with specific technical criteria. Seed and Idriss (1982, p. 94–95; Seed and others, 1985) specified several procedural guidelines that must be accommodated by the penetration test: (1) the test must comply with some of the SPT guidelines described by the American Society for Testing and Materials (ASTM) (1982) and (2) the test should incorporate several additional guidelines not stipulated by ASTM. By using these screening criteria, we determined that most of the penetration data that are available from the San Bernardino Valley region are not appropriate for susceptibility evaluations, leaving only those data from localities shown on plate 1.

Determination of Cyclic-Stress Ratios

For all sites where penetration-resistance values were obtained by using appropriate SPT procedures, we evaluated site-specific liquefaction susceptibilities by using analytical methods described by Seed and Idriss (1982). This analysis requires (1) estimates of peak horizontal ground acceleration resulting from each scenario earthquake, (2) data on depth to ground water, (3) values for the median grain size of tested materials, and (4) estimates of overburden pressure and effective stress, which in turn require assumptions about unit weights, neutral stress, and pore pressures. These factors are integrated with the penetration data to calculate two parameters (cyclic-stress ratios) that determine liquefaction susceptibility.

Cyclic-stress ratios[2] are unitless parameters that characterize the response of a given sediment type at a particular subsurface depth to ground-shaking conditions of specified strength and duration. One cyclic-stress ratio [$(\tau_{av} / \sigma_o')_{dev}$, referred to hereafter as C_d] describes the cyclic-loading conditions expected to develop at a location during a given earthquake; the other cyclic-stress ratio [$(\tau_{av} / \sigma_o')_{liq}$, referred to hereafter as C_l] describes the loading conditions required at the location for liquefaction to occur. If C_d exceeds C_l, then liquefaction is likely at the test location for that earthquake; if C_d is less than C_l, then liquefaction is unlikely. In this study we calculated C_d by using a formula provided by Seed and Idriss (1982) and C_l by using penetration-resistance values from the San Bernardino Valley region and a chart from Seed and Idriss (1982).

Determination of C_d

The cyclic-stress ratio that can be expected to develop at the location of each SPT as the result of a given earthquake can be determined by

$$C_d = 0.65 \cdot \frac{\sigma_o}{\sigma_o'} \cdot \frac{A_{max}}{g} \cdot r_d \,. \qquad (1)$$

The ratio of total overburden stress to effective overburden stress (σ_o / σ_o') quantifies the inherent resistance to deformation of a particular sediment at a particular subsurface depth given particular ground-water conditions. We calculated σ_o and σ_o' by using standard engineering relations, but to do so we had to make simplifying assumptions about pore-fluid pressures and saturated and unsaturated unit weights for sediments. The ratio of maximum horizontal ground-surface acceleration to gravitational acceleration (A_{max} / g) quantifies the strength of ground shaking expected at a particular site during a specified earthquake. We estimated values for A_{max} by stipulating scenario earthquakes of specified magnitude for specific faults and then by using attenuation curves provided by Seed and Idriss (1982) to scale ground-shaking strength at a specific site according to distance from the causative fault (figs. 2, 3). The parameter r_d is a stress-reduction coefficient that compensates for the fact that the shear stress affecting a sediment mass at a given subsurface depth during an earthquake is less than the maximum value because the overlying sediment column is flexible rather than rigid. Values for r_d are obtained by using figure 4.

Determination of C_l

Derivation of C_l relies mainly on penetration resistance (N) determined at specific sites. The raw penetration data cannot be used directly but must be modified to compensate for several factors, including (1) a numerical compensation for SPT tests conducted at shallow subsurface depths, (2) normalization of N to an overburden pressure of 2,000 lb/ft^2 to compensate for the effect of overburden pressure (obtained from fig. 5), and (3) a numerical compensation applied to N for SPT determinations in silty or partly silty materials. These adjustments to N yield a modified penetration resistance N_1 that can be used to determine C_l values for specific earthquakes by using empirical curves proposed by Seed and Idriss (1982, fig.

[2] The cyclic stress ratio (τ_{av} / σ_o') is the ratio between average shear stress (τ_{av}) induced by the ground shaking and the effective overburden pressure (σ_o') affecting a saturated sediment at a given subsurface depth. See Appendix B for details.

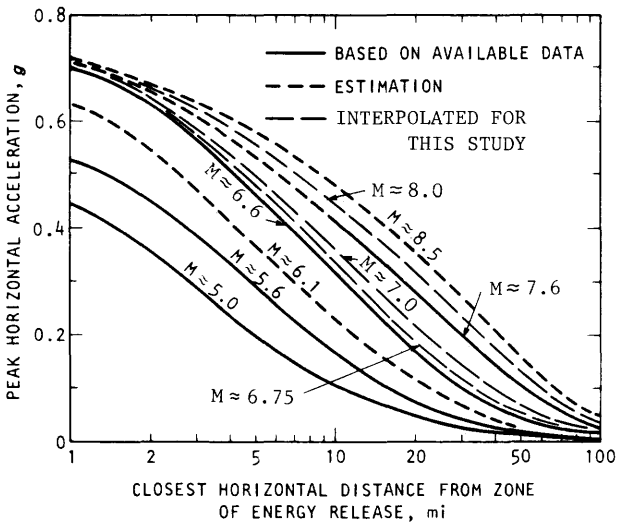

Figure 2. Attenuation of peak horizontal bedrock acceleration (A_{max}) with distance from the causative earthquake (modified from Seed and Idriss, 1982, fig. 17). M = earthquake magnitude; g = gravitational acceleration. Published with permission of the Earthquake Engineering Research Institute.

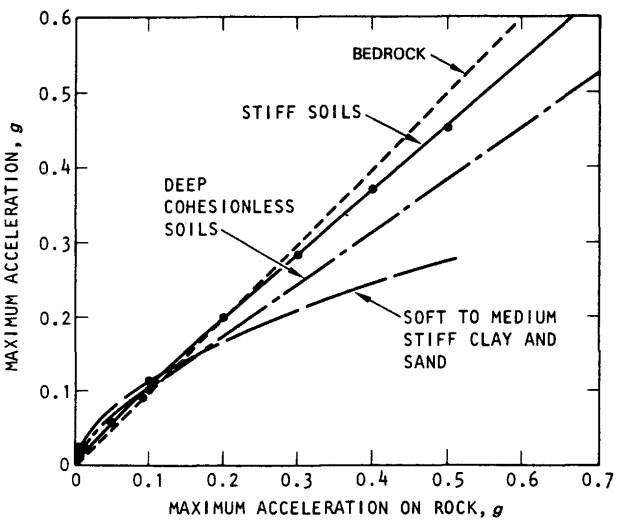

Figure 3. Approximate relation between peak horizontal accelerations on bedrock and peak accelerations at sites underlain by surficial sedimentary materials (modified from Seed and Idriss, 1982, fig. 19). g = gravitational acceleration. Published with permission of the Earthquake Engineering Research Institute.

57; fig. 6 of this report).[3] (Note: for deeper SPT samples, where values of effective overburden pressure greater than about 3,380 lb/ft^2 are encountered, C_l values obtained by using fig. 6 must be corrected by using factors like those obtained by using fig. 7). Figure 8 shows the range of N_1 values determined for penetration tests from the San Bernardino Valley region.

Susceptibility Evaluation—Susceptibility Ratios and Factors of Safety

To determine liquefaction susceptibility at an individual site, the two cyclic-stress ratios C_l and C_d for each of the three scenario earthquakes are compared as the ratio FS where:

$$FS = \frac{C_l}{C_d} . \qquad (2)$$

The ratio FS defines a factor of safety against liquefaction. If C_d is equal to or greater than C_l, FS=1.0 or less, and the materials evaluated by the penetration test have no margin of safety against liquefaction during the specified earthquake. Where C_d is less than C_l, FS is greater than 1.0, and the materials evaluated by the penetration test have a margin of safety against liquefaction that increases as the ratio FS increases.

No appropriate margin of safety is widely agreed upon as a standard for liquefaction-hazard recognition, "...primarily because the degree of conservatism thought desirable at this point depends upon the extent of the conservatism already introduced in assigning the design earthquake" (National Research Council, 1985, p. 96). If the specified ground-shaking conditions are deemed reasonable, factors of safety of about 1.35 generally are acceptable, although Seed and Idriss (1982, p. 123–124) suggest a range of 1.25 to 1.5. If the ground-shaking conditions are deemed excessively conservative to begin with, factors of safety only slightly above unity are acceptable. Given the conservative ground-shaking conditions generated by the large scenario earthquakes specified in our analysis and given the degree of conservatism introduced by some of the assumptions incorporated in our analysis, we specified a nonconservative margin of safety against liquefaction where FS=1.0. We explore the implications of this choice in the section on Evaluation of Results.

Regional Evaluation of Liquefaction Susceptibility

Statistical Evaluation

Although FS values calculated for individual sites indicate whether the materials at each penetration test are likely to liquefy, individually they do not provide informa-

[3] Seed and others (1985) recently introduced refined curves that correlate N_1 with C_l. As discussed in the section on Evaluation of Results, the new curves narrow the range of N_1 values that yield susceptible conditions, which thus could modify the results of our study where N_1 is relatively high—particularly at deeper subsurface depths.

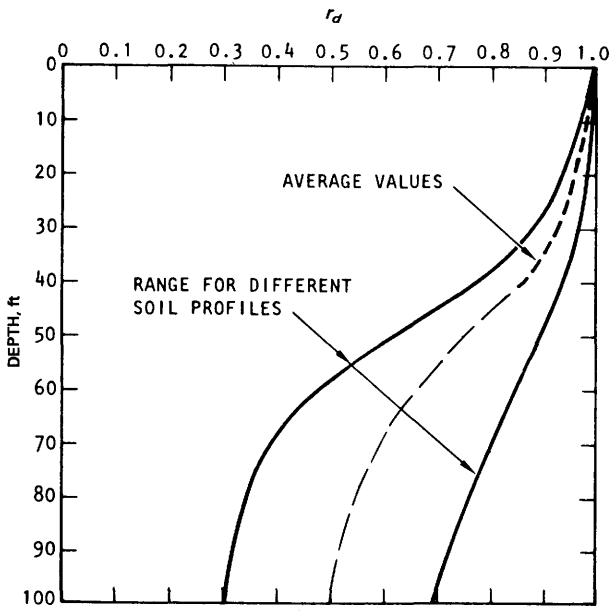

Figure 4. Range of r_d values (stress-reduction coefficients) for different sedimentary materials (modified from Seed and Idriss, 1982, fig. 40). Short dashes represent average values suggested by Seed and Idriss; long dashes represent our extrapolation of that average curve to deeper subsurface depths. Published with permission of the Earthquake Engineering Research Institute.

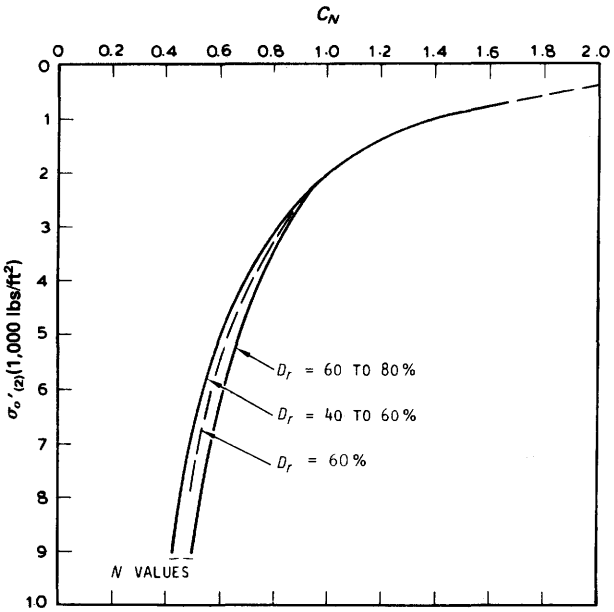

Figure 5. Values used to obtain the correction factor (C_N) applied to field penetration resistance (N) to determine the modified penetration resistance (N_1) applicable for overburden pressure normalized to 2,000 lb/ft ($\sigma_o'_{(2)}$) (modified from Seed and Idriss, 1982, fig. 47). Dashed curves are extrapolations used in our investigation. D_r = relative density. Published with permission of the Earthquake Engineering Research Institute.

tion on susceptibilities for other conditions or for other locations. To apply the local results throughout the San Bernardino Valley region, we used a correlation process whereby susceptible conditions at local sites were linked to particular geologic units and ground-water intervals that then were mapped throughout the region, thereby extending the susceptible conditions from areas where site-specific results are abundant to areas where site-specific results are sparse. This correlation process was accomplished by pooling the individual *FS* results into statistical groups or populations defined by different combinations of geologic unit, ground-water interval, and fault distance. Ratings (high, moderately high, moderate, and low) for each of the scenario earthquakes were then assigned to a given statistical population depending on what percentage of site-specific analyses within that population indicated susceptible conditions. Tables 1 through 7 summarize overall susceptibility ratings for the San Bernardino Valley region.

Of fundamental importance to our statistical-evaluation method is the way we combined the susceptibility ratings for narrowly defined statistical categories to yield overall susceptibility ratings. The overall ratings, identified on the right-hand side of tables 1 through 7, represent statistical groupings whose boundaries—geologic unit, depth to ground water, and distance to causative fault—enclose subordinate groupings whose susceptibility ratings are fairly similar to each other. The overall susceptibility categories treat as statistical groups the following categories: (1) results for sand and silty sediment from both unit Qh_2 and unit Qh_1, (2) results from the 10- to 30-ft and 30- to 50-ft ground-water intervals, and (3) results from fault-distance intervals that are 4 mi wide for the San Andreas and San Jacinto faults and as much as 8 mi wide for the Cucamonga fault.

We combined the narrow categories into broader ones because susceptibility results from the narrower categories were so similar that the categories could not be distinguished as statistically distinct populations. For example, we found that susceptibility results within 1 mi of a causative fault were not much different from results 2 mi from the fault, results 2 mi from a fault were not much different from those 3 mi from the fault, and so forth for any given population of results compared with the immediately adjacent population 1 mi nearer or closer to the fault. Thus, groupings of susceptibility results that were defined by fault-distance boundaries only 1 mi wide were too narrow, and we adopted the broader fault-distance categories incorporated on tables 1–7. A similar situation developed where we attempted to group susceptibility results for sand-sized materials separately from those for silty materials, and results for unit Qh_2 separately from those for unit Qh_1: the differences in susceptibility that separated narrowly defined

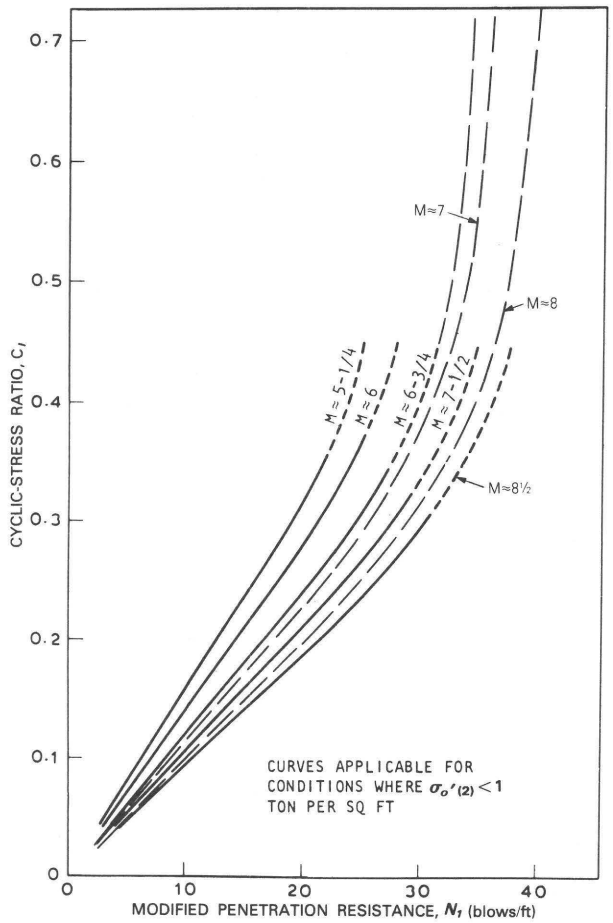

Figure 6. Relation between modified penetration resistance (N_1) and the cyclic-stress ratio (C_l) required to cause liquefaction for specific earthquakes (modified from Seed and Idriss, 1982, fig. 57). Curves having long dashes represent extrapolations used in our investigation. M = earthquake magnitude; $\sigma_o'_{(2)}$ = effective overburden pressure. Published with permission of the Earthquake Engineering Research Institute.

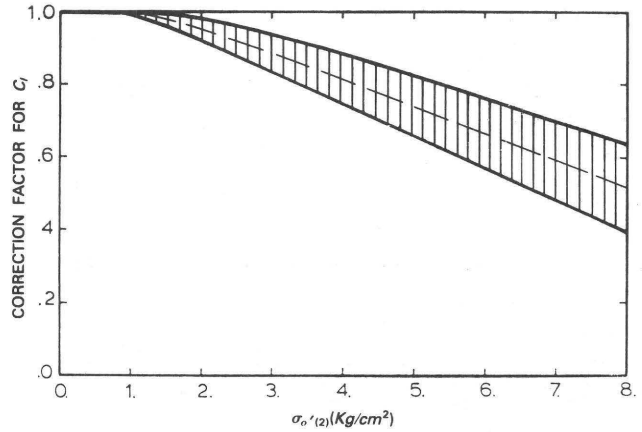

Figure 7. Values used to obtain correction factors that are applied to C_l values obtained by using figure 6 when effective overburden pressure ($\sigma_o'_{(2)}$) is greater than about 3,380 lb/ft² (1.5 kg/cm²). C_l = cyclic-stress ratio causing liquefaction for specific ground-shaking conditions. Unpublished chart provided by H. Bolton Seed and used with permission (oral commun., 1984).

groupings commonly were so minor that the categories best were merged together.[4] Ultimately, even the five individual ground-water categories were best combined into three—partly to better separate statistically distinct populations of susceptibility results and partly to accommodate prevailing opinion that liquefaction susceptibility can be evaluated effectively for the intervals 0 to 10 ft, 10 to 30 ft, and 30 to 50 ft subsurface.

The overall susceptibility categories for the San Bernardino Valley region have the following boundaries:

Fault-distance intervals.—0 to 4 mi, 4 to 8 mi, 8 to 15 mi, and greater than 15 mi.

Ground-water intervals.—0 to 10 ft, 10 to 30 ft, and 30 to 50 ft subsurface.

Geologic unit and sediment type.—Sandy and silty materials from units Qh_2 and Qh_1 were grouped together and separated from sediment in unit Qp.

Susceptibility Ratings

For each statistical cluster of *FS* values, the group susceptibility to liquefaction was assigned by determining the percentage of *FS* values that are less than or equal to 1.0 (where *FS* values less than or equal to 1.0 are susceptible). Susceptibility ratings are defined by the following classes:

High (H): 80 percent or more of the *FS* values are less than or equal to 1.0.

Moderately High (MH): Between 60 and 80 percent of the *FS* values are less than or equal to 1.0.

Moderate (M): Between 30 and 60 percent of the *FS* values are less than or equal to 1.0.

Low (L): Less than 30 percent of the *FS* values are less than or equal to 1.0.

Both single ratings (for example, High) and compound ratings (for example, Moderately High to Moderate) are used. Single ratings apply to the entire subsurface interval under consideration. Compound ratings are applied to the 10- to 30-ft and 30- to 50-ft ground-water intervals and indicate that the overall rating for these subsurface intervals varies with depth. For these 20-ft intervals, the first part of the compound rating applies to the shallower

[4] Individual *FS* values were grouped according to the geologic unit that occurs at the surface where the site is located (units Qh_1, Qh_2, and Qp). Because we had no means of consistently determining how far into the subsurface the surface unit extended before it passed downward into an older unit, in most cases we assumed that the surface unit extended for the entire interval down to 50 ft subsurface.

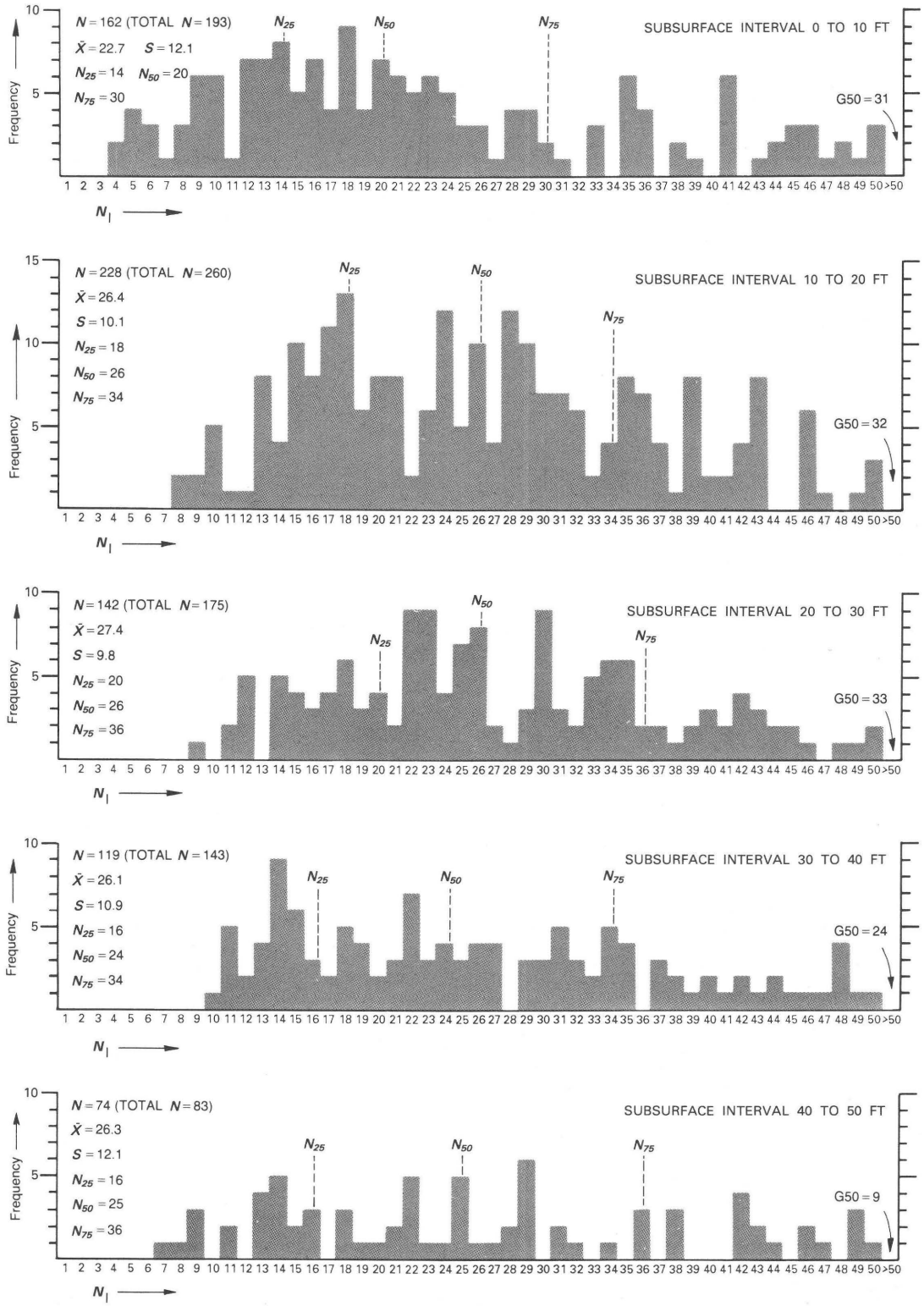

Figure 8. Frequency distribution of modified penetration values (N_1) determined for this investigation; data are classified by 10-ft stratigraphic intervals (0 to 10 ft, 10 to 20 ft, and so forth). Note that N_1 values greater than 50 are grouped within a single frequency class; the number of values within this class is shown as G50. Statistical parameters (mean, $\overline{X}$; standard deviation, s; quartiles, N_{25}, N_{50}, N_{75}) are calculated for N_1 values between 1 and 50 and do not include values greater than 50.

10-ft interval, while the second part of the rating applies to the deeper interval.

Compilation of Liquefaction Susceptibility Maps

When the susceptibility evaluation of *FS* groupings was completed, we prepared maps that show the areal distribution of the four susceptibility ratings (H, MH, M, L). By combining threshold distances from the San Andreas, San Jacinto, and Cucamonga faults with geologic and depth-to-ground-water information, the maps include all of the geotechnical information necessary for identifying the factors that define the statistical groupings. The boundaries between areas having different susceptibility ratings can correspond with any of the criteria used to define the *FS* groupings (that is, depth to ground water, geologic-unit boundary, or fault distance), although depth to ground water generally determines the pattern of susceptibility zones. Three different susceptibility maps were prepared, each dealing with liquefaction of sand for the specified scenario earthquake: an M_s=8.0 earthquake on the San Andreas fault (pl. 3), an M_s=7.0 earthquake on the San Jacinto fault (pl. 4), and an M_s=6.75 earthquake on the Cucamonga fault (pl. 5).

As delineated on plates 3–5, the boundaries between susceptibility zones appear to be located with a high degree of accuracy and precision. This is because the susceptibility-zone boundaries coincide with boundaries between geologic or hydrologic features (ground-water depths, fault distances, and geologic units) that themselves are sharply defined. Some zonal boundaries actually are abrupt, such as the sharp transition from H to L susceptibility that occurs at contacts between loose Holocene deposits and firm Pleistocene deposits. However, the susceptibility-zone boundaries in most cases are gradational because liquefaction susceptibility gradually decreases with increasing depth to ground water, increasing distance away from the causative fault, and increasing geologic age of materials. Susceptibility zones on plates 3–5 ideally would grade from high (where ground water is shallowest, fault distance closest, and geologic age youngest) to low (where ground water is deepest, fault distance greatest, and geologic age oldest). However, such refinements are not possible because of the limited geotechnical data base that is available for this study.

RESULTS

San Andreas Fault

The strong ground-shaking conditions generated by an M_s=8.0 earthquake on the San Andreas fault (pl. 3) yield elevated liquefaction susceptibilities wherever ground water is shallow. Within 0 to 4 mi of the fault, the overall susceptibility of Holocene and latest Pleistocene sands and silty sands is H, even where ground water is as deep as 30 to 50 ft subsurface (table 1). The few silty-sand samples (N=42) have lower susceptibilities (MH to L), but the numerical abundance (N=137) of susceptible sand samples pulls the overall susceptibility rating up to H even at deeper ground-water levels. The elevated susceptibilities at depth can be attributed to the strong ground shaking that is likely to be encountered within 0 to 4 mi of an M_s=8.0 earthquake on the San Andreas fault. There, peak horizontal bedrock accelerations could range between 0.6 and 0.7 *g* (Seed and Idriss, 1982, fig. 17; see our fig. 2) or even higher if accelerations generated by a M_s=8.0 shock were to exceed the 0.7- to 0.9-*g* accelerations predicted by Boore and Joyner (1982, fig. 13) for a smaller M=7.5 earthquake.

For areas 4 to 8 mi from the San Andreas fault, peak horizontal bedrock accelerations may range between 0.45 and 0.6 *g* (Seed and Idriss, 1982, fig. 17; see fig. 2 of this report); Boore and Joyner (1982) presumably would assign even higher accelerations. Here, overall susceptibilities remain H where ground water is shallower than 10 ft subsurface but decline to M where ground water is deeper (table 2). Silty samples (N=266) have lower susceptibilities at the deeper subsurface levels, especially in unit Qh_1 where L susceptibility occurs at ground-water levels deeper than 30 ft subsurface. Again, however, the overall susceptibilities are influenced by the numerical abundance (N=481) of susceptible sand samples.

San Jacinto Fault

The distribution of susceptibilities accompanying moderately strong to strong ground shaking generated by an M_s=7.0 earthquake on the San Jacinto fault (pl. 4) depends on fault distance and ground-water conditions. Elevated susceptibilities (H, MH) occur within 0 to 4 mi of the fault wherever ground water is shallower than 20 ft (table 3) and within 4 to 8 mi of the fault wherever ground water is shallower than 10 ft (table 4). At these fault-distance intervals, peak horizontal bedrock accelerations could range between 0.55 and 0.7 *g* (0 to 4 mi) and between 0.4 and 0.55 *g* (4 to 8 mi) (Seed and Idriss, 1982, fig. 17; see fig. 2 of this report. Boore and Joyner, 1982, fig. 13, indicate a similar range of acceleration values). Despite these strong shaking conditions, overall susceptibilities decline to M within 0 to 4 mi from the fault wherever ground water is deeper than 20 ft subsurface (table 3) and decline to M and L within 4 to 8 mi from the fault where ground water is deeper than 30 ft subsurface (table 4). In general, the silty samples (N=277+32=309) appear to be less susceptible than the sand samples (N=536+94=630), especially at ground-water levels below 30 ft subsurface.

Table 1. Susceptibility ratings for various combinations of geologic unit, sediment type, and ground-water interval for an M_s=8.0 earthquake on the San Andreas fault (fault-distance interval = 0 to 4 mi)

[M_S, surface-wave magnitude; Qh_2, uppermost Holocene sedimentary materials; Qh_1, Holocene and uppermost Pleistocene sedimentary materials; L, low susceptibility; M, moderate susceptibility; MH, high susceptibility; H, high susceptibility; N, number of standard penetration test samples; N_1, modified penetration resistance]

	Qh_2			Qh_1			Qh_2 + Qh_1			
Ground-water interval (ft)	Sand	Silt	Sand + silt	Sand	Silt	Sand + silt	Sand	Silt	Sand + silt	Overall susceptibility rating
0 to 10	100:0 **H** N=16	91:9 **H** N=11	96:4 **H** N=27 59:41	100:0 **H** N=1	100:0 **H** N=2	100:0 **H** N=3 33:67	100:0 94:6 **H** N=17	92:8 85:15 **H** N=13	97:3 **H** N=30 57:43	**H**
10 to 20	100:0 **H** N=26	50:50 **M** N=16	81:19 **H** N=42 62:38	100:0 **H** N=3	50:50 **M** N=2	80:20 **H** N=5 60:40	100:00 90:10 **H** N=29	50:50 89:11 **M** N=18	81:19 **H** N=47 62:38	**H**
20 to 30	89:11 **H** N=28	60:40 **MH** N=5	85:15 **H** N=33 85:15	75:25 **MH–M** N=4	0:100 **L** N=1	60:40 **MH** N=5 80:20	88:12 88:12 **H** N=32	50:50 83:17 **H** N=6	82:18 **H** N=38 84:16	
30 to 40	87:13 **H** N=30	100:0 **H** N=2	88:12 **H** N=32 94:6	100:0 **H** N=1	0:100 **L** N=1	50:50 **M** N=2 50:50	87:13 97:3 **H** N=31	67:33 67:33 **MH** N=3	85:15 **H** N=34 91:9	**H**
40 to 50	96:4 **H** N=28	50:50 **M** N=2	93:7 **H** N=30 93:7				96:4 100:0 **H** N=28	50:50 100:0 **M** N=2	93:7 **H** N=30 93:7	
Total N_1 values	128	36	164	9	6	15	137	42	179	
	477			15			179			

Table 2. Susceptibility ratings for various combinations of geologic unit, sediment type, and ground-water interval for an M_s=8.0 earthquake on the San Andreas fault (fault-distance interval = 4 to 8 mi)

[M_S, surface-wave magnitude; Qh_2, uppermost Holocene sedimentary materials; Qh_1, Holocene and uppermost Pleistocene sedimentary materials; L, low susceptibility; M, moderate susceptibility; MH, moderately high susceptibility; H, high susceptibility; N, number of standard penetration test samples; N_1, modified penetration resistance]

	Qh_2			Qh_1			Qh_2 + Qh_1			
Ground-water interval (ft)	Sand	Silt	Sand + silt	Sand	Silt	Sand + silt	Sand	Silt	Sand + silt	Overall susceptibility rating
0 to 10	94:6 **H** N=34	90:10 **H** N=50	92:8 **H** N=84 40:60	92:8 **H** N=73	76:24 **MH** N=58	85:15 **H** N=131 56:44	93:7 36:68 **H** N=107	82:18 46:54 **H** N=108	87:13 **H** N=215 50:50	**H**
10 to 20	67:33 **H** N=79	76:24 **M** N=38	70:30 **H** N=117 68:32	68:32 **H** N=82	58:42 **M** N=38	65:35 **H** N=120 68:32	68:32 49:51 **H** N=161	67:33 50:50 **M** N=76	68:32 **H** N=237 68:32	**MH–M**
20 to 30	41:59 **M** N=58	54:46 **M** N=28	45:55 **M** N=86 67:33	66:34 **MH** N=35	18:82 **L** N=17	50:50 **M** N=52 67:33	51:49 62:38 **M** N=93	40:60 62:38 **M** N=45	47:53 **M** N=138 67:33	
30 to 40	46:54 **M** N=57	48:52 **M** N=21	46:54 **M** N=78 73:27	67:33 **MH** N=21	14:86 **L** N=7	54:46 **M** N=28 75:25	51:49 73:27 **M** N=78	39:61 75:25 **M** N=28	48:52 **M** N=106 74:26	**M**
40 to 50	44:56 **M** N=27	0:100 **L** N=8	34:66 **M** N=35 77:23	53:47 **M** N=15	0:100 **L** N=1	50:50 **M** N=16 94:6	48:52 64:36 **M** N=42	0:100 89:11 **L** N=9	39:61 **M** N=51 82:18	
Total N_1 values	255 400	145	400	226 347	121	347	481 747	266	747	

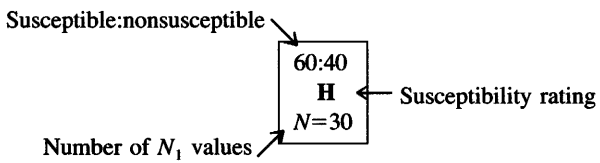

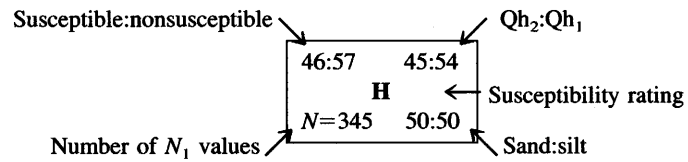

Table 3. Susceptibility ratings for various combinations of geologic unit, sediment type, and ground-water interval for an M_s=7.0 earthquake on the San Jacinto fault (fault-distance interval = 0 to 4 mi)

[M_s, surface-wave magnitude; Qh_2, uppermost Holocene sedimentary materials; Qh_1, Holocene and uppermost Pleistocene sedimentary materials; L, low susceptibility; M, moderate susceptibility; MH, moderately high susceptibility; H, high susceptibility; N, number of standard penetration test samples; N_1, modified penetration resistance]

	Qh_2			Qh_1			Qh_2 + Qh_1			
Ground-water interval (ft)	Sand	Silt	Sand + silt	Sand	Silt	Sand + silt	Sand	Silt	Sand + silt	Overall susceptibility rating
0 to 10	96:4 **H** N=44	72:28 **MH** N=57	82:18 **H** N=101 44:56	94:6 **H** N=65	69:31 **MH** N=58	82:18 **H** N=123 53:47	95:5 40:60 **H** N=109	70:30 50:50 **MH** N=115	82:18 **H** N=224 49:51	**H**
10 to 20	70:30 **MH** N=91	73:27 **MH** N=44	71:29 **MH** N=135 67:33	61:39 **MH** N=77	58:42 **M** N=38	60:40 **MH** N=115 67:33	66:34 54:46 **MH** N=168	66:34 54:46 **MH** N=82	66:34 **MH** N=250 67:33	**MH–M**
20 to 30	56:44 **M** N=71	65:35 **MH** N=23	59:41 **M** N=94 76:24	66:34 **MH** N=35	25:75 **L** N=16	53:47 **M** N=51 69:31	59:41 67:33 **M** N=106	49:51 59:41 **M** N=39	57:43 **M** N=145 73:27	
30 to 40	55:45 **M** N=71	50:50 **M** N=20	54:46 **M** N=91 78:22	62:38 **MH** N=21	20:80 **L** N=10	48:52 **M** N=31 68:32	57:43 77:23 **M** N=92	40:60 67:33 **M** N=30	52:48 **M** N=122 75:25	**M**
40 to 50	59:41 **M** N=46	10:90 **L** N=10	50:50 **M** N=56 82:18	53:47 **M** N=15	0:100 **L** N=1	50:50 **M** N=16 94:6	57:43 75:25 **M** N=61	9:91 91:9 **L** N=11	50:50 **M** N=72 85:15	
Total N_1 values	323	154	477	213	123	336	536	277	813	
	477			336			813			

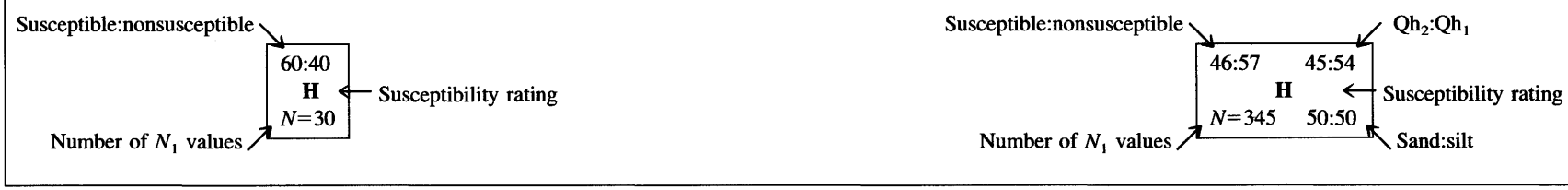

Table 4. Susceptibility ratings for various combinations of geologic unit, sediment type, and ground-water interval for an M_s=7.0 earthquake on the San Jacinto fault (fault-distance interval = 4 to 8 mi)

[M_s, surface-wave magnitude; Qh_2, uppermost Holocene sedimentary materials; Qh_1, Holocene and uppermost Pleistocene sedimentary materials; L, low susceptibility; M, moderate susceptibility; MH, moderately high susceptibility; H, high susceptibility; *N*, number of standard penetration test samples; N_1, modified penetration resistance]

	Qh_2			Qh_1			Qh_2 + Qh_1			
Ground-water interval (ft)	Sand	Silt	Sand + silt	Sand	Silt	Sand + silt	Sand	Silt	Sand + silt	Overall susceptibility rating
0 to 10	100:0 **H** *N*=10	86:14 **H** *N*=7	94:6 **H** *N*=17 59:41	100:0 **H** *N*=7	100:0 **H** *N*=5	100:0 **H** *N*=12 58:42	100:0 59:41 **H** *N*=17	92:8 58:42 **H** *N*=12	97:3 **H** *N*=29 59:41	**H**
10 to 20	56:44 **M** *N*=16	36:64 **M** *N*=11	48:52 **M** *N*=27 59:41	78:22 **MH** *N*=9	0:100 **L** *N*=2	64:36 **MH** *N*=11 82:18	64:36 64:36 **MH** *N*=25	31.69 85:15 **M** *N*=13	53:47 **M** *N*=38 66:34	**M**
20 to 30	63:37 **MH** *N*=16	50:50 **M** *N*=4	60:40 **MH** *N*=20 80:20	60:40 **MH** *N*=5	0:100 **L** *N*=1	50:50 **M** *N*=6 83:17	62:38 76:24 **MH** *N*=21	40:60 80:20 **M** *N*=5	58:42 **M** *N*=26 81:19	
30 to 40	87:13 **H** *N*=15	0:100 **L** *N*=1	81:19 **H** *N*=16 94:6	33:67 **M** *N*=3	 *N*=0	33:67 **M** *N*=3 100:0	78:22 83:17 **MH** *N*=18	0:100 100:0 **L** *N*=1	74:26 **MH** *N*=19 95:5	**M–L**
40 to 50	69:31 **MH** *N*=13	0:100 **L** *N*=1	64:36 **MH** *N*=14 93:7	 *N*=0	 *N*=0	 *N*=0	69:31 100:0 **MH** *N*=13	0:100 100:0 **L** *N*=1	64:36 **MH** *N*=14 93:7	
Total N_1 values	70	24	94	24	8	32	94	32	126	
	94			32			126			

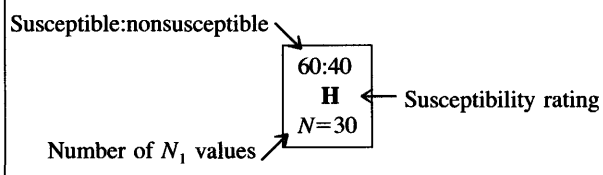

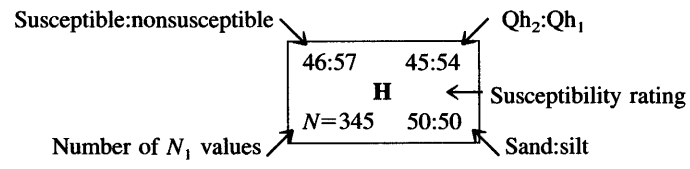

Cucamonga Fault

Elevated susceptibilities accompanying an M_s=6.75 earthquake on the Cucamonga fault (pl. 5) are not so widespread as those for larger earthquakes on the San Andreas and San Jacinto faults. Within 0 to 4 mi of the fault, H to MH susceptibilities probably occur where ground water is shallow (pl. 5), but penetration data from this fault-distance interval were not available for our investigation. Susceptibility ratings here are inferred based on their comparison with susceptibility results from equivalent ground-water intervals at greater distances from the fault. High or MH susceptibility occurs wherever ground water is shallower than 10 ft at all distances between 4 and 15 mi from the fault, but at all these fault distances susceptibility declines to M and L where ground water is deeper than 10 ft (tables 5–7).

Discussion

The shape and size of the susceptibility zones largely are controlled by depth to ground water and distance to the causative fault, although the age and type of sediment also influence its susceptibility. The main zones of elevated susceptibility accompanying earthquakes on the San Andreas, San Jacinto, and Cucamonga faults are associated with shallow ground-water zones that occur beneath the flood plains of Cajon Creek, Warm Creek, and the Santa Ana River (pls. 3–5). These areas are underlain by recently deposited Holocene sediments (unit Qh_2) that would be expected to have lower penetration resistance and higher susceptibilities than older sediments (unit Qh_1). However, even the older Holocene and latest Pleistocene sediments have elevated susceptibilities comparable to those in the younger deposits (tables 1–7), which accounts for zones of H and MH susceptibility that extend laterally away from the active flood plains and into adjacent areas underlain by older deposits. Additional areas of elevated susceptibility are represented by isolated zones along the base of the San Bernardino Mountains that occur downstream from the mouths of canyons.

The influence of fault distance and earthquake magnitude on regional susceptibility patterns can be seen in the way that liquefaction susceptibility decreases as distance to the causative faults increases and as earthquake magnitude decreases. For example, a comparison of regional susceptibility patterns for the three scenario earthquakes (pls. 3–5) shows that, all other factors being equal, susceptibilities are higher and more widespread for the larger earthquakes than for the smaller and are highest close to the causative faults but gradually diminish with increasing distance. These relations are not surprising and in fact illustrate the interdependence between liquefaction susceptibility and ground-shaking strength as measured by peak acceleration (A_{max}): larger earthquakes generate larger A_{max} values and longer durations of ground shaking, which lead to larger values for C_d and lower values for FS (that is, higher susceptibility).

Because older geologic units in the study area tend to yield higher values for N_1 that result in higher values for C_l, the age of the geologic unit occurring at the ground surface also influences susceptibility to liquefaction. For otherwise similar conditions, susceptibility generally is greatest in very young Holocene deposits, slightly less in older Holocene deposits, and least in Pleistocene deposits. These differences in susceptibility influence the susceptibility maps accordingly.

Because they largely are based on ground-water patterns, the susceptibility patterns portrayed on plates 3–5 should not be viewed as permanent features. The boundaries between susceptibility zones will shift geographically as ground-water conditions change. For example, if ground-water reservoirs become depleted because of decreased natural and artificial recharge or because of dewatering measures, water tables would fall and the zones of elevated susceptibilities would decrease in geographic extent.

EVALUATION OF RESULTS

The results of this investigation can be critiqued from two points of view: (1) our study does not incorporate refined geotechnical procedures recently published by Seed and others (1985) and (2) our seismic-risk analysis incorporates ground-shaking conditions considerably stronger than those incorporated by probabilistic analyses that model ground response for 50- or 100-yr return periods. In this section we address concerns raised by these two points of view.

Application of Up-to-date Susceptibility Curves

Seed and others (1985) introduced revised susceptibility curves that correlate modified penetration resistance (N_1) with the cyclic-stress ratio (C_l) required for liquefaction. For a given N_1 value, the new curves (fig. 9) will indicate greater cyclic strength (resistance to liquefaction) than indicated by the older curves of Seed and Idriss (1982). Of concern here is the disparity between C_l values obtained using the old and new curves and the potential impact this disparity will have on susceptibility results we report for the San Bernardino Valley region.

To address this concern, we conducted a pilot study in which the penetration data collected by the U.S. Geological Survey (Carson and others, 1986) were reanalyzed by using the new susceptibility curves. Table 8 presents the

Table 5. Susceptibility ratings for various combinations of geologic unit, sediment type, and ground-water interval for an M_s=6.75 earthquake on the Cucamonga fault (fault-distance interval = 4 to 8 mi)

[M_s, surface-wave magnitude; Qh_2, uppermost Holocene sedimentary materials; Qh_1, Holocene and uppermost Pleistocene sedimentary materials; L, low susceptibility; M, moderate susceptibility; MH, moderately high susceptibility; H, high susceptibility; N, number of standard penetration test samples; N_1, modified penetration resistance]

	Qh_2			Qh_1			Qh_2 + Qh_1			
Ground-water interval (ft)	Sand	Silt	Sand + silt	Sand	Silt	Sand + silt	Sand	Silt	Sand + silt	Overall susceptibility rating
0 to 10	100:0 **H** N=1	 N=0	100:0 **H** N=1 100:0	100:0 **H** N=4	 N=0	100:0 **H** N=4 100:0	100:0 20:80 **H** N=5	 N=0	100:0 **H** N=5 100:0	**H**
10 to 20	 N=0	0:100 **L** N=1	0:100 **L** N=1 0:100	0:100 **L** N=2	0:100 **L** N=1	0:100 **L** N=3 67:33	0:100 0:100 **L** N=2	0:100 50:50 **L** N=2	0:100 **L** N=4 50:50	**M–L**
20 to 30	 N=0	100:0 **H** N=1	100:0 **H** N=1 0:100	0:100 **L** N=1	 N=0	0:100 **L** N=1 100:0	0:100 0:100 **L** N=1	100:0 100:0 **H** N=1	50:50 **M** N=2 50:50	
30 to 40	25:75 **L** N=4	100:0 **H** N=1	40:60 **M** N=5 80:20	0:100 **L** N=1	 N=0	0:100 **L** N=1 100:0	20:80 80:20 **L** N=5	100:0 100:0 **H** N=1	33:67 **M** N=6 83:17	**M–L**
40 to 50	50:50 **M** N=4	 N=0	50:50 **M** N=4 100:0	 N=0	 N=0	 N=0	50:50 100:0 **M** N=4	 N=0	50:50 **M** N=4 100:0	
Total N_1 values	9	3	12	8	1	9	17	4	21	
	12			9			21			

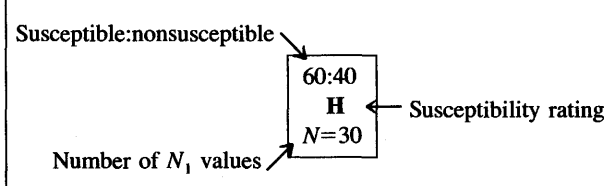

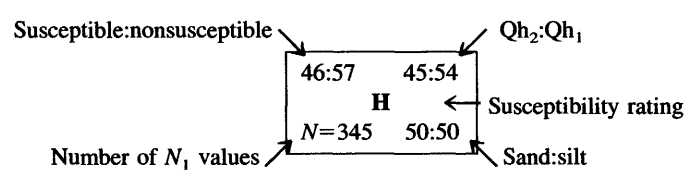

Table 6. Susceptibility ratings for various combinations of geologic unit, sediment type, and ground-water interval for an M_s=6.75 earthquake on the Cucamonga fault (fault-distance interval = 8 to 15 mi)

[M_s, surface-wave magnitude; Qh_2, uppermost Holocene sedimentary materials; Qh_1, Holocene and uppermost Pleistocene sedimentary materials; L, low susceptibility; M, moderate susceptibility; MH, moderately high susceptibility; H, high susceptibility; N, number of standard penetration test samples; N_1, modified penetration resistance]

	Qh_2			Qh_1			Qh_2 + Qh_1			
Ground-water interval (ft)	Sand	Silt	Sand + silt	Sand	Silt	Sand + silt	Sand	Silt	Sand + silt	Overall susceptibility rating
0 to 10	88:12 **H** N=50	68:32 **MH** N=63	77:23 **MH** N=113 44:56	100:0 **H** N=1	53:47 **M** N=40	54:46 **M** N=41 2:98	88:12 98:2 **H** N=51	62:38 61:39 **MH** N=103	71:29 **MH** N=154 33:67	**MH**
10 to 20	33:67 **M** N=112	25:75 **L** N=48	31:69 **M** N=160 70:30	26:74 **L** N=40	9:91 **L** N=34	19:81 **L** N=74 54:46	32:68 74:26 **M** N=152	18:82 59:41 **L** N=82	27:73 **L** N=234 65:35	**L**
20 to 30	17:83 **L** N=84	14:86 **L** N=28	16:84 **L** N=112 75:25	13:87 **L** N=30	0:100 **L** N=16	9:91 **L** N=46 65:35	16:84 74:26 **L** N=114	9:91 64:36 **L** N=44	14:86 **L** N=158 72:28	
30 to 40	26:74 **L** N=87	13:87 **L** N=24	23:77 **L** N=111 78:22	17:83 **L** N=12	0:100 **L** N=10	9:91 **L** N=22 55:45	25:72 88:12 **L** N=99	9:91 71:29 **L** N=34	21:79 **L** N=133 74:26	**L**
40 to 50	35:65 **L** N=51	0:100 **L** N=9	30:70 **L** N=60 85:15	0:100 **L** N=11	0:100 **L** N=1	0:100 **L** N=12 92:8	29:71 82:18 **L** N=62	0:100 90:10 **L** N=10	25:75 **L** N=72 86:14	
Total N_1 values	384	172	556	94	101	195	478	273	751	
	576			195			751			

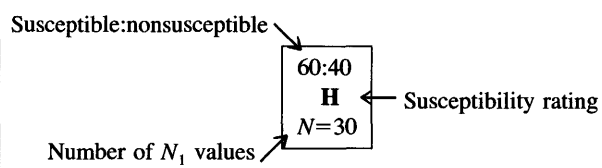

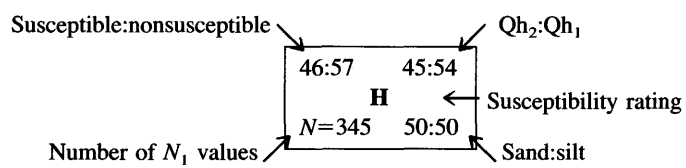

Table 7. Susceptibility ratings for various combinations of geologic unit, sediment type, and ground-water interval for an M_s=6.75 earthquake on the Cucamonga fault (fault-distance interval >15 mi)

[M_s, surface-wave magnitude; Qh_2, uppermost Holocene sedimentary materials; Qh_1, Holocene and uppermost Pleistocene sedimentary materials; L, low susceptibility; M, moderate susceptibility; MH, moderately high susceptibility; H, high susceptibility; N, number of standard penetration test samples; N_1, modified penetration resistance]

Ground-water interval (ft)	Qh_2			Qh_1			Qh_2 + Qh_1			Overall susceptibility rating
	Sand	Silt	Sand + silt	Sand	Silt	Sand + silt	Sand	Silt	Sand + silt	
0 to 10	100:0 **H** N=2	0:100 **L** N=2	50:50 **M** N=4 50:50	77:23 **MH** N=62	59:41 **M** N=22	73:27 **MH** N=84 74:26	78:22 3:97 **MH** N=64	54:56 8:92 **M** N=24	72:28 **MH** N=88 73:27	**MH**
10 to 20	100:0 **L** N=2	0:100 **L** N=4	0:100 **L** N=6 33:67	4:96 **L** N=47	0:100 **L** N=5	4:96 **L** N=52 90:10	4:96 4:96 **L** N=49	0:100 44:56 **L** N=9	3:97 **L** N=58 84:16	**L**
20 to 30	N=0	0:100 **L** N=4	0:100 **L** N=4 0:100	8:92 **L** N=12	0:100 **L** N=1	8:92 **L** N=13 92:8	8:92 0:100 **L** N=12	0:100 80:20 **L** N=5	6:94 **L** N=17 71:29	
30 to 40	N=0	0:100 **L** N=2	0:100 **L** N=2 0:100	0:100 **L** N=8	N=0	0:100 **L** N=8 100:0	0:100 0:100 **L** N=8	0:100 100:0 **L** N=2	0:100 **L** N=10 80:20	**L**
40 to 50	N=0	N=0	N=0	0:100 **L** N=6	N=0	0:100 **L** N=6 100:0	0:100 0:100 **L** N=6	N=0	0:100 **L** N=6 100:0	
Total N_1 values	4	12	16	135	28	163	139	40	179	
	16			163			179			

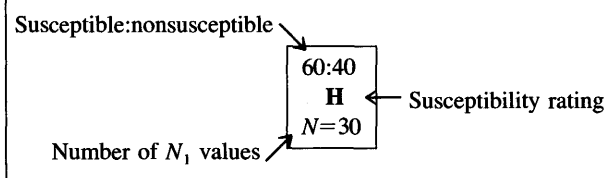

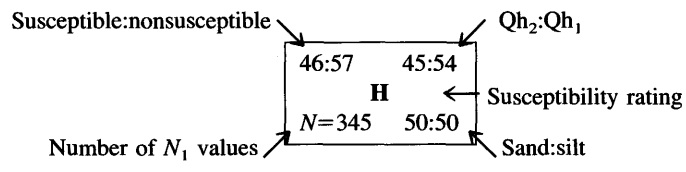

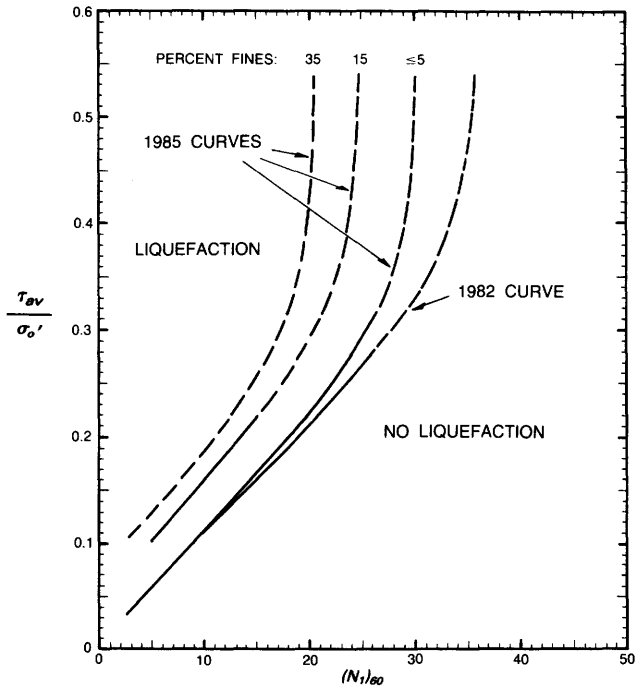

Figure 9. Comparison of liquefaction-susceptibility curves proposed by Seed and Idriss (1982) and Seed and others (1985). Modified from figure 6 of Seed and others (1985) by our addition of curve for M=7.5 earthquake obtained from figure 57 of Seed and Idriss (1982). τ_{av}/σ_o' = cyclic-stress ratio (C_l) causing liquefaction for particular ground-shaking conditions; $(N_1)_{60}$ = modified penetration resistance. Published with permission of the American Society of Civil Engineers.

results of this pilot study together with results obtained by using the 1982 curves.[5]

The pilot study indicates that, for N_1 values smaller than 25, susceptibility determinations obtained by using the 1982 curves would not be changed by application of the 1985 curves—that is, most of the determinations found to be susceptible by using the older curves would remain susceptible by using the new ones, although the specific *FS* value might change somewhat. For N_1 values between 3 and 25, only a single *FS* determination (table 8, DSS–21–11.5′) changed from susceptible to nonsusceptible, and this was for an SPT sample greater than 8 mi from an M_s=6.75 earthquake on the Cucamonga fault. This consistency in results applies both to sands (using the 5 percent curve of Seed and others, 1985) and to silty sands (using their curves for 15 percent fines and 35 percent fines) and can be attributed to the small disparity between C_l values that are derived from the 1982 and 1985 curves: C_l values differ by only 6 to 10 percent for an M_s=8.0 earthquake and by only 4 to 8 percent for M_s=7.0 and 6.75 earthquakes.

At about N_1=25, the slopes of the 1982 and 1985 susceptibility curves begin to diverge significantly (fig. 9), so that with increasing N_1 the new curves yield progressively larger C_l values (greater cyclic strength) than the older curves. For N_1=25 to 27, C_l values for all three scenario earthquakes differ by about 7 to 17 percent—a disparity that in the pilot study did not lead to changes in susceptibility rating for either sandy or silty SPT samples. However, for N_1 between 27 and 30, where C_l values differ by about 17 to 29 percent for an M_s=8.0 earthquake and by about 13 to 22 percent for M_s=7.0 and 6.75 earthquakes, the pilot study indicates that the disparity between cyclic strengths would have a significant impact on the susceptibility evaluations. This can be seen in table 8, where several SPT samples having N_1 values between 27 and 30 yielded *FS* ratios less than 1.0 by using the 1982 curves but greater than 1.0 by using the 1985 curves (DRQ–02–32′, DSS–04–11′, DSS–12–22′, DSS–15–24′, DSS–15–32.5′, and DSS–17–11.5′).

For sediments having N_1 greater than 30, the impact of the new curves on our results might be even greater. Seed and others (1985) indicate that the cyclic strength of sediments having N_1>30 is so great that liquefaction leading to large strains will not occur. This new finding would have a significant effect on our results because, in some cases, we concluded that sedimentary materials having N_1>30 are susceptible.[6] This generally was not the case for SPT samples occurring deeper than 30 ft subsurface, where overburden pressures are great enough to prevent liquefaction for these N_1 ranges. However, at depths less than 30 ft subsurface, some N_1 values between 30 and 35 yielded *FS* ratios less than 1.0, chiefly because of the strong ground-shaking conditions specified in our analysis. Susceptible results would not be obtained by using the new curves that indicate that materials this dense would not liquefy—even if they attained pore pressures equal to 100 percent of the confining pressure. Thus, our determination that some SPTs having N_1=30–35 are susceptible to liquefaction could bias the overall susceptibility ratings for the shallow ground-water intervals.

To test for the degree of bias, we reexamined the data for our entire study to determine how the overall ratings would be affected if all SPT samples having N_1>30 were assigned nonsusceptible factors of safety. For the 10- to

[5] For the pilot study, we assumed that the cable-and-clutch system with downhole safety hammer used by the U.S. Geological Survey (Carson and others, 1986) yields modified penetration-resistance data comparable to $(N_1)_{60}$ of Seed and others (1985). Therefore, we applied no energy-ratio correction to these data. The USGS system actually has a driving efficiency of 68 percent (T.L. Holzer, oral commun., 1986).

[6] The susceptibility curves proposed by Seed and Idriss (1982, fig. 57) indicate that N_1 values between 30 and 35 could be susceptible given the appropriate C_d value. We incorporated this assumption into our analysis and embellished upon it by extending the curves as described in Appendix B.

20-ft and 20- to 30-ft ground-water intervals, we found that the susceptible/nonsusceptible ratios would not change significantly, and thus there would be no change in the overall susceptibility ratings. However, for the 0-to-10 ft ground-water interval, the overall ratings for an M_s=8.0 earthquake on the San Andreas fault (4 to 8 mi) and for an M_s=7.0 earthquake on the San Jacinto fault (0 to 4 mi and 4 to 8 mi) conceivably could be decreased from H to MH (tables 2–4). We are not certain how valid this across-the-board conversion would be, however, because the N_1 values between 30 and 35 mainly are from data sources that could have generated anomalously high penetration resistance. Many of these penetration data were collected using rope-and-pulley energy-delivery systems that, when corrected to $(N_1)_{60}$, will yield values lower than 30, which then would yield susceptible or nonsusceptible ratings depending on site conditions.

Summary.—We conclude that application of the new susceptibility curves proposed by Seed and others (1985) would refine the numerical results of our analysis but would not significantly change the overall susceptibility ratings we assign to sediments in the San Bernardino Valley region. For $N_1 \leq 27$, our pilot study indicates that cyclic-stress ratios (C_l) obtained by using the 1985 curves will be within 6 to 17 percent of those obtained by using the 1982 curves—a disparity that does not lead to significant changes in *FS* ratios because the C_d values called for by the scenario earthquakes specified in our analysis are so large. For N_1 values between 27 and 30, the disparity between C_l values obtained using the 1982 and 1985 curves increases, and many *FS* values no doubt would increase from <1.0 to >1.0, depending on the subsurface depth of the SPT and its distance to the causative earthquake. Those N_1 values between 30 and 35 that we interpret to be susceptible by using the 1982 curves now must be viewed as potentially nonsusceptible. However, many of these penetration data were collected by private drilling companies by using rope-and-pulley systems with a donut hammer and by CalTrans from borings having narrow 2.5-in diameters. Both of these conditions lead to N_1 values that must be corrected to lower values to make them compatible with $(N_1)_{60}$ of Seed and others (1985). Thus, an unknown percentage of N_1 values between 30 and 35 could fall below 30 and might still yield susceptible results. Any N_1 value greater than 36 yielded nonsusceptible results in our investigation.

Ground-Shaking Conditions

Several techniques and strategies for modeling or predicting earthquake ground response are available (see chapters on predicting earthquake ground motion in Ziony, 1985), and the choice of one predictive model or another greatly influences the results of liquefaction-susceptibility evaluations. To calculate the cyclic-stress ratio (C_d) developed throughout the San Bernardino Valley during a specified earthquake, we estimated peak horizontal ground acceleration (A_{max}) by using attenuation curves to determine site response to large scenario earthquakes on the San Andreas, San Jacinto, and Cucamonga faults. These large local earthquakes resulted in large values for A_{max}. This empirical approach contrasts with probabilistic approaches (Idriss, 1985) that evaluate the strength of expected ground shaking by estimating the likelihood (probability) that a specified ground acceleration will be exceeded during a specified time period (for example, 50, 100, or 250 yr).

Probabilistic estimates of A_{max} generally are lower than the A_{max} values we used in our scenario-earthquake approach because most probabilistic estimates model their ground-shaking conditions by using relatively short return periods for earthquakes that are presumed to occur randomly in time. This premise leads to reduced A_{max} values for two reasons: (1) For relatively short return periods, lower rather than higher peak accelerations are likely by comparison with long return periods because patterns of historical seismicity and earthquake occurrence demonstrate that small to moderate earthquakes occur more frequently than large to great earthquakes. For metropolitan areas where noncritical structures are planned, probabilistic seismic-risk analyses commonly are for 50-yr or 100-yr earthquake-return periods. This approach leads to relatively low values for A_{max} because a given 50- or 100-yr period is more likely to witness a smaller earthquake yielding lower peak accelerations than a larger earthquake yielding larger peak accelerations. (2) For probabilistic approaches based on the statistical premise that earthquakes occur randomly in time, the annual probability for earthquake occurrence is the same from year to year given a Poisson (random) probability distribution. If the earthquake-return period modeled by such an analysis is relatively short (50 to 100 yr), the impending occurrence of a large earthquake having a 150- or 250-yr return period is not accommodated by the analysis. As a result, the actual seismic risk may be greater than implied by the annual probability for a 50- to 100-yr event, and the peak-acceleration values (A_{max}) modeled for these events may be underestimated.

Application of empirical or probabilistic analyses to the San Bernardino Valley depends largely on how the seismic potential of the region is interpreted. The valley is flanked by active traces of the San Jacinto and San Andreas faults that are capable of generating large and great earthquakes of M_s=7.0 and 8.0, respectively. Other faults in the region are capable of generating earthquakes in the M_s=6.0 to 7.0 range, including the Cucamonga fault and possibly faults in the Crafton Hills and San Gorgonio Pass fault complexes. Although microseismicity is associated with all of these faults except the San Andreas, none of them is known to have generated a moderate to large earthquake in historic time, and little is known about the repeat time for

Table 8. Parameters used to evaluate liquefaction susceptibility for standard-penetration-test samples collected by susceptibility results (factors of safety) determined by using methods recommended by Seed and Idriss (1982) and Seed

[For convenience in comparing slightly different results obtained by using one method or the other, the factor-of-safety information is emphasized in bold because N_1 too high; N, field penetration resistance; C_N, correction factor applied to N to yield N_1; N_1, modified penetration resistance; expected to develop during a given earthquake; A_{max}, peak horizontal ground acceleration; W_1, interpolated value for water-table depth; σ_o' effective

Borehole	Geologic unit	SPT sampling depth (ft)	SPT N	C_N	Correction for silt	N_1	A_{max}			Ground water depth (W_1) (ft)	σ_o' (lb/ft²)	$C_d=\left(\frac{\tau_{av}}{\sigma_o'}\right)_{dev}$		
							SAF	SJF	CF			SAF	SJF	CF
DRQ–02	Qh_1	8	7	1.5	--	7.8	0.55	0.45	0.25	0	541	0.688	0.563	0.313
DRQ–02	Qh_1	13	19	1.2	--	22.8	.55	.45	.25	10	1,253	.390	.319	.177
DRQ–02	Qh_1	27	27	.9	--	24.3	.55	.45	.25	20	2,573	.397	.325	.181
DRQ–02	Qh_1	32	36	.8	--	28.8	.55	.45	.25	30	3,285	.334	.273	.152
DSN–02	Qh_2	4.5	5	1.9	7.5	14.6	.60	.50	.35	0	304	.750	.625	.438
DSN–03	Qh_2	5	3	1.8	--	4.1	.65	.45	.35	0	338	.813	.563	.438
DSN–03	Qh_2	9.5	11	1.4	7.5	19.1	.65	.45	.35	0	642	.813	.563	.438
DSS–01	Qh_1	6	14	1.7	7.5	25.4	.50	.65	.30	0	405	.625	.813	.375
DSS–01	Qh_1	17.5	23	1.0	--	23	.50	.65	.30	10	1,557	.402	.522	.241
DSS–01	Qh_1	28.5	76	.9	6.5	74.4	.50	.65	.30	20	2,674	.370	.481	.222
DSS–01	Qh_1	33.5	74	.8	--	59.2	.50	.65	.30	30	3,387	.374	.487	.225
DSS–02	Qh_2	25	29	.9	7.5	33.6	.50	.65	.30	20	2,438	.348	.453	.209
DSS–02	Qh_2	28.5	40	.9	4.5	40.5	.50	.65	.30	20	2,674	.370	.481	.222
DSS–02	Qh_2	32	33	.8	7.5	33.9	.50	.65	.30	30	3,285	.304	.395	.182
DSS–02	Qh_2	42	45	.8	--	36	.50	.65	.30	40	4,335	.284	.369	.170
DSS–03	Qh_2	17.5	34	1.1	--	37.4	.50	.65	.35	10	1,557	.402	.522	.281
DSS–03	Qh_2	34	30	.9	--	27	.50	.65	.35	30	2,420	.314	.408	.220
DSS–04	Qh_1	11	17	1.3	7.5	29.6	.50	.65	.35	10	1,118	.343	.446	.240
DSS–04	Qh_1	21	34	1.0	7.5	41.5	.50	.65	.35	20	2,168	.318	.413	.222
DSS–04	Qh_1	31	17	.8	7.5	21.1	.50	.65	.35	30	3,218	.298	.288	.209
DSS–05	Qh_1	12.5	12	1.2	.5	14.9	.55	.55	.30	10	1,219	.383	.383	.209
DSS–05	Qh_1	21.5	24	.9	--	21.6	.55	.55	.30	20	2,201	.354	.354	.193
DSS–05	Qh_1	29.5	33	.8	--	26.4	.55	.55	.30	20	2,742	.391	.391	.213
DSS–05	Qh_1	32	42	.8	5.0	38.6	.55	.55	.30	30	3,285	.334	.334	.182
DSS–06	Qh_2	4	4	2.0	.5	6.5	.45	.65	.30	0	270	.563	.813	.375
DSS–07	Qh_2	9	12	1.5	3.0	16.5	.50	.60	.30	0	608	.625	.750	.375
DSS–07	Qh_2	29.5	11	1.0	--	11	.50	.60	.30	20	2,742	.356	.427	.213
DSS–08	Qh_2	18.5	27	1.1	--	29.7	.50	.60	.30	10	1,624	.410	.492	.246
DSS–09	Qh_2	3.5	12	2.0	--	18	.55	.50	.30	0	237	.688	.625	.375
DSS–09	Qh_2	8.5	13	1.5	6.0	20.6	.55	.50	.30	0	574	.688	.625	.375
DSS–10	Qh_1	5	26	1.8	7.5	42.6	.50	.60	.30	0	338	.625	.750	.375
DSS–10	Qh_1	15	15	1.1	7.5	24	.50	.60	.30	10	1,388	.378	.454	.227
DSS–10	Qh_1	35	23	.8	--	18.4	.50	.60	.30	30	3,488	.319	.382	.191
DSS–11	Qh_2	6	10	1.7	5.0	17.8	.50	.55	.30	0	405	.625	.688	.375
DSS–11	Qh_2	15	20	1.1	6.5	28.5	.50	.55	.30	10	1,388	.378	.416	.227
DSS–11	Qh_2	32	14	.8	--	11.2	.50	.55	.30	30	3,285	.304	.334	.182
DSS–12	Qh_2	3	4	2.0	--	6	.50	.60	.30	0	203	.625	.750	.375
DSS–12	Qh_2	13	22	1.2	--	26.4	.50	.60	.30	10	1,253	.355	.426	.213
DSS–12	Qh_2	19	39	1.0	3.5	42.5	.50	.60	.30	10	1,658	.413	.496	.248
DSS–12	Qh_2	22	28	1.0	2.0	30	.50	.60	.30	20	2,235	.326	.391	.196
DSS–13	Qh_2	7	3	1.6	7.5	11.1	.50	.60	.30	0	473	.625	.750	.375
DSS–13	Qh_2	12	18	1.2	--	21.6	.50	.60	.30	10	1,185	.359	.431	.216
DSS–14	Qh_2	5	6	1.8	7.5	15.6	.50	.60	.30	0	338	.625	.750	.375
DSS–14	Qh_2	21	34	1.0	6.0	40	.50	.60	.30	20	2,168	.318	.381	.191
DSS–15	Qh_1	3	8	2.0	7.5	19.5	.45	.65	.30	0	203	.563	.813	.375
DSS–15	Qh_1	9.5	11	1.4	4.5	16.1	.45	.65	.30	0	642	.563	.813	.375
DSS–15	Qh_1	13	13	1.3	7.5	24.4	.45	.65	.30	10	1,253	.319	.461	.213
DSS–15	Qh_1	24	22	1.0	7.5	29.5	.45	.65	.30	20	2,370	.307	.444	.205

the U.S. Geological Survey (Carson and others, 1986). For comparison, tabulated information includes liquefaction- and others (1985)

text, and individual results flagged with an asterisk where factors of safety greater than 1.0 were obtained by using 1985 methods. N.O., not obtainable

$\left(\frac{\tau_{av}}{\sigma_o'}\right)_{liq}$ = C_l = cyclic-loading characteristics required at a location for liquefaction to occur; $\left(\frac{\tau_{av}}{\sigma_o'}\right)_{dev}$ = C_d = cyclic-loading characteristics

overburden stress; STP, standard penetration test; SAF, San Andreas fault; SJF, San Jacinto fault; CF, Cucamonga fault]

$C_l=\left(\frac{\tau_{av}}{\sigma_o'}\right)_{liq}$ (1982)[1]			Factor of safety (1982) $(C_l / C_d)^2$			$\left(\frac{\tau_{av}}{\sigma_o'}\right)_{liq}$ (1985)[3]			Factor of safety (1985) $(C_l / C_d)^2$			C_l corrected by using curves for fines[4]	
SAF	SJF	CF	SAF	SJF	CF	SAF	SJF	CF	SAF	SJF	CF	15 percent	35 percent
0.072	0.082	0.086	**0.11**	**0.15**	**0.28**	0.084	0.094	0.099	**0.12**	**0.174**	**0.32**	--	--
.219	.255	.266	**.56**	**.80**	**1.50**	.253	.285	.300	**.65**	**.89**	**1.70**	--	--
.240	.281	.293	**.60**	**.86**	**1.62**	.269	.303	.320	**.68**	**.93**	**1.77**	--	--
.286	.337	.356	**.86***	**1.23**	**>2.0**	.388	.437	.461	**1.16***	**1.60**	**>2.0**	--	--
.138	.159	.167	**.18**	**.25**	**.38**	.150	.169	.179	**.20**	**.27**	**.41**	--	--
.040	.046	.049	**.05**	**.08**	**.11**	.043	.048	.051	**.05**	**.09**	**.12**	--	--
.188	.215	.225	**.23**	**.38**	**.51**	.201	.227	.240	**.25**	**.40**	**.55**	--	--
.250	.294	.307	**.40**	**.36**	**.82**	.280	.316	.333	**.45**	**.39**	**.89**	--	0.314
.230	.268	.280	**.57**	**.51**	**1.16**	.247	.278	.294	**.61**	**.53**	**1.23**	--	--
	N.O.		**>2.0**	**>2.0**	**>2.0**		N.O.		**>2.0**	**>2.0**	**>2.0**	--	--
	N.O.		**>2.0**	**>2.0**	**>2.0**		N.O.		**>2.0**	**>2.0**	**>2.0**	--	--
.359*	.448*	.508*	**1.03**	**.99***	**>2.0**		N.O.		**>2.0**	**>2.0**	**>2.0**	N.O.*	N.O.*
.680*	N.O.	N.O.	**1.84**	**>2.0**	**>2.0**		N.O.		**>2.0**	**>2.0**	**>2.0**	N.O.	N.O.
.359*	.448*	.508*	**1.18**	**1.14**	**>2.0**		N.O.		**>2.0**	**>2.0**	**>2.0**	N.O.	N.O.
.405*	.599*	.950*	**1.42**	**1.62**	**>2.0**		N.O.		**>2.0**	**>2.0**	**>2.0**	--	--
.464*	.770*	N.O.	**1.16**	**1.47**	**>2.0**		N.O.		**>2.0**	**>2.0**	**>2.0**	--	--
.259	.305	.321	**.83**	**.75**	**1.46**	.311	.350	.370	**.99**	**.86**	**1.68**	--	--
.299	.355	.376	**.87***	**.80***	**1.57**	.412	.464	.490	**1.2**	**1.04**	**>2.0**	--	N.O.*
	N.O.		**>2.0**	**>2.0**	**>2.0**		N.O.		**>2.0**	**>2.0**	**>2.0**	--	N.O.
.290	.242	.253	**.70**	**.62**	**1.21**	.224	.253	.267	**.75**	**.65**	**1.28**	0.202	.233
.138	.159	.167	**.36**	**.42**	**.80**	.156	.176	.185	**.41**	**.46**	**.89**	.208	--
.209	.242	.253	**.59**	**.68**	**1.31**	.230	.259	.274	**.65**	**.73**	**1.42**	--	--
.261	.307	.322	**.67**	**.78**	**1.50**	.300	.338	.357	**.77**	**.87**	**1.68**	--	--
.510*	N.O.	N.O.	**1.53**	**>2.0**	**>2.0**		N.O.		**>2.0**	**>2.0**	**>2.0**	N.O.	N.O.
.061	.070	.074	**.12**	**.09**	**.20**	.071	.080	.085	**.13**	**.10**	**.23**	.113	.140
.157	.181	.190	**.25**	**.24**	**.51**	.173	.195	.206	**.28**	**.26**	**.55**	.202	--
.109	.127	.133	**.31**	**.30**	**.62**	.116	.131	.138	**.33**	**.31**	**.65**	--	--
.299	.355	.376	**.73**	**.73**	**1.53**	.406	.458	.484	**.99**	**.93**	**1.97**	--	--
.177	.203	.213	**.26**	**.32**	**.57**	.190	.214	.226	**.28**	**.34**	**.60**	--	--
.198	.228	.238	**.29**	**.36**	**.63**	.218	.245	.259	**.32**	**.39**	**.69**	.212	--
	N.O.		**1.6**	**>2.0**	**>2.0**		N.O.		**>2.0**	**>2.0**	**>2.0**	N.O.	--
.240	.281	.293	**.63**	**.62**	**1.29**	.261	.294	.311	**.69**	**.65**	**1.37**	.236	--
.168	.193	.202	**.53**	**.50**	**1.06**	.194	.218	.231	**.61**	**.57**	**1.21**	--	--
.167	.192	.201	**.27**	**.28**	**.54**	.186	.210	.222	**.30**	**.31**	**.59**	.192	.220
.286	.337	.356	**.76**	**.81**	**1.57**	.353	.398	.420	**.93**	**.96**	**1.85**	.335	--
.109	.127	.133	**.36**	**.38**	**.73**	.122	.137	.145	**.40**	**.41**	**.80**	--	--
.061	.070	.074	**.10**	**.09**	**.20**	.067	.075	.079	**.11**	**.10**	**.21**	--	--
.261	.307	.322	**.74**	**.72**	**1.51**	.301	.339	.358	**.85**	**.80**	**1.68**	--	--
	N.O.		**>2.0**	**>2.0**	**>2.0**		N.O.		**>2.0**	**>2.0**	**>2.0**	N.O.	--
.313	.375	.399	**.96***	**.96***	**>2.0**	.442	.498	.526	**1.36***	**1.27***	**>2.0**	--	--
.109	.127	.133	**.17**	**.17**	**.35**	.119	.134	.141	**.19**	**.18**	**.38**	--	.113
.209	.242	.253	**.58**	**.56**	**1.17**	.232	.261	.276	**.65**	**.61**	**1.28**	--	--
.148	.170	.179	**.24**	**.23**	**.48**	.163	.184	.194	**.26**	**.25**	**.52**	--	.163
.680*	N.O.	N.O.	**>2.0**	**>2.0**	**>2.0**		N.O.		**>2.0**	**>2.0**	**>2.0**	N.O.	--
.188	.215	.225	**.33**	**.26**	**.60**	.204	.230	.243	**.36**	**.28**	**.65**	--	.210
.157	.181	.190	**.28**	**.22**	**.51**	.169	.191	.201	**.30**	**.24**	**.54**	.176	.205
.240	.281	.293	**.75**	**.61**	**1.38**	.266	.300	.316	**.83**	**.65**	**1.48**	.240	.290
.299	.355	.376	**.97***	**.80***	**1.84**	.399	.449	.475	**1.30***	**1.01***	**>2.0**	.332*	N.O.*

Table 8. Parameters used to evaluate liquefaction susceptibility for standard-penetration-test samples collected by susceptibility results (factors of safety) determined by using methods recommended by Seed and Idriss (1982) and Seed

[For convenience in comparing slightly different results obtained by using one method or the other, the factor-of-safety information is emphasized in bold because N_1 too high; N, field penetration resistance; C_N, correction factor applied to N to yield N_1; N_1, modified penetration resistance; expected to develop during a given earthquake; A_{max}, peak horizontal ground acceleration; W_1, interpolated value for water-table depth; σ_o' effective

Borehole	Geologic unit	SPT sampling depth (ft)	SPT N	C_N	Correction for silt	N_1	A_{max}			Ground water depth (W_1) (ft)	σ_o' (lb/ft^2)	$C_d=\left(\frac{\tau_{av}}{\sigma_o'}\right)_{dev}$		
							SAF	SJF	CF			SAF	SJF	CF
DSS–15	Qh_1	29	29	0.9	7.5	33.6	0.45	0.65	0.30	20	2,708	0.336	0.485	0.224
DSS–15	Qh_1	32.5	27	.9	6.0	30.3	.45	.65	.30	30	3,319	.276	.398	.184
DSS–16	Qp	18.5	12	1.0	7.5	19.5	.50	.65	.30	10	1,624	.410	.533	.246
DSS–17	Qh_2	6.5	9	1.7	7.5	18.9	.45	.65	.25	0	439	.563	.813	.313
DSS–17	Qh_2	11.5	17	1.3	7.5	29.6	.45	.65	.25	10	1,151	.316	.457	.176
DSS–20	Qh_1	17	12	1.1	--	13.2	.50	.60	.30	10	1,523	.397	.477	.238
DSS–20	Qh_1	20	14	1.0	7.5	21.5	.50	.60	.30	20	2,100	.309	.371	.185
DSS–21	Qh_2	4	9	2.0	4.5	18	.50	.60	.30	0	270	.625	.750	.375
DSS–21	Qh_2	8	6	1.5	6.5	13.3	.50	.60	.30	0	541	.625	.750	.375
DSS–21	Qh_2	11.5	8	1.3	7.5	17.9	.50	.60	.30	10	1,151	.351	.422	.211

[1] C_l values determined by using susceptibility curves of Seed and Idriss (1982). *, value obtained by using extended susceptibility curves.

[2] *, factor-of-safety value determined to be susceptible by using 1982 curves, but nonsusceptible by using 1985 curves; >2.0, factor of safety greater than 2.0.

major seismic events along them. Thus, it might be argued that a random-probability model would be appropriate for evaluating seismic risk and ground response in the San Bernardino Valley and that A_{max} values for earthquakes having a 50-yr repeat time would be appropriate for evaluations of liquefaction susceptibility.

We believe that the scenario-earthquake approach used in this report is an appropriate measure of the seismic potential of the San Bernardino Valley region, given the premise that most local fault segments may be in the later stages of their recurrence cycles. Although little is known about the repeat time or last occurrence of earthquakes on most of these faults, they are not known to have generated significant shocks in the last 140 yr or so, and most workers assign moderate to high probabilities for failure within the next few decades (Raleigh and others, 1982; Lindh, 1983; Sykes and Nishenko, 1984). These studies indicate that although statistical uncertainties are significant—reflecting uncertainty about the earthquake history of important faults in the region over the last 10,000 yr—the seismic potential for the San Bernardino Valley is great and includes an increasing probability of large to very large earthquakes in the range M=7–8 during the next 20 to 30 yr.

A significant seismic potential for the San Bernardino Valley region is in keeping with the overall tectonic framework of the region, which consists of an integrated network of faults that have active seismicity (Green, 1983; Webb and Kanamori, 1985; Nicholson and others, 1986) or that display clear geological evidence for recurrent earthquake activity over the last 10,000 to 100,000 yr (Matti and others, 1982; Weldon and Sieh, 1985; Harden and others, 1986; Morton and Matti, 1987). These faults generate earthquakes not by random chance but according to time- and strain-dependent scenarios that develop as the faults interact systematically in response to the regional budget of crustal strain (Weldon and Humphreys, 1985; Matti and others, 1985). Although a large-magnitude earthquake may not occur until 75 or 100 yr from now—thus legitimizing a seismic-risk analysis that models ground-response parameters on the basis of a 50-yr return period for moderate-magnitude earthquakes—such an earthquake also could occur tomorrow. Prevailing opinions are that it will be sooner rather than later, and this philosophy governed our choice of the scenario-earthquake approach and our selection of large local earthquakes to evaluate liquefaction susceptibilities throughout the San Bernardino Valley region.

The Effect of r_d Uncertainty at Depth

As shown in figure 4, the stress-reduction factor r_d in equation 1 can be determined fairly accurately for depths shallower than about 40 ft subsurface. However, for depths between 40 and 50 ft subsurface, the range in r_d values increases significantly, and it becomes more difficult to select a representative value. As a result, the validity of C_d values calculated for this subsurface depth is difficult to

the U.S. Geological Survey (Carson and others, 1986). For comparison, tabulated information includes liquefaction-and others (1985)—Continued

text, and individual results flagged with an asterisk where factors of safety greater than 1.0 were obtained by using 1985 methods. N.O., not obtainable

$\left(\frac{\tau_{av}}{\sigma_o'}\right)_{liq}$ = C_l = cyclic-loading characteristics required at a location for liquefaction to occur; $\left(\frac{\tau_{av}}{\sigma_o'}\right)_{dev}$ = C_d = cyclic-loading characteristics

overburden stress; STP, standard penetration test; SAF, San Andreas fault; SJF, San Jacinto fault; CF, Cucamonga fault]

$C_1=\left(\frac{\tau_{av}}{\sigma_o'}\right)_{liq\ (1982)}$[1]			Factor of safety (1982) $(C_l / C_d)^2$			$\left(\frac{\tau_{av}}{\sigma_o'}\right)_{liq\ (1985)}$[3]			Factor of safety (1985) $(C_l / C_d)^2$			C_l corrected by using curves for fines[4]	
SAF	SJF	CF	SAF	SJF	CF	SAF	SJF	CF	SAF	SJF	CF	15 percent	35 percent
0.359	0.448*	0.508*	**1.07**	**0.92***	**>2.0**	N.O.	N.O.	N.O.	**>2.0**	**>2.0***	**>2.0**	--	N.O.*
.313	.375	.399	**1.14**	**.94***	**>2.0**	N.O.	N.O.	N.O.	**>2.0**	**>2.0***	**>2.0**	0.453*	--
.188	.215	.225	**.46**	**.40**	**.92**	.204	.230	.243	**.50**	**.43**	**.99**	--	0.210
.177	.203	.213	**.31**	**.25**	**.68**	.200	.225	.237	**.36**	**.28**	**.76**	--	.205
.299	.355	.376	**.95***	**.78***	**>2.0**	.409	.460	.486	**1.29***	**1.01***	**>2.0**	--	N.O.
.129	.148	.156	**.32**	**.31**	**.65**	.141	.158	.167	**.36**	**.33**	**.70**	--	--
.209	.242	.253	**.68**	**.65**	**1.37**	.228	.257	.271	**.74**	**.69**	**1.47**	.196	.228
.177	.203	.213	**.28**	**.27**	**.57**	.190	.214	.226	**.30**	**.29**	**.60**	.198	.232
.129	.148	.156	**.21**	**.20**	**.42**	.141	.158	.167	**.23**	**.21**	**.45**	.120	.147
.167	.192	.210	**.48**	**.46**	**.95***	.190	.214	.226	**.54**	**.51**	**1.07***	--	--

[3] Values obtained by a two-stage procedure: (1) C_l value for a M=7.5 earthquake first was determined from figure 5 of Seed and others (1985); (2) This value then was converted to C_l values for scenario earthquakes of this report by using correction factors obtained from table 4 of Seed and others (1985): C_l for M=8.0 = [(0.95) · (C_l for M=7.5)]; C_l for M=7.0 = [(1.07) · (C_l for M=7.5)]; C_l for M=6.75 = [(1.13) · (C_l for M=7.5)].

[4] C_l values listed here are for a M=7.5 earthquake determined from figure 6 of Seed and others (1985). Equivalent C_l values for M=6.75, 7.0, and 8.0 earthquakes can be derived by using correction factors described in footnote 3. *, value yields nonsusceptible factor-of-safety value, in contrast with susceptible factor-of-safety value obtained by using 1982 susceptibility curves and correction to N_1 for silt.

evaluate, and the credibility of susceptibility determinations derived from the ratio between C_d and C_l is unknown.

Evaluation of Results—Summary

We recognize elevated (H to MH) susceptibility to earthquake-induced liquefaction in the San Bernardino Valley region wherever ground water is shallower than 10 to 20 ft subsurface and locally where ground water is as deep as 30 to 50 ft subsurface. The susceptibility ratings mainly reflect the physical characteristics of surficial sediments in the valley region and their likely response to the ground-shaking conditions specified in our analysis. However, the susceptibility patterns on plates 3–5 may overstate the distribution of elevated susceptibilities, for two reasons: (1) the susceptibility patterns reflect generalizations and assumptions that we consciously employed to achieve our intended goal of identifying on a regional basis all areas that have any significant possibility of experiencing liquefaction and (2) our pilot study shows that, for sediments having N_1 values between 27 and 30, use of 1982-vintage susceptibility curves to determine liquefaction thresholds led to our assigning susceptible *FS* determinations to some (but not all) sediments that actually may not be susceptible. To accommodate this uncertainty in our results, we offer the following evaluations:

(1) We are confident in our conclusion that ground-water saturated sediments in the interval 0 to 10 ft subsurface have H to MH susceptibility to liquefaction. Sands and silty sands having $N_1 \leq 27$ are abundant in this subsurface interval, and loose sediments with N_1 between 9 and 24 are common (fig. 8). Many of these sediment layers probably will liquefy under ground-shaking conditions like those modeled in our study.

(2) We are confident in our conclusion that ground-water saturated sedimentary materials between 10 and 30 ft subsurface have MH to M susceptibility to liquefaction. Sands and silty sands having $N_1 \leq 27$ are common in this interval, although moderately dense to dense sands with $N_1 \geq 27$ also are abundant (fig. 8). Some of these sediments will liquefy under ground-shaking conditions like those modeled in our study.

(3) Between 30 and 50 ft subsurface, the degree of susceptibility for saturated sedimentary materials generally declines to M for earthquakes on the San Jacinto and San Andreas faults, although within 0 to 4 mi of an M_s= 8.0 earthquake on the San Andreas fault we show H susceptibility extending to depths as great as 50 ft subsurface. This evaluation may prove to be valid. On the other hand, subsequent site-specific investigations that incorporate improved procedural methods may identify lower susceptibilities for these depth intervals using the same ground-shaking conditions. Consider-

able opinion exists about the likelihood of liquefaction between 30 and 50 ft subsurface. Resolution of this controversy is beyond the scope and capabilities of our investigation.

POTENTIAL FOR LIQUEFACTION-INDUCED GROUND FAILURE

Although plates 3–5 indicate the distribution of geologic and hydrologic conditions shown by our analysis to have varying degrees of liquefaction susceptibility, the maps are not intended to be liquefaction-hazard maps— that is, they do not portray the potential for liquefaction-induced ground failures. Liquefaction of sedimentary materials in itself does not pose a hazard or risk to structures or life—the hazard is posed by ground failures that can be induced by liquefaction. Ground failures do not always accompany subsurface liquefaction, however, and many areas underlain by susceptible materials may experience no ground failure at all if the physical effects of liquefaction do not propagate to near-surface zones.

The prediction and evaluation of liquefaction-induced ground failures and their attendant risks are state-of-the-art endeavors that require engineering judgments that are beyond the scope and purpose of our investigation. However, the potential for ground failure in the San Bernardino Valley region can be estimated in a general way (1) by comparing the geologic and geomorphic setting of sedimentary materials in the study area with settings in other areas where liquefaction-induced ground failures have occurred and (2) by considering the layering characteristics of the sedimentary fill.

Geomorphic Setting and Ground-Failure Potential

The scale of potential ground failure in the San Bernardino Valley region can be estimated on the basis of average slope conditions. For example, liquefaction-induced ground failures typically are more catastrophic on steeper rather than shallower slopes. Slope gradients throughout most of the San Bernardino Valley region average about 0.5° to 1.0°, although gradients steepen to as much as 4.0° on alluvial-fan surfaces adjacent to the San Bernardino Mountains. According to Tinsley and others (1985, p. 266–267), slopes of 0.5° to 1.0° typically result in lateral spreads, ground oscillation, and differential settlements; more catastrophic flow failures typically occur on slopes steeper than 3°. However, this observation does not minimize the potential hazard created by ground failure on gentle slopes, as such slopes experienced damaging liquefaction-induced ground failures during the 1971 San Fernando earthquake (M_L=6.4; Tinsley and others, 1985, figs. 127 and 128). Thus, low-slope conditions in the San Bernardino Valley give some insight into the scale of ground failure that might occur given the appropriate ground-shaking conditions.

The presence of a locally steepened slope—such as an excavation or near-vertical river bluff, fault scarp, or other steep-sided alluvial landform—can facilitate ground failure by providing a free face that can collapse and allow downslope movement of material occurring upslope from the face. In the San Bernardino Valley, young channel deposits (unit Qh_2) of the Santa Ana River are separated from older higher standing alluvial deposits (unit Qh_1) to the north and south by a river bluff that in some places is rounded and subdued because of natural erosion and urban modification but commonly forms a steep near-vertical free face. Under appropriate ground-water conditions, liquefaction upslope from such a free face could lead to ground failure that would be facilitated if the free face were to fail by landsliding or collapse.

The potential scale of ground failure in the San Bernardino Valley can be estimated from evidence in subsurface excavations and from examination of aerial photographs. Trenches and pits excavated at specific sites in the valley locally reveal sand injections, convolute layering, pillow-and-ball structures, and other evidence of soft-sediment deformation related to liquefaction, but, to our knowledge, no evidence of large-scale deformations has been documented. Long continuous trenches designed specifically to evaluate liquefaction-induced ground failures have not been excavated, however, so the fragmentary evidence from isolated excavations can only hint at the potential style and scale of ground failure.

Our examination of 1931- and 1938-vintage aerial photographs of the San Bernardino Valley did not reveal geomorphic evidence of catastrophic ground failure in the recent past. Although urbanization has obscured many primary landscape features, we suspect that large-scale features such as hummocky ground, lateral-spread crown areas, and local collapse of the river-bluff free face adjacent to the Santa Ana River would be identifiable despite information loss due to urbanization and agriculture.

Depth to Liquefied Layer and Ground-Failure Potential

Ishihara (1985, p. 359–362, figs. 84, 85, and 88) has shown that the thickness of the nonliquefied layer or mantle overlying a liquefied layer influences whether the physical effects of liquefaction will be expressed as ground failure within the overlying mantle (figs. 10, 11). For light ground shaking (A_{max} = 0.2 to 0.25 g), the liquefied layer must be at least as thick as the nonliquefied surface mantle in order for ground failure to occur; moreover, ground failure is not likely to occur if the surface mantle is thicker than about 10 ft (3 m; fig. 11). These tentative results suggest that, for relatively light ground-shaking conditions, liquefaction-induced ground failure probably will not occur if the water

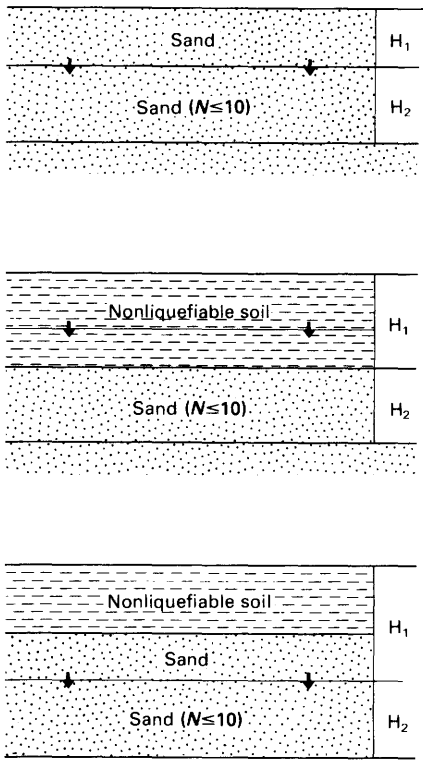

Figure 10. Relations among the water table, a liquefied layer having $N \leq 10$ (H_2), and a nonliquefied surface mantle overlying the water table (H_1) (from Ishihara, 1985, fig. 84). N = field penetration resistance. Published with permission of A.A. Balkema Press.

table is deeper than about 10 ft subsurface or if the liquefied layer is too thin relative to the thickness of the nonliquefied mantle.

For stronger ground-shaking conditions (A_{max} = 0.4 to 0.5 g), liquefaction events fairly deep in the subsurface can yield ground failures, even if the overlying nonliquefied layer is as much as 30 ft thick (9 to 10 m; fig. 11); moreover, the liquefied layer need not be as thick as the nonliquefied surface mantle. These two observations, based on investigations of liquefaction-induced ground failures that accompanied the 1976 M=7.8 earthquake in Tangshan, China, may apply to the San Bernardino Valley region, where ground-shaking conditions resulting from large earthquakes on the San Andreas and San Jacinto faults are likely to be intense (A_{max} = 0.5 to 0.8 g) and where individual liquefied layers typically will be thinner than the overlying nonliquefied layer (discussed in the following section). Results from the large Tangshan earthquake suggest that ground failure in the San Bernardino Valley region may occur even if the liquefaction events are relatively deep seated or occur in relatively thin layers.

Layering Character and Ground-Failure Potential

The general character of sedimentary materials underlying the San Bernardino Valley region may control the type and scale of ground failure. The sediments consist of interlayered materials of different grain sizes, relative densities, and cohesiveness (Carson and others, 1986). At any given location, the layering sequence may include loose liquefiable sands and silty sands, dense nonliquefiable sands and silts, permeable gravel deposits, and firm, impermeable deposits of cohesive clay. Any given layer may be a few inches to several feet thick.

This stratigraphic setting has conflicting implications for liquefaction susceptibility. On the one hand, where susceptible layers are enclosed by impermeable clay layers that do not allow drainage of pore waters and the reduction of pore pressure, the potential for liquefaction of specific sediment layers might be fairly high. On the other hand, individual liquefied layers may be no thicker than a few inches to a few feet, in which case the findings of Ishihara (1985) suggest that ground failure would be unlikely unless the failed layer were within 10 ft of the surface. Under these conditions, the scale and type of ground failure might be less catastrophic than ground failures that might occur if the region were underlain by thick bodies of loose sand and

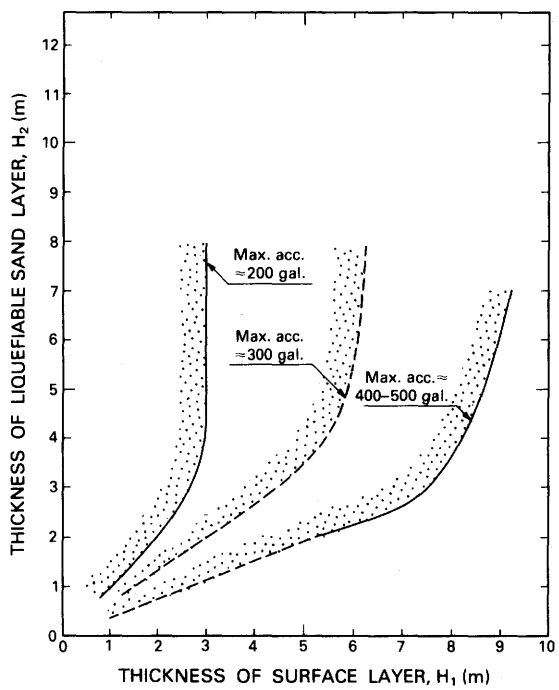

Figure 11. Correlation of ground-failure potential at specific sites with thickness of nonliquefied surface layer, thickness of liquefied layer, and peak ground acceleration (from Ishihara, 1985, fig. 88). gal. = gravitational acceleration in milligal. Published with permission of A.A. Balkema Press.

silty sand that experienced extensive liquefaction. Moreover, if liquefied layers are too thin, the resulting uplift pressure may not be great enough to induce deformation or collapse of the surface mantle (Ishihara, 1985, p. 359). Thus, the scale of liquefaction-induced ground failure in the San Bernardino Valley region may be limited to deformations associated with local failure of one or more individual layers, although the ground-failure potential might be greater if more than one thin layer liquefied, thereby yielding a cumulative impact on the surficial mantle. These speculations illustrate the difficulties inherent in predicting the style and pattern of liquefaction-induced ground failure.

The heterogeneous layering sequence within the sedimentary fill of the San Bernardino Valley region affects the potential for liquefaction-induced ground failure in another way: not all susceptible materials within the sequence have the same potential for inducing ground failures. Up to this point in our discussion, we have referred to sediments that have *FS* ratios <1.0 as liquefiable but have not distinguished between liquefaction events that lead to significant deformations of the sediment layer and those that lead to minor deformations. Relatively loose sand can sustain large deformations (strains) when they liquefy, whereas denser sands sustain relatively minor deformations (cyclic mobility with limited strain potential; Seed, 1979). This distinction is important because the degree of deformation (shear strain) sustained by a sediment mass may influence the potential for ground failure and damage to structures.

Seed and others (1985, fig. 8, p. 144; fig. 12 of this report) indicate that relatively loose sands [$(N_1)_{60}$ between 1 and 20] have high damage potential, moderately dense sands [$(N_1)60$ between 20 and 30] have moderate damage potential, and dense sands [$(N_1)_{60}$ greater than 30] have low damage potential. Surficial deposits of the San Bernardino Valley region include a mix of loose, moderately dense, and dense materials interlayered together (fig. 8). In the 0- to 10-ft interval, this mix seems to be dominated by looser sediments, a trend that weakly continues to 30 ft subsurface (fig. 8); however, the 30- to 40-ft and 40- to 50-ft intervals consist of a more heterogeneous mix in terms of N_1. The heterogenous mixture of sediments having different relative densities makes the prediction of regional ground-failure potential using the criteria of Seed and others (1985, fig. 8) difficult because the sequence, thickness, and lateral extent of sedimentary layers having a particular damage potential vary from site to site.

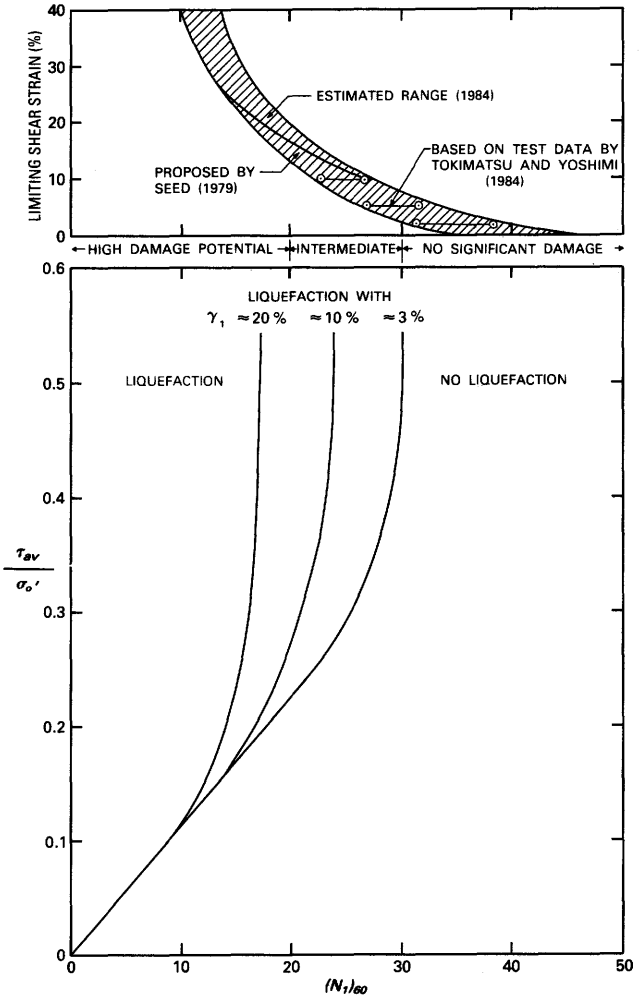

Figure 12. Tentative relation among cyclic-stress ratio, modified penetration resistance $(N_1)_{60}$, and limiting strains for natural deposits of clean sand (modified from Seed and others, 1985, fig. 8). Published with permission of the American Society of Civil Engineers.

Summary of Ground-Failure Implications

Although we assign H to MH susceptibility to parts of the San Bernardino Valley region where ground water is shallow, it is not possible to predict with confidence the degree of hazard posed by liquefaction-induced ground failures. Preliminary evidence leads to the following provisional generalizations: (1) Ground failure is more likely to develop where liquefaction occurs at shallow subsurface levels rather than at deeper levels. Thus, in the San Bernardino Valley region, liquefaction-induced failures are more likely to occur in areas where ground water is shallower than 30 ft subsurface than in areas where ground water is deeper than 30 ft subsurface. (2) Slope conditions for most areas having moderate and greater susceptibility are very low (0.5° to 1.0°), which suggests that potential ground failures will be small-scale lateral spreads and differential settlements. (3) Interlayering of loose sands and silty sands with dense sands and silts and with firm impermeable clay deposits suggests that liquefaction most likely will be confined to specific layers that may be thin. Although ground failures induced by such events can cause significant damage, large-scale catastrophic failures induced by wholescale liquefaction of large volumes of

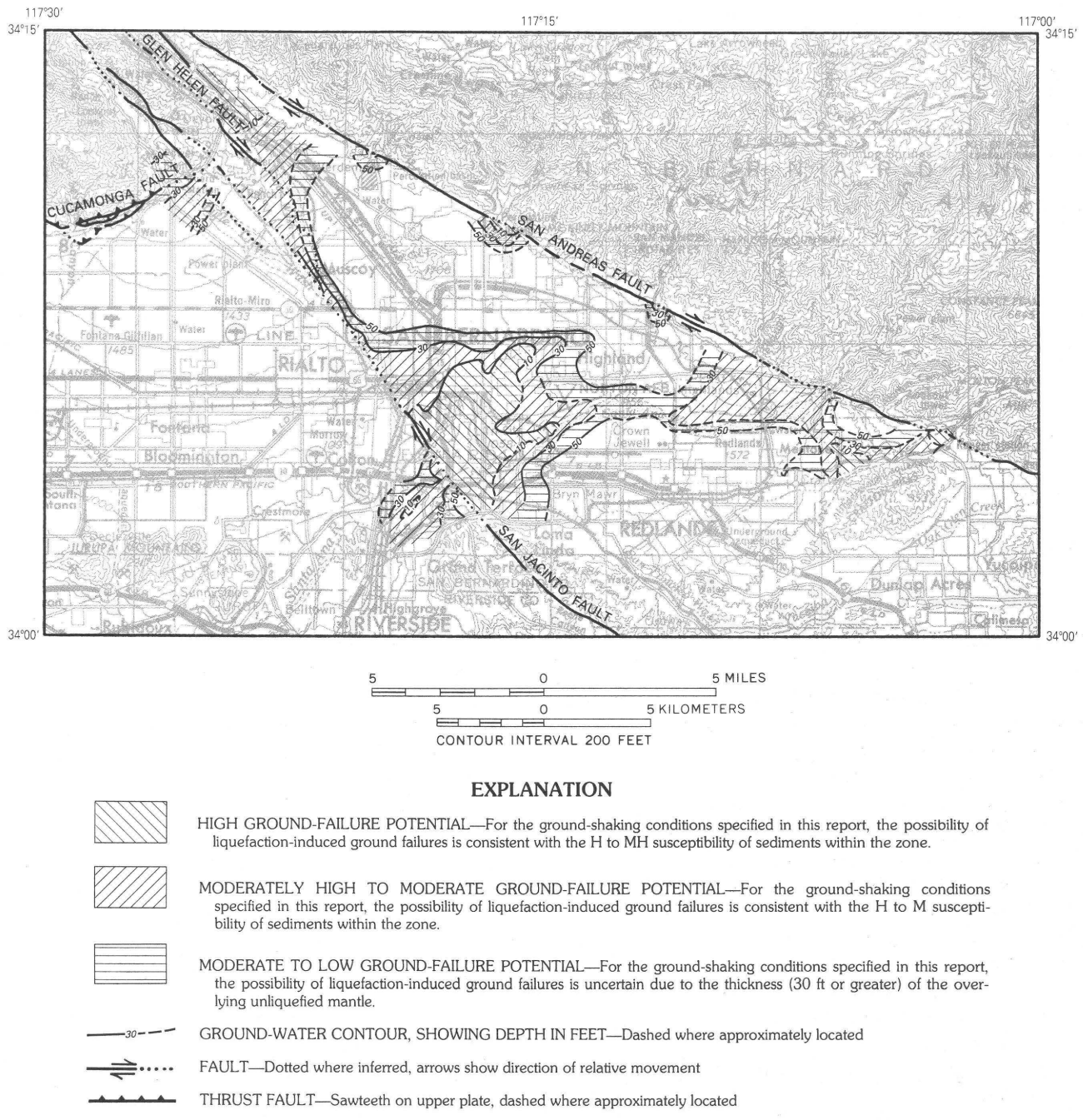

Figure 13. Preliminary estimate of liquefaction-induced ground-failure potential for the San Bernardino Valley and vicinity, southern California. See text for discussion. (**H**, high; **MH**, moderately high; **M**, moderate.)

sand may not be likely. Moreover, the potential for ground failure will depend on how deep and thick the liquefied layer is in relation to the thickness of the nonliquefied surface mantle (Ishihara, 1985) and will depend upon the density of the liquefied layers (Seed and others, 1985) and their abundance within the layering sequence. (4) Large-scale catastrophic ground failures in sediments of the San Bernardino Valley region are unlikely given the heterogeneous nature of the layering types and sequences. Active flood plains of Cajon Creek, Warm Creek, and the Santa Ana River, where relatively thick bodies of loose sand are likely to occur, may be an exception.

Figure 13 is a generalized ground-failure-potential map that is based partly on the susceptibility results of tables 1–7 and partly on what is known about the geomorphic setting and layering character of surficial deposits in the San Bernardino Valley region. The map incorporates the following ground-failure-potential zones:

High.—Areas where ground water is shallower than 10 ft subsurface. The sediments are characterized by an abundance of loose to moderately loose sands and silts having N_1 less than 24 (fig. 8) and by a large percentage of SPT's having susceptibility ratios ≤ 1.0 for all fault distances (tables 1–7). The possibility of ground failure is consistent with the H to MH susceptibility of sediments in the zones.

Moderately High to Moderate.—Areas where ground water is 10 to 30 ft subsurface. The sediments are characterized by mixtures of loose to dense sands and silts. The possibility of ground failure is consistent with the MH to M susceptibility rating of sediments in the zone, but the heterogenous nature of the layering sequence makes the scale and extent of ground failure difficult to evaluate.

Moderate to Low.—Areas where ground water is 30 to 50 ft subsurface. The sediments are characterized by mixtures of loose to dense sands and silty sands, but the thickness of the overlying unliquefied mantle (30 ft or greater) makes the scale and extent of ground failure difficult to evaluate.

RECOMMENDATIONS

On the basis of our regional evaluation of liquefaction susceptibility in the San Bernardino Valley region, we offer the following recommendations for the application of results developed in this report:

(1) In areas having H or MH susceptibility, where the probability of liquefaction is greatest and liquefaction-induced ground failures are possible, special attention is warranted in general land-use planning activities. Site-specific geotechnical studies to assess liquefaction hazards may be advisable.

(2) Where site-specific investigations are required, they should incorporate one of the established methods for evaluating liquefaction susceptibility outlined in scientific papers. The site report should describe all equipment and procedures and should present all geotechnical data utilized in the susceptibility analysis. These stringent requirements would allow the site-specific study to be evaluated by an independent reviewer.

(3) If hazard-mitigation measures are planned on the basis of the regional susceptibility evaluation presented in this report, we recommend that areas of concern be prioritized in the following order: (a) all areas where ground water is shallower than 10 ft subsurface but especially the flood plains of the Santa Ana River and Cajon, Lytle, and Warm Springs Creeks, where young loose sedimentary materials are abundant; (b) areas where we recognize elevated susceptibilities in the interval 10 to 30 ft subsurface; and (c) areas where we recognize elevated susceptibilities in the interval 30 to 50 ft subsurface.

CONCLUSIONS

Our investigation has demonstrated that some sedimentary materials underlying the San Bernardino Valley region are susceptible to earthquake-induced liquefaction. The level of susceptibility and the geographic extent of susceptibility zones depend mainly on two factors: (1) the depth to the ground-water table and (2) the intensity and duration of ground shaking as determined by the magnitude of the earthquake and distance to the causative fault. We used these two factors in combination with penetration-resistance data from various sites throughout the valley to provide a regional zonation of liquefaction susceptibilities accompanying three scenario earthquakes: an M_s=8.0 earthquake on the San Andreas fault, an M_s=7.0 shock on the San Jacinto fault, and an M_s=6.75 earthquake on the Cucamonga fault. Our analysis led to the following conclusions:

(1) Where ground water is shallower than 10 ft subsurface in Holocene and latest Pleistocene sedimentary materials, all three scenario earthquakes are accompanied by H to MH susceptibilities at all fault distances.

(2) Where ground water is between 10 and 30 ft subsurface in Holocene and latest Pleistocene sedimentary materials, liquefaction susceptibilities accompanied by the three scenario earthquakes depend on distance to the causative fault. Susceptibilities remain H within 0 to 4 mi of an M_s=8.0 earthquake on the San Andreas fault but decline to M at greater distance from the fault. Susceptibilities are M within 0 to 8 mi of an M_s=7.0 earthquake on the San Jacinto fault. At all fault distances, an M_s=6.75 earthquake on the Cucamonga Fault is accompanied by L susceptibilities.

(3) Where ground water is between 30 and 50 ft subsurface in Holocene and latest Pleistocene sedimentary materials, susceptibilities for the three scenario earthquakes depend on distance to the causative fault. Susceptibility remains H within 0 to 4 mi of an M_s=8.0 earthquake on the San Andreas fault but declines to M at greater distances from the fault. Susceptibilities are M within 0 to 4 mi of an M_s=7.0 earthquake on the San Jacinto fault but decline to L within 4 to 8 mi of the fault. At all fault distances, an M_s=6.75 earthquake on the Cucamonga fault is accompanied by L susceptibility.

The susceptibility maps can be used in conjunction with what is known about the geomorphic setting and layering characteristics of sedimentary materials underlying the San Bernardino Valley region to estimate where liquefaction-induced ground failures are most and least likely to occur, at least on a regional basis. Where ground water is shallower than 10 ft subsurface, the possibility of ground failure is consistent with the H to MH susceptibility of sediments within this ground-water interval. These areas require special attention during future land-use planning and development, and mitigation of existing hazards may be

advisable. In areas of deeper ground water, where liquefaction susceptibility is M to L, liquefaction-induced ground failures are less likely but cannot be ruled out.

ACKNOWLEDGMENTS

Many people assisted us during this investigation, although they are not responsible for its results or conclusions. John C. Tinsley of the U.S. Geological Survey (USGS) provided valuable technical advice at many different stages of our studies, and A.T.F. Chen and T.L. Holzer of the USGS discussed various aspects of our analytical approach. T. Leslie Youd, formerly of the USGS and now with Brigham Young University, assisted us during the early stages of our investigation and directed us to the study by Ishihara (1985). We benefited from conversations with H. Bolton Seed of the University of California, Berkeley, who discussed with us various aspects of his approach to liquefaction evaluation. Professor Seed graciously allowed us to use unpublished curves to correct C_l values where overburden pressures are excessive (fig. 7). Leslie F. Harder of the California Department of Water Resources provided technical advice pertaining to various aspects of susceptibility evaluation. Building and safety officials from various municipal and county agencies in the San Bernardino Valley region allowed us to examine geotechnical site investigations filed with their offices in compliance with permitting procedures. Larry Lauro, A.T. Roodsari, and G. Davis of the U.S. Army Corps of Engineers, Los Angeles Office, assisted us in obtaining copies of subsurface-boring logs prepared by the Corps in the San Bernardino Valley region. K.A. Miller of the San Bernardino Valley Flood Control District provided us with additional boring logs prepared by the Corps of Engineers for various flood-control measures in the valley region. Joseph F. Stejskal of the City of San Bernardino Municipal Water Department provided us with weekly updates of groundwater levels in the metropolitan San Bernardino area and assisted us during our subsurface-drilling investigations. Sam Shaler of the USGS operated the USGS drilling rig, and Constance K. Throckmorton, Jane Koch, and Michael M. Kelley of the USGS assisted in various aspects of the drilling investigation. Research for this investigation was sponsored by the Regional Hazards Assessment Element of the USGS National Earthquake Hazards Reduction Program.

REFERENCES CITED

Algermissen, S.T., and Perkins, D.M., 1976, A probabilistic estimate of maximum acceleration in rock in the contiguous United States: U.S. Geological Survey Open-File Report 76–416, 45 p.

Allen, C.R., 1968, The tectonic environments of seismically active and inactive areas along the San Andreas fault system, *in* Dickinson, W.R., and Grantz, Arthur, eds., Proceedings of conference on geologic problems of San Andreas fault system: Stanford University Publications in Geological Sciences, v. XI, p. 70–82.

———1981, The modern San Andreas fault, *in* Ernst, W.G., ed., The geotectonic development of California: Englewood Cliffs, New Jersey, Prentice-Hall, Inc., p. 511–534.

Ambraseys, N.N., and Sarma, S., 1969, Liquefaction of soils induced by earthquakes: Bulletin of the Seismological Society of America, v. 59, no. 2, p. 651–664.

American Society of Civil Engineers, 1958, Glossary of terms and definitions in soil mechanics: Journal of the Soil Mechanics and Foundations Division, American Society of Civil Engineers, v. 84, no. SM4, pt. 1, p. 1826–1, 1826–43.

American Society for Testing and Materials, 1982, Standard method for penetration test and split-barrel sampling of soils, *in* Procedures for testing soils: Philadelphia, American Society for Testing and Materials, D1586–67, p. 292–294.

Anderson, L.R., Keaton, J.R., Aubry, Kevin, and Ellis, S.J., 1982, Liquefaction potential map for Davis County, Utah: Unpublished technical report submitted to Earthquake Hazards Program, U.S. Geological Survey, Contract No. 14–08–0001–19127.

Bonilla, M.G., Mark, R.K., and Lienkaemper, J.J., 1984, Statistical relations among earthquake magnitude, surface rupture length, and surface fault displacement: Bulletin of the Seismological Society of America, v. 75, no. 6, p. 2379–2411.

Boore, D.M., and Joyner, W.B., 1982, The empirical prediction of ground motion: Bulletin of the Seismological Society of America, v. 72, no. 6, p. S43–S60.

Campbell, K.W., 1981, Near-source attenuation of peak horizontal acceleration: Bulletin of the Seismological Society of America, v. 71, p. 2039–2070.

Carson, S.E., and Matti, J.C., 1985, Contour map showing minimum depth to ground water, upper Santa Ana River valley, California: U.S. Geological Survey Miscellaneous Field Studies Map MF–1802, 22 p., scale 1:48,000.

———1986, Contour map showing minimum depth to ground water, San Bernardino Valley and vicinity, California, 1973–1983: U.S. Geological Survey Open-File Report 86–169, 10 p., scale 1:48,000.

Carson, S.E., Matti, J.C., Throckmorton, C.K., and Kelly, M.M., 1986, Stratigraphic and geotechnical data from a drilling investigation in the San Bernardino Valley and vicinity, California: U.S. Geological Survey Open-File Report 86–225, 83 p., scale 1:48,000.

Castro, Gonzalo, 1969, Liquefaction of sands: Harvard Soil Mechanics Series, no. 81, 112 p.

Cox, B.F., and Morton, D.M., 1978, Generalized map of surficial materials in northwestern Riverside and southwestern San Bernardino Counties, California: U.S. Geological Survey Open-File Report 78–978, scale 1:48,000.

Dutcher, L.C., and Garrett, A.A., 1963, Geologic and hydrologic features of the San Bernardino area, California—With special reference to underflow across the San Jacinto fault: U.S. Geological Survey Water-Supply Paper 1419, 114 p.

Evernden, J.F., and Thomson, J.M., 1985, Predicting seismic intensities, *in* Ziony, J.I., ed., Evaluating earthquake hazards

in the Los Angeles region—An earth-science perspective: U.S. Geological Survey Professional Paper 1360, p. 151–202.

Fife, D.L., 1976, Map showing surface waters and marshes in the late 1800's and generalized depth to ground water (1960, 1972), upper Santa Ana Valley, southwestern San Bernardino County, plates 4A and 4B, *in* Fife, D.L., Rodgers, D.A., Chase, G.W., Chapman, R.H., and Sprotte, E.C., Geologic hazards in southwestern San Bernardino County, California: California Division of Mines and Geology Special Report 113, 40 p.

Fife, D.L., Rodgers, D.A., Chase, G.W., Chapman, R.H., and Sprotte, E.C., 1976, Geologic hazards in southwestern San Bernardino County, California: California Division of Mines and Geology Special Report 113, 40 p.

Fumal, T.E., and Tinsley, J.C., 1985, Mapping shear-wave velocities of near-surface geologic materials, *in* Ziony, J.I., ed., Evaluating earthquake hazards in the Los Angeles region—An earth-science perspective: U.S. Geological Survey Professional Paper 1360, p. 127–149.

Ghaboussi, Jamshid, and Wilson, E.L., 1973, Liquefaction and analysis of saturated granular soils: World Conference on Earthquake Engineering, Rome, 1973, 5th, Proceedings.

Gibbs, H.J., and Holtz, W.G., 1957, Research on determining the density of sands by spoon penetration testing: International Conference on Soil Mechanics and Foundation Engineering, London, 1957, 4th, Proceedings, v. 1, p. 35–39.

Green, S.M., 1983, Seismotectonic study of the San Andreas, Mission Creek, and Banning fault system: Los Angeles, University of California, unpublished Master of Science thesis, 52 p.

Greensfelder, R.W., 1974, Maximum credible rock acceleration from earthquakes in California: California Division of Mines and Geology, Map Sheet 23.

Hadley, D.M., and Combs, Jim, 1974, Microearthquake distribution and mechanisms of faulting in the Fontana-San Bernardino area of southern California: Bulletin of the Seismological Society of America, v. 64, no. 5, p. 1477–1499.

Hadley, D.M., and Smith, S.W., 1973, Two geophysical investigations in the San Bernardino Valley area, California, *in* Geological Investigations of the San Jacinto fault zone, and aspects of the socio-economic impact of earthquakes in the Riverside-San Bernardino area, California: University of California, Riverside, Campus Museum Contributions, no. 3, September 1973.

Hanks, T.C., Hileman, J.A., and Thatcher, Wayne, 1975, Seismic moments of the larger earthquakes of the southern California region: Geological Society of America Bulletin, v. 86, p. 1131–1139.

Harden, J.W., Matti, J.C., and Terhune, Christina, 1985, Late Quaternary slip rates along the San Andreas fault near Yucaipa, California, derived from soil development on fluvial terraces: Geological Society of America Abstracts with Programs, v. 18, no. 2, p. 113.

Hays, W.W., 1980, Procedures for estimating earthquake ground motions: U.S. Geological Survey Professional Paper 1114, 77 p.

Hoose, S.N., Wilson, R.C., and Rosenfeld, J.H., 1978, Liquefaction-caused ground failure during the February 4, 1976, Guatemala earthquake: International Symposium on the February 4, 1976, Guatemalan Earthquake and the Reconstruction Process, Guatemala City, 1978, 11th, Proceedings, v. 1, p. 418–464.

Idriss, I.M., 1985, Evaluating seismic risk in engineering practice: International conference on soil mechanics and foundation engineering, 11th, Proceedings, v. 1, p. 255–320.

Ishihara, Kenji, 1985, Stability of natural deposits during earthquakes: International conference on soil mechanics and foundation engineering, San Francisco, 1985, 11th, Proceedings, Rotterdam, Netherlands, v. 1, p. 321–374.

Joyner, W.B., and Boore, D.M., 1981, Peak horizontal acceleration and velocity from strong-motion records including records from the 1979 Imperial Valley, California, earthquake: Bulletin of the Seismological Society of America, v. 71, no. 6, p. 2011–2038.

Joyner, W.B., and Fumal, T.E., 1985, Predictive mapping of earthquake ground motion, *in* Ziony, J.I., ed., Evaluating earthquake hazards in the Los Angeles region—An earth-science perspective: U.S. Geological Survey Professional Paper 1360, p. 203–220.

Kovacs, W.D., Evans, J.C., and Griffith, A.H., 1975, A comparative investigation of the Mobile Drilling Company's Safe-T-Driver with the standard cathead with manila rope for the performance of the Standard Penetration Test: Geotechnical Engineering Report, Purdue University, Lafayette, Indiana, 127 p.

———1977, Towards a more standardized SPT: International Conference on Soil Mechanics and Foundation Engineering, Tokyo, 1977, 9th, Proceedings.

Kovacs, W.D., and Salomone, L.A., 1982, SPT hammer energy measurement: Journal of the Geotechnical Engineering Division, American Society of Civil Engineers, v. 108, no. GT4, p. 599–620.

Lamar, D.L., Merifield, P.M., and Proctor, R.J., 1973, Earthquake recurrence intervals on major faults in southern California, *in* Moran, D.E., Slosson, J.E., Stone, R.O., and Yelverton, C.A., eds., Geology, seismicity, and environmental impact: Association of Engineering Geologists Special Publication, p. 265–276.

Lange, N.A., and Forker, G.M., 1961, Handbook of chemistry (10th ed.): New York, McGraw-Hill, 1969 p.

Laughlin, H., Arnold, R., and Kew, W.S.W., 1923, Southern California earthquake of July 22, 1923: Bulletin of the Seismological Society of America, v. 13, no. 3, p. 105–106.

Lee, K.L. and Seed, H.B., 1967, Cyclic stress conditions causing liquefaction of sand: Journal of the Soil Mechanics and Foundations Division, American Society of Civil Engineers, v. 93, no. SM1, p. 47–70.

Lindh, A.G., 1983, Preliminary assessment of long-term probabilities for large earthquakes along selected fault segments of the San Andreas fault system in California: U.S. Geological Survey Open-File Report 83–63, 15 p.

Martin, R., 1979, Bunker Hill artesian zone study: San Bernardino Valley Municipal Water District unpublished report, 53 p.

Matti, J.C., Morton, D.M., and Cox., B.F., 1985, Distribution and geologic relations of fault systems in the vicinity of the

Central Transverse Ranges, southern California: U.S. Geological Survey Open-File Report 85–365, 27 p. scale 1:250,000.

Matti, J.C., Tinsley, J.C., Morton, D.M., McFadden, L.D., 1982, Holocene faulting history as recorded by alluvial history within the Cucamonga fault zone—A preliminary view, *in* Tinsley, J.C., McFadden, L.D., and Matti, J.C., eds., Late Quaternary pedogenesis and alluvial chronologies of the Los Angeles and San Gabriel Mountains areas, southern California: Field trip 12, Geological Society of America, Cordilleran Section, 78th, Anaheim, California, Guidebook, p. 21–44.

McLean, F.G., Frankin, A.G., and Dahlstrand, T.K., 1975, Influence of mechanical variables on the SPT: Proceedings of the Conference on In-Site Movement of Soil Properties, June 1–4, 1975, North Carolina State University, Raleigh, North Carolina, Specialty Conference of the Geotechnical Engineering Division, American Society of Civil Engineers, v. 1, p. 287–318.

Mendenhall, W.C., 1905, The hydrology of San Bernardino Valley, California: U.S. Geological Survey Water-Supply Paper 142, 124 p.

Miller, F.K., 1979, Geologic map of the San Bernardino North quadrangle, California: U.S. Geological Survey Open-File Report 79–770, scale 1:24,000.

Morton, D.M., 1975, Synopsis of the geology of the eastern San Gabriel Mountains, southern California, *in* Crowell, J.C., ed., San Andreas fault in southern California: California Division of Mines and Geology Special Report 118, p. 170–176.

———1978a, Geologic map of the Redlands quadrangle, San Bernardino and Riverside Counties, California: U.S. Geological Survey Open-File Report 78–21, 1 pl., scale 1:24,000.

———1978b, Geologic map of the San Bernardino South quadrangle, San Bernardino and Riverside Counties, California: U.S. Geological Survey Open-File Report 78–20, 1 pl., scale 1:24,000.

———1978c, Geologic map of the Sunnymead quadrangle, Riverside County, California: U.S. Geological Survey Open-File Report 78–22, 1 pl., scale 1:24,000.

Morton, D.M., and Matti, J.C., 1987, The Cucamonga fault zone—Geological setting and Quaternary history, *in* Morton, D.M., and Yerkes, R.F., Recent reverse faulting in the Transverse Ranges, California: U.S. Geological Survey Professional Paper 1339, p. 179–203, scale 1:24,000.

National Earthquake Prediction Evaluation Council, 1988, Probabilities of large earthquakes occurring in California on the San Andreas fault: U.S. Geological Survey Open-File Report 88–398, 62 p.

National Research Council, 1985, Liquefaction of sands during earthquakes: Washington, D.C., National Academy Press, 240 p.

Nicholson, Craig, Seeber, Leonardo, Williams, Patrick, and Sykes, L.R., 1986, Seismicity and fault kinematics through the eastern Transverse Ranges, California—Block rotation, strike-slip faulting and low-angle thrusts: Journal of Geophysical Research, v. 91, no. B5, p. 4891–4908.

Nishenko, S.P., and Sykes, L.R., 1982, Probabilities of occurrences of large plate rupturing earthquakes for the San Andreas, San Jacinto, and Imperial faults, California, 1983–2003: American Geophysical Union Transactions, v. 64, no. 18, p. 258.

Page, R.A., Boore, D.M., and Dieterich, J.H., 1975, Estimation of bedrock motion at the ground surface, *in* Borcherdt, R.D., ed., Studies for seismic zonation of the San Francisco Bay region: U.S. Geological Survey Professional Paper 941–A, p. A31–A38.

Poulos, S.J., Castro, Gonzalo, and France, J.W., 1985, Liquefaction evaluation procedure: Journal of Geotechnical Engineering, American Society of Civil Engineers, v. 111, p. 772–791.

Raleigh, C.B., Sieh, K.E., Sykes, L.R., and Anderson, D.L., 1982, Forecasting southern California earthquakes: Science, v. 217, p. 1097–1104.

Rasmussen, G.S., 1981, San Andreas fault geometry and maximum probable earthquakes in southern California: Geological Society of America Abstracts with Programs, v. 13, no. 2, p. 102.

Real, C.R., Toppozada, T.R., and Parke, D.L., 1978, Earthquake epicenter map of California: California Division of Mines and Geology Map sheet 39, scale 1:1,000,000.

Richter, C.F., 1958, Elementary seismology: San Francisco, W.H. Freeman, 768 p.

Sanders, C.O., and Kanamori, Hiroo, 1984, A seismotectonic analysis of the Anza seismic gap, San Jacinto fault zone, southern California: Journal of Geophysical Research, v. 89, no. B7, p. 5873–5890.

Schmertmann, J.H., 1979, Statics of SPT: Journal of the Geotechnical Engineering Division, American Society of Civil Engineers, v. 105, no. GT5, p. 655–670.

Schnabel, P.B., and Seed, H.B., 1973, Accelerations in rock for earthquakes in the Western United States: Bulletin of the Seismological Society of America, v. 63, no. 2, p. 501–516.

Schwartz, D.P., and Coppersmith, K.J., 1984, Fault behavior and characteristic earthquakes—Examples from the Wasatch and San Andreas fault zones: Journal of Geophysical Research, v. 89, no. B7, p. 5681–5698.

Seed, H.B., 1968, Landslides during earthquakes due to soil liquefaction: Journal of the Soil Mechanics and Foundations Division, American Society of Civil Engineers, v. 93, no. SM5, p. 1053–1122.

———1979, Soil liquefaction and cyclic mobility evaluation for level ground during earthquakes: Journal of the Geotechnical Engineering Division, American Society of Civil Engineers, v. 105, no. GT2, p. 201–255.

Seed, H.B., and Idriss, I.M., 1967, Analysis of soil liquefaction— Niigata earthquake: Journal of the Soil Mechanics and Foundations Division, American Society of Civil Engineers, v. 93, no. SM3, p. 83–108.

———1971, Simplified procedure for evaluating soil liquefaction potential: Journal of the Soil Mechanics and Foundations Division, American Society of Civil Engineers, v. 97, no. SM9, p. 1249–1273.

———1982, Ground motions and soil liquefaction during earthquakes: Berkeley, California, Earthquake Engineering Research Institute, 134 p.

Seed, H.B., and Peacock, W.H., 1971, Test procedures for measuring soil liquefaction characteristics: Journal of the

Geotechnical Engineering Division, American Society of Civil Engineers, v. 108, no. GTZ, p. 265–283.

Seed, H.B., Ramesh Murarka, John Lysmer, and I.M. Idriss, 1975, Relationships between maximum acceleration, maximum velocity, distance from source and local site conditions for moderately strong earthquakes: University of California, Berkeley, Earthquake Engineering Research Center, report no. EERC 75–25, 23 p.

Seed, H.B., Tokimatsu, K., Harder, L.F., and Chung, R.M., 1985, Influence of SPT procedures in soil liquefaction resistance evaluations: Journal of Geotechnical Engineering, v. 111, no. 12, p. 1425–1445.

Sieh, K.E., 1978, Prehistoric large earthquakes produced by slip on the San Andreas fault at Pallett Creek, California: Journal of Geophysical Research, v. 83, no. B8, p. 3907–3939.

———1981, A review of geological evidence for recurrence times of large earthquakes, *in* Simpson, D.W., and Richards, P.G., eds., Earthquake prediction—An international review: American Geophysical Union Maurice Ewing Series, no. 4, p. 181–207.

———1984, Lateral offsets and revised dates of large prehistoric earthquakes at Pallett Creek, southern California: Journal of Geophysical Research, v. 89, no. B9, p. 7641–7670.

Sowers, G.F., 1979, Introductory soil mechanics and foundations: Geotechnical engineering (4th ed.): New York, Macmillan Publishing Co., Inc., 621 p.

Sykes, L.R., and Nishenko, S.P., 1984, Probabilities of occurrence of large plate-rupturing earthquakes for the San Andreas, San Jacinto, and Imperial faults, California, 1983–2003: Journal of Geophysical Research, v. 89, no. B7, p. 5905–5927.

Sykes, L.R., and Seeber, Leonardo, 1982, Great earthquakes and great asperities along the San Andreas fault, southern California: Eos, American Geophysical Union Transactions, v. 63, no. 45, p. 1030.

———1985, Great earthquakes and great asperities, San Andreas fault, southern California: Geology, v. 13, no. 12, p. 835–838.

Terzaghi, Karl, and Peck, R.B., 1948, Soil mechanics in engineering practice: New York, John Wiley and Sons, 566 p.

Thatcher, Wayne, 1984, The earthquake deformation cycle, recurrence, and the time-predictable model: Journal of Geophysical Research, v. 89, no. B7, p. 5674–5680.

Thatcher, Wayne, Hileman, J.A., and Hanks, T.C., 1975, Seismic slip distribution along the San Jacinto fault zone, southern California, and its implications: Geological Society of America Bulletin, v. 86, p. 1140–1146.

Thenhaus, P.C., Perkins, D.M., Ziony, J.I., and Algermissen, S.T., 1980, Probabilistic estimates of maximum seismic horizontal ground motion on rock in coastal California and the adjacent outer continental shelf: U.S. Geological Survey Open-File Report 80–924, 69 p.

Tinsley, J.C., Youd, T.L., Perkins, D.M., and Chen, A.T.F., 1985, Evaluating liquefaction potential, *in* Ziony, J.I., ed., Evaluating earthquake hazards in the Los Angeles region—An earth-science perspective: U.S. Geological Survey Professional Paper 1360, p. 263–315.

Tokimatsu, K., and Yoshimi, Y., 1984, Correlation of soil liquefaction with SPT and fines content: World Conference on earthquake engineering, 8th, Proceedings, v. 3, p. 255–262.

Toppozada, T.R., and Parke, D.L., 1982, Areas damaged by California earthquakes, 1900–1949: California Division of Mines and Geology Open File Report 82–17SAC, 65 p.

Webb, T.H., and Kanamori, Hiroo, 1985, Earthquake focal mechanisms in the eastern Transverse Ranges and San Emigdio Mountains, southern California, and evidence for a regional decollement: Bulletin of the Seismological Society of America, v. 75, no. 3, p. 737–757.

Weldon, R.J., II, 1985, The late Cenozoic geology of Cajon Pass— Implications for tectonics and sedimentation along the San Andreas fault: Pasadena, California Institute of Technology, unpublished Ph.D. thesis, 382 p.

Weldon, Ray, and Humphreys, Eugene, 1985, A kinematic model of southern California: Tectonics, v. 5, no. 1, p. 33–48.

Weldon, R.J., II, and Sieh, K.E., 1985, Holocene rate of slip and tentative recurrence interval for large earthquakes on the San Andreas fault, Cajon Pass, southern California: Geological Society of America Bulletin, v. 96, p. 793–812.

Wesson, R.L., and Wallace, R.E., 1985, Predicting the next great earthquake in California: Scientific American, v. 252, no. 2, p. 35–43.

Youd, T.L., 1973, Liquefaction, flow, and associated ground failure: U.S. Geological Survey Circular 688, 11 p.

Youd, T.L., and Hoose, S.N., 1977, Liquefaction susceptibility and geologic setting: World Conference on Earthquake Engineering, 6th, New Delhi, 1977, Proceedings, v. 3, p. 2189–2194.

Youd, T.L., and Perkins, D.M., 1978, Mapping liquefaction-induced ground failure potential: Journal of the Geotechnical Engineering Division, ASCE, v. 104, no. GT4, p. 433–446.

Youd, T.L., Tinsley, J.C., Perkins, D.M., King, E.J., and Preston, R.F., 1978, Liquefaction potential of the San Fernando Valley: International Conference on Microzonation for Safer Construction-Research and Applications, San Francisco, 1978, 2d, Proceedings, v. 1, p. 267–278.

Ziony, J.I., ed., 1985, Evaluating earthquake hazards in the Los Angeles region—An earth-science perspective: U.S. Geological Survey Professional Paper 1360, 505 p.

Ziony, J.I., and Yerkes, R.F., 1985, Evaluating earthquake and surface-faulting potential, *in* Ziony, J.I., ed., Evaluating earthquake hazards in the Los Angeles region—An earth-science perspective: U.S. Geological Survey Professional Paper, 1360, p. 43–91.

APPENDIXES A–C

APPENDIX A

STANDARD PENETRATION TESTS—SCREENING PROCEDURES

Penetration data from the sources described in the text were generated by using a variety of field methods that incorporate different equipment and procedures. Differences in methodology can lead to significant differences in blow count for sedimentary materials having identical physical characteristics—a shortcoming that creates problems for liquefaction evaluations that use blow-count data to compare the relative susceptibilities of sedimentary materials. This problem can be circumvented if the penetration test is standardized to comply with specific technical criteria. Seed and Idriss (1982, p. 94–95; Seed and others, 1985) specify several guidelines that must be followed during the penetration test: (1) the test must comply with some of the SPT guidelines described by the American Society for Testing and Materials (ASTM, 1982) and (2) the test should incorporate several additional guidelines not stipulated by ASTM (1982), including (a) specific standards to be met by the energy-delivery system, (b) a relatively small-diameter hole approximately 4 in. in diameter, and (c) drilling mud to support the sides of the hole. We used these criteria to screen the penetration data available from the San Bernardino Valley region.

ASTM Guidelines

The ASTM (1982, p. 292–294, Designation: D1586) provides specifications for equipment and procedures for SPTs that have various engineering applications. The borehole diameter must range between 2.25 and 8 in., and the sampling device itself must have a 2-in. outside diameter and a 1⅜-in. inside diameter. A 140-lb drive weight falling freely 30 in. must be used to drive the sampler through a total penetration interval of 18 in. Hammer strikes during the first 6 in. are used to seat the sampler and do not figure into the actual penetration resistance; the blow count (N) is the number of blows required to advance the sampler through the 12-in. interval between 6 and 18 in.

According to Seed and Idriss (1982, p. 94–95), penetration procedures that depart from these particular ASTM specifications for the SPT are not appropriate for liquefaction analyses based on their approach—a standard we generally conformed to in our study of the San Bernardino Valley. When a log sheet or description of field methods or our inquiries to the source company or agency indicated that a penetration test actually was an SPT performed according to ASTM guidelines, we assumed that the blow-count data were usable. However, if the log sheet or description of field methods outlined penetration procedures that were not compatible with ASTM guidelines, or if test procedures were not specifically described, we assumed that the penetration test was incompatible with the SPT procedures specified by Seed and Idriss (1982) and we did not use the blow-count data.

ASTM guidelines requiring borehole diameters between 2.25 and 8 in. proved to be the most easily applied screen for penetration-resistance data from the San Bernardino Valley region. Much of these data were collected for engineering purposes other than liquefaction evaluations, and typically were obtained by using large-diameter bucket augers in the range of 16 to 36 in. The U.S. Army Corps of Engineers and many private geotechnical firms use bucket augers of this type. Correction factors conceivably could be applied to penetration data collected by using large-diameter borings, thus making the data comparable to those derived using SPT procedures specified by ASTM (1982) and by Seed and Idriss (1982). However, the applicability of such factors had not been documented at the time we conducted our investigation, especially factors that accommodate disturbance of sedimentary material at the bottom of large-diameter boreholes. Dynamic-penetration data collected by CalTrans also are not compatible with ASTM guidelines for the SPT, and we did not use these data.

Supplemental Criteria

Penetration data that met the ASTM standard were examined for their compliance with the three supplemental guidelines specified by Seed and Idriss (1982; Seed and others, 1985)—energy-delivery standards, 4-inch borehole requirement, and use of drilling mud. This screen was more difficult to apply than the ASTM screen because many log sheets and descriptions of field investigations do not fully discuss penetration-test procedures. We clarified some ambiguities by telephone, but where questions were not resolved, we either made assumptions about the procedures or rejected the data as incompatible with the three supplemental guidelines discussed in this section.

Energy-delivery standards

Many SPT data from the San Bernardino Valley region were generated by using a rope-and-pulley system to lift the driving weight and drop it on the impact block (anvil) of the drill string. The Corps of Engineers generally employs the rope-and-pulley system (J. Ralston, E. Stokes, and E. Ketchum, oral commun., 1984), and geotechnical firms whose investigations make up the bulk of the local-agency data generally use this procedure. To minimize

variation in N that can be introduced by procedural differences in using the rope-and-pulley system, Seed and others (1985, p. 1426–1427) recommend standardized procedures for the number of rope turns around the pulley (two turns) and the driving rate (blows per minute, 30 to 40). It is not possible to implement this screen for the rope-and-pulley data set collected from the San Bernardino Valley region because the drilling logs generally do not include such procedural details.

Cable-and-clutch systems commonly are used instead of rope-and-pulley systems to lift and release the SPT hammer. For example, the cable-and-clutch system routinely is used by CalTrans, is occasionally employed by private geotechnical firms (oral communication from several local drillers), and was used by Carson and others (1986). We analyzed SPT data that were generated by using the cable-and-clutch system because the technique produces penetration results that are fairly compatible with those of the rope-and-pulley system (Kovacs and others, 1975; L.F. Harder, oral commun., 1984). However, cable-and-clutch systems have driving energies that are more efficient than those of rope-and-pulley systems employing the same hammer and will generate N values that are somewhat lower than those generated by rope-and-pulley hardware.

Seed and others (1985, p. 1430–1432, table 3) describe procedures for normalizing penetration values obtained using various energy-delivery systems and hammers. With the use of correction factors, N from any hardware system can be converted to N_{60}—the penetration resistance obtained if the energy delivered to the drill stem by the hammer is 60 percent of the energy associated with a free-falling hammer. These correction factors were published after we completed our investigation and were not available for our analysis; hence, N values obtained by using different energy-delivery systems and different hammer types were analyzed without correcting for driving-energy differences between them. In any event, it would be difficult to apply such criteria to the San Bernardino Valley data set.

Four-in. Borehole Requirement

Seed and Idriss (1982) specify a hole diameter of approximately 4 in. because smaller or larger hole diameters can greatly influence penetration resistance.[1] If the borehole is significantly narrower than 4 in., overburden pressure at the bottom of the hole can be increased; moreover, the sides of the hole may impede the progress of the SPT sampler. Either of these effects can increase penetration resistance. If the borehole diameter is significantly larger than 4 in., overburden pressure is reduced at the bottom of the boring, which can result in reduced penetration resistance (L.F. Harder, oral commun. 1984). Moreover, sediment disturbance resulting from the rotation of large-diameter augers also tends to reduce penetration resistance. With either undersize or oversize borehole diameters, N will not accurately reflect the liquefaction susceptibility at a given site.

A stringent borehole requirement is desirable because it minimizes blow-count variability stemming from hardware differences. However, with the exception of the large-diameter boreholes discussed above, we did not rigorously incorporate the 4-in. borehole requirement because such a stringent screening criterion would have eliminated most of the penetration data available for the San Bernardino Valley region. For example, soil and foundation reports on file with local agencies indicate that a wide variety of borehole diameters are used by private companies; many diameters measure up to 8 in. Penetration tests performed by CalTrans generally use borehole diameters of 3 in., and tests performed by the USGS (Carson and others, 1986) used a 6.25-in. diameter. To accommodate variation in borehole diameter but still comply to some degree with the stringent figure recommended by Seed and Idriss (1982), we extended the range of acceptable borehole diameters within the San Bernardino Valley data set to include those between 2.25 in. and 8 in. This allowed us to use much of the local-agency SPT data, as well as all of the SPT data obtained by CalTrans and the USGS.

Use of Drilling Mud

Seed and Idriss (1982, p. 95) recommend the use of drilling mud while penetration tests are performed above the water table to minimize the decrease in overburden pressure at the bottom of the hole. As material is removed during the excavation of a borehole, the overburden pressure on the material at the bottom of the hole is reduced, which tends to result in reduced resistance during the penetration test. The use of drilling mud, or water in appropriate cases, minimizes this pressure reduction and leads to appropriate penetration resistance. This procedure is necessary in large-diameter holes where the loss of overburden pressure has a greater impact; in small-diameter holes within the 2¼- to 8-in. range, the loss of overburden pressure is not as great and the requirement for drilling mud may not be so critical. Where penetration tests in the San Bernardino Valley were completed above the water table, we incorporated their results even if drilling muds were not used. This may result in our inclusion of N values that are slightly lower than those generated by using the guidelines of Seed and Idriss (1982). In any event, it is difficult to apply the drilling-mud criterion to SPT's completed above the water table because drilling records from most investigations do not discuss the use or nonuse of mud in this zone.

Below the water table, an additional factor—heaving—becomes significant. If drilling mud or water is

[1] Seed and others (1985, p. 1432) broadened the range of acceptable boreholes to include those 5 in. in diameter.

not added when the drill stem is below the water table, water from the surrounding sediment tends to flow into the hole and disturb and loosen the material around and at the bottom of the boring. Heaving of this type may lower penetration resistance. The use of drilling mud or water in the hole, with the level of the mud or water above that of the water table, eliminates the inflow of water and attendant heaving.

All of the SPT investigations that we used in this report employed either drilling mud or water below the water table. Although geotechnical reports by private consultants seldom indicate whether drilling muds were used, Seed and Idriss (1982, p. 95) and several drillers with whom we conversed indicate that private consultants commonly use drilling muds or water when drilling below the water table. CalTrans uses mud whenever possible (A. Goldschmidt, oral commun., 1984), and the USGS (Carson and others, 1986) added water to the borings when below the water table.

Other Factors

Numerous procedural factors other than the three supplemental guidelines affect penetration resistance, including: (1) the use or nonuse of liners in standard samplers designed to accept liners (Schmertmann, 1979), (2) rope age and the method used to release the rope into the drill rig cathead (Kovacs and others, 1977), and (3) the length and type of rod used to drive the sampler during the penetration test (McLean and others, 1975; Seed and others, 1985). The qualitative effect of these factors on penetration resistance is fairly well understood. However, their quantitative effect on blow counts has not been documented fully, and it is not clear to what degree they affect an evaluation of liquefaction susceptibility based on penetration resistance. These factors probably would not alter the results of this study in any significant way, although they would refine the results somewhat. We made no attempt to modify, eliminate, or correct the penetration values used in this study based on these additional factors.

APPENDIX B

PROCEDURES FOR SITE-SPECIFIC ANALYSIS OF LIQUEFACTION SUSCEPTIBILITY

Although we characterize this phase of our analysis as "site-specific"—implying that our evaluation at each site utilizes field data for each of the geotechnical parameters required by the analysis—we modified the site-specific methods proposed by Seed and Idriss (1982) to adapt them to regional rather than local evaluations of liquefaction susceptibility. Ideally, site investigations obtain specific values for such geotechnical parameters as ground-water depth, overburden pressure, and physical characteristics of the geologic materials (such as lithologic variation, relative density, unit weights). Unfortunately, specific field data for many of these geotechnical parameters either are not reported by the site investigations available to us, or are so variable from site to site as to prohibit meaningful comparisons between sites. Consequently, we modified the Seed-Idriss site-specific method by making generalizations and assumptions about most geotechnical parameters and by simplifying some parts of the Seed-Idriss procedure. In this Appendix we describe our procedural methods and discuss the generalizations entailed by our regional application of site-specific techniques.

Cyclic-stress Ratios

Comparisons between two types of cyclic-stress ratio form the basis of the Seed-Idriss method for determining liquefaction susceptibility. Cyclic-stress ratios are unitless parameters that characterize the response of a given sediment type at a particular subsurface depth to ground-shaking conditions of specified strength and duration. At the location and depth of each SPT, the cyclic-stress ratio that would be expected to develop during a particular earthquake (C_d) is compared to that which would be required to cause liquefaction at that location during the same earthquake (C_l) to yield the susceptibility ratio (FS):

$$FS = \frac{C_l}{C_d}.$$

If C_d is equal to or greater than C_l, $FS = 1.0$ or less and the materials are considered susceptible. In this study, we calculated C_d by using a formula provided by Seed and Idriss (1982) and C_l by using penetration-resistance values from the San Bernardino Valley region and a chart from Seed and Idriss (1982).

Determination of C_d

The cyclic-stress ratio that can be expected to develop at the location of each SPT as the result of a given earthquake can be determined by:

$$C_d = 0.65 \cdot \frac{\sigma_o}{\sigma_o'} \cdot \frac{A_{max}}{g} \cdot r_d \qquad (1)$$

where C_d is an abbreviation for $(\tau_{av} / \sigma_o')_{dev}$, g is the acceleration due to gravity, A_{max} is the maximum ground-surface acceleration expected at the site of the SPT (some fractional multiple of 1.0), σ_o is the total overburden stress, σ_o' is the effective overburden stress, and r_d is a stress-reduction coefficient. The equation is solved by determining appropriate values for A_{max}, σ_o, σ_o', and r_d.

Determination of A_{max}

Maximum or peak ground acceleration (A_{max}) commonly is used as a measure of the strength of earthquake-induced ground shaking. Its value at a particular site is a function of many factors, including earthquake magnitude, distance to the causative earthquake, various seismic-source parameters, site location relative to direction of energy propagation, and geologic conditions at the site (Page and others, 1975; Hays, 1980). To select maximum-acceleration values at various SPT sites in the San Bernardino Valley region, we identified scenario earthquakes having specified surface-wave magnitudes (M_s) for specific faults within the study area. For these earthquakes, we utilized attenuation curves to specify A_{max} at various SPT sites located at different distances from the causative faults.

Scenario earthquakes.—To identify the maximum distribution of areas having any significant liquefaction susceptibility, we modeled ground response for the San Bernardino Valley region by using local scenario earthquakes having large, reasonably-expectable surface-wave magnitudes. Large nearby earthquakes will generate larger A_{max} values than smaller or more distant earthquakes and will lead to maximum values for C_d calculated in equation 1. Because large C_d values are more likely to exceed C_l values, determinations of C_d for large local earthquakes would identify the maximum distribution of areas susceptible to liquefaction. The large-magnitude scenario-earthquake approach admittedly is conservative because it incorporates earthquake magnitudes and maximum accelerations that lead to worst-case conditions. However, this approach is consistent with the goal of this investigation, which is to identify on a regional basis the maximum distribution of areas having any significant susceptibility to liquefaction.

The San Andreas, San Jacinto, and Cucamonga faults have the greatest potential for generating earthquakes large enough to induce liquefaction in the San Bernardino Valley region. Accordingly, we used scenario earthquakes on these

faults for evaluating liquefaction susceptibility in the region. Earthquakes on other faults also may have the potential for inducing liquefaction in the San Bernardino Valley, but these faults generally are more distant and fault-length considerations (Bonilla and others, 1984) suggest that they are not capable of generating earthquakes with magnitudes as large as those on the three major faults.

San Andreas fault: This study incorporates an estimated Richter surface-wave magnitude of 8.0 (M_s=8.0) on the modern trace of the San Andreas fault (Sieh, 1978, 1981; Raleigh and others, 1982; Lindh, 1983; Sykes and Nishenko, 1984; Sykes and Seeber, 1985; Ziony and Yerkes, 1985).

San Jacinto fault: This study incorporates an estimated M_s=7.0 earthquake on the San Jacinto fault (Ziony and Yerkes, 1985).

Cucamonga fault: This study incorporates an estimated M_s=6.75 earthquake on the Cucamonga fault (Lamar and others, 1973; J.C. Matti, D.M. Morton, J.C. Tinsley, and L.D. McFadden, unpublished data).

Attenuation curves and site-specific determination of A_{max}. —Site-specific values for A_{max} resulting from the three scenario earthquakes were determined by using attenuation curves. Maximum accelerations decrease (attenuate) as distance from the source fault increases. Models correlating magnitude and fault distance with A_{max} have been proposed by many workers, including Schnabel and Seed (1973), Greensfelder (1974), Seed and others (1975), Algermissen and Perkins (1976), Thenhaus and others (1980), Joyner and Boore (1981), Campbell (1981), Boore and Joyner (1982), Seed and Idriss (1982), and Joyner and Fumal (1985). We used curves developed by Seed and Idriss (1982, fig. 17, p. 29–40) because they allow consistent application of the Seed-Idriss method of evaluating liquefaction. Use of alternative curves proposed by other authors probably would not significantly affect the results of this investigation.

To determine A_{max} values resulting from the three scenario earthquakes, we used the two-stage procedure described by Seed and Idriss (1982). (1) We used graphical attenuation curves (fig. 2, modified from fig. 17 of Seed and Idriss, 1982) to determine peak bedrock accelerations throughout the San Bernardino Valley region. The curves for M_s=7.0 and 8.0 earthquakes are interpolated in figure 2 because Seed and Idriss (1982) do not show curves for shocks of these magnitudes. (2) Because estimates of bedrock accelerations may not be appropriate for sites underlain by sedimentary materials like those in the San Bernardino Valley, the accelerations obtained from figure 2 had to be correlated with accelerations for various sedimentary materials. Figure 3 (modified from Seed and Idriss, 1982, fig. 19) shows curves that correlate A_{max} on rock with A_{max} on sedimentary materials, including stiff soils, deep cohesionless soils, and soft to medium-stiff clay and sand. Seed and Idriss (1982, p. 35–37) do not provide a full description of these soil categories, so it is difficult to determine which soil type applies to sedimentary materials in the study area. However, our conversations with Seed (oral commun., 1984) suggest that the stiff-soil category-(cohesionless soils or stiff clays with shear-wave velocities of about 2,500 ft/s or less to depths of about 200 ft or less) generally is appropriate for sedimentary materials occurring in the San Bernardino Valley region. These materials consist of interlayered gravel, sand, silt, and clay (Carson and others, 1986) and have shear-wave velocities ranging from a few hundred ft/s to about 2,500 ft/s (Hadley and Smith, 1973; Hadley and Combs, 1974; Fumal and Tinsley, 1985).

To determine values for A_{max}, we measured the closest horizontal distance from each SPT site to the fault in question. This figure then was used to estimate A_{max} values on rock (fig. 2) and the corresponding A_{max} values on stiff soil (fig. 3). Values for A_{max} were determined to the nearest 0.05 *g* for each SPT location.

Determination of Total Stress, Effective Stress, and Neutral Stress

In equation 1, the ratio of total stress to effective stress (σ_o / σ_o') is a term that quantifies the inherent resistance to deformation of a particular sediment at a particular subsurface depth given particular ground-water conditions. Determinations of both σ_o and σ_o' require site-specific values or estimates for the unit weight and thickness of sedimentary materials overlying a given SPT sample and estimates for the neutral stress exerted by ground water.

Relations among total stress, effective stress, and neutral stress can be illustrated by considering the stresses acting upon a unit volume of soil buried at depth *z* in a sedimentary column. The column of sediment and ground water overlying the unit volume exerts a vertical stress on the unit volume equal to the weight of the column divided by its cross-sectional area. This stress is the total vertical stress (σ_o) due to overburden pressure. The total vertical load is supported mainly by the point contacts between individual sediment grains, but pore-water pressure (u, or neutral stress) in the unit volume also helps to support some of the load. The difference between the total vertical stress (σ_o) and the pore-water pressure (u) is the effective vertical stress (σ_o'). Many laboratory investigations of cohesionless material, of which liquefiable sand is an example, have shown that resistance to deformation depends on the magnitude of the effective stress.

Unit-weight calculations. —Both σ_o and σ_o' require information about the unsaturated and saturated unit weights (γ_u and γ_s, respectively) of sedimentary materials overlying each SPT sample. At any given depth

$$\sigma_o = \gamma \cdot z \quad (2)$$

and

$$\sigma_o' = \sigma_o - u \quad (3)$$

where γ is the unit weight of the overlying material, z is the depth, and u is the neutral stress caused by water pressure within the soil voids. Because unit-weight values were not routinely available on log sheets accompanying SPT's compiled for this study, we made assumptions about their value on the basis of work by other studies in other regions. Terzaghi and Peck (1948) summarized unit-weight values for 10 different sediment categories—four of which characterize the majority of surficial materials encountered in borings in the San Bernardino Valley and vicinity: uniform loose sand, uniform dense sand, mixed-grained loose sand, and mixed-grained dense sand. For these sediment types, Terzaghi and Peck provide approximations of dry unit weight γ_d ranging from 90 lb/ft^3 to 116 lb/ft^3 and saturated unit weight γ_s ranging from 118 lb/ft^3 to 135 lb/ft^3. To select a single representative value from these unit-weight ranges, we used rounded-up arithmetic means. For γ_d we derived an arithmetic mean by determining the value that is halfway between 90 lb/ft^3 and 116 lb/ft^3, or 103 lb/ft^3; for γ_s we derived an arithmetic mean by determining the value that is halfway between 118 lb/ft^3 and 135 lb/ft^3, or 126.5 lb/ft^3. Because borings in the San Bernardino Valley and vicinity primarily encountered dense and mixed-grain sands, and because Terzaghi and Peck indicate that these types of sands generally have unit weights greater than the arithmetic means calculated above, we rounded the arithmetic means up to the nearest multiple of 5—thus deriving values of 105 lb/ft^3 for γ_d and 130 lb/ft^3 for γ_s.

We used values of γ_d to estimate γ_u. However, because γ_d is the unit weight when completely dry and γ_u is the unit weight with natural field moisture, γ_d tends to be lower than γ_u in most natural settings. By rounding-up the arithmetic mean for γ_d we were able to partly compensate for this difference between the two values and provide a more accurate estimate of γ_u.

We believe our approximations of saturated and unsaturated unit weight are appropriate substitutes for their actual site-specific values. Where we compared these generalized values with actual values reported on the log sheets for borings completed in the San Bernardino Valley region, we found general agreement. Furthermore, when we tested small adjustments to γ_u and γ_s we discovered no significant impact on the susceptibility calculations completed for this study.

Calculation of neutral stress.—As discussed above, ground water plays an important role in the mechanics of soil-particle interactions because it influences both total stress and effective stress by exerting pore pressure (neutral stress, u) which reduces intergranular stress. Estimates for u require information about the height of the ground-water column overlying a given sediment mass.

Site-specific investigations that evaluate the impact of u on σ_o' typically would incorporate the actual depth to the water table at the site. However, in our analysis we did not utilize actual values for three reasons: (1) Many geotechnical site investigations available to us were conducted at times when ground-water levels were considerably deeper than they are today, and most of the subsurface borings did not penetrate the water table; (2) ground-water levels fluctuate so dramatically according to cycles of withdrawal and recharge that a water-level measurement obtained at a given site at a particular time might not be representative of typical ground-water conditions; and (3) site-specific liquefaction analyses that utilize water-level values unique to each site are not amenable to regional extrapolation of site-specific results.

To circumvent these problems, we modeled the effect of u on σ_o' by evaluating interpolated ground-water conditions. We posed the following question: for a given SPT sample at a particular depth, what would be the value of u and σ_o' (equation 3), σ_o (equation 2), and C_d (equation 1) if the water table were at a depth (W_1) equal to the nearest multiple of 10 ft overlying the SPT sample? For example, for an SPT sample at 28 ft subsurface, we estimated u, σ_o', σ_o, and C_d for a ground-water level at 20 ft subsurface and thus for the neutral-stress effects created by an overlying water column 8 ft high. In this fashion, all SPT samples were evaluated under neutral-stress conditions created by the water-column height between the sample position and the immediately overlying 10-ft ground-water multiple (W_1).

Use of interpolated water levels in our analysis created hypothetical estimates for effective stress (which we refer to as $\sigma_{o(1)}'$). In turn, this procedure led to values for C_d that are approximations of their actual value: the closer W_1 approximates the actual water-level depth W_2 the closer C_d is to its actual value for a given SPT. This approach has the advantage that each C_d value can be grouped with other values having the same assumed depth to ground water to determine the typical susceptibility to liquefaction for a specific ground-water interval (0 to 10 ft, 10 to 20 ft, and so forth). Typical susceptibilities thus calculated correspond to ground-water contours compiled for this study (pl. 2) and provide a means for easily evaluating susceptibility to liquefaction across large regions.

Determination of Stress-Reduction Coefficient (r_d)

The stress-reduction coefficient (r_d) in equation 1 compensates for the difference between the total and actual shear stresses induced within a soil mass during an earthquake. The actual stress is less than the total stress because the soil column overlying a sediment mass is flexible rather than rigid, and deformation of this flexible column reduces

the applied shear stress induced by the earthquake (Seed and Idriss, 1982, p. 74–75). Average values for r_d vary from 1.0 at the surface to smaller values at depth, as determined to the nearest 0.05 units from the dashed line in figure 4 (modified from Seed and Idriss, 1982, fig. 40). As shown in figure 4, the accuracy with which r_d can be determined decreases with depth because the envelope of possible values widens with depth. Average values of r_d generally can be determined with an error of less than 5 percent to subsurface depths of 30 to 40 ft (Seed and Idriss, 1982, p. 75). However, at depths greater than about 40 ft subsurface the error is larger; this introduces uncertainty in r_d and in turn introduces uncertainty in c_d values that are calculated for these subsurface depths.

Determination of C_l

C_l $[(\tau_{av} / \sigma_o')_{liq}$ of Seed and Indriss (1982)] is the threshold cyclic-stress ratio required for liquefaction to occur at a particular site as the result of a given earthquake. Derivation of C_l requires determinations or estimates of such site factors as effective overburden pressure and relative density of sedimentary materials to evaluate the cyclic loading characteristics that will promote failure of the materials under specified shaking conditions.

Modifications to penetration resistance (N)

Derivation of C_l relies mainly on penetration resistance (N) obtained during the SPT. However, raw values for N determined in the field cannot be used to derive C_l because raw penetration resistance must be modified to compensate for various factors.

Compensation for differences in rod length.—Values for N from shallow depths must be adjusted to compensate for a loss of driving energy that results because only a short length of rod is needed between the ground surface and the penetration sample. This adjustment is described by Seed and Idriss (1982, p. 177; also see Seed and others, 1985) and requires a simple correction coefficient of 0.75 for SPT depths less than 10 ft subsurface. No adjustment is necessary for greater depths.

Compensation for effective overburden pressure ($\sigma_o'_{(2)}$).—Penetration resistance reflects not only the physical properties of the soil tested (compaction, cementation), but also the influence of effective overburden pressure at the depth of the SPT. Because it is desirable to compare the physical properties of various soils independent of their response to overburden pressures that vary with the thickness and relative density of overburden, Seed and Idriss (1982, p. 93) recommend that N be converted to a normalized penetration resistance (N_1) that would be obtained under an effective overburden pressure of 2,000 lb/ft^2, where

$$N_1 = C_N \cdot N \qquad (4)$$

where C_N is a function of the effective overburden pressure at the depth of the SPT.

Values for C_N can be derived from figure 5, but only after the effective overburden pressure is calculated at the location of the SPT. Effective overburden pressure ($\sigma_o'_{(2)}$), like effective stress ($\sigma_o'_{(1)}$), is derived by equations 2 and 3 using similar values for unsaturated and saturated unit weights (105 lb/ft^3 and 130 lb/ft^3, respectively). However, whereas we calculated $\sigma_o'_{(1)}$ by using hypothetical values for ground-water depth (W_1), calculations of $\sigma_o'_{(2)}$ are based on actual depths to ground water (W_2) measured at the time and location of each SPT.

Once we calculated $\sigma_o'_{(2)}$, the relative density (D_r) at the SPT had to be determined before C_N could be read from figure 5. For values of $\sigma_o'_{(2)}$ less than about 2,500 lb/ft^2, figure 5 has a single curve that applies regardless of D_r considerations. For values of $\sigma_o'_{(2)}$ greater than about 2,500 lb/ft^2, this single curve bifurcates (solid lines in figure 5) with one limb applicable where the average D_r falls in the range 40 to 60 percent and the other where average D_r falls between 60 and 80 percent (Seed and Idriss, 1982, p. 92; H.B. Seed, oral commun., 1984). Because values for D_r are not routinely available for SPT's from the San Bernardino Valley region and to avoid preferencing one limb over the other, we used an assumed value of 60 percent for D_r and added a new limb to the figure that is halfway between the original two. This interpolated curve was used to calculate values of C_N at SPT locations where $\sigma_o'_{(2)}$ was greater than approximately 2,500 lb/ft^2.

As originally published by Seed and Idriss (1982, fig. 47), the curve in figure 5 did not accommodate $\sigma_o'_{(2)}$ less than about 800 lb/ft^2. To determine C_N for effective overburden conditions less than 800 lb/ft^2, we extended the curve by adding a linear extrapolation. This new portion of the curve extends to $\sigma_o'_{(2)}$ as low as 400 lb/ft^2, where C_N equals 2.0; where $\sigma_o'_{(2)}$ was less than 400 lb/ft^2, we assumed that C_N equals 2.0. This extended portion of the curve typically was used to calculate C_N values at depths less than about 10 ft. Because the slope and position of the extrapolated curve are not controlled by actual data, we have less confidence in C_N values determined for these shallow depths and in the susceptibility evaluations that depend on those extrapolated values.

After compensations for driving energy and effective overburden stress are applied, normalized overburden stress ($\sigma_o'_{(2)}$) can be used in conjunction with relative density (D_r) to determine C_N to the nearest 0.1 for each SPT (fig. 5). These C_N values are used to convert raw penetration resistance (N) to modified penetration resistance (N_1) (equation 4).

Compensation for silt.—An adjustment to N_1 is required for silty or partly silty materials. If the median grain size (D_{50}) of the tested materials is greater than 0.16 in. (0.25 mm), no adjustment is necessary, but at smaller values of D_{50} adjustments are required. If D_{50} is 0.09 in.

or less, 7.5 is added to N_1. If D_{50} is between 0.16 in. and 0.09 in., we increased N_1 by an amount interpolated linearly between 0 and 7.5.[2]

Graphical Determination of C_l

After C_N and N_1 have been determined, figure 6 is used to determine C_l for each of the scenario earthquakes on the San Andreas fault (M_s=8.0), San Jacinto fault (M_s=7.0), and Cucamonga fault (M_s=6.75). Figure 6 is modified from figure 57 of Seed and Idriss (1982), who provided susceptibility-threshold curves for M=5.25, 6, 6.75, 7.5, and 8.5 events. We used their M=6.75 curve to determine values of C_l for the Cucamonga fault. However, we had to interpolate threshold curves for scenario earthquakes on the San Jacinto and San Andreas faults. We also had to extend the slopes of all three threshold curves in order to accommodate N_1 values that we determined for SPT samples from extremely shallow (less than 10 ft) anddeep (greater than about 35 ft) subsurface levels in the San Bernardino Valley region. In figure 6, the threshold curves have been extended downward by linear extrapolation and upward by continuing the existing slope trend. The accuracy of results for C_l determined by using these extrapolated curves is more questionable than results for the range between 10 and 35 ft subsurface. Improved curves for extremely shallow or deep SPT data would greatly enhance the results of this investigation.

The threshold curves in figure 6 only are applicable for values of $\sigma_o'_{(2)}$ less than about 2,000 lb/ft^2 (Seed and Idriss, 1982, p. 112, 118). Where $\sigma_o'_{(2)}$ exceeds this value, figure 6 tends to predict values for C_l that are too high. However, according to Seed (oral commun., 1984), correction factors can be used to compensate for these excessive overburden pressures, and figure 7 represents one approach to identifying such factors. According to figure 7, effective overburden pressure must exceed approximately 3,380 lb/ft^2 (1.5 kg/cm^2) before a correction is required.

C_d and C_l—Summary

From the preceeding description of procedures used to calculate C_d and C_l, it should be clear that we employed various assumptions, approximations, and generalizations with regard to the geotechnical parameters manipulated in the calculations, and we adopted minor modifications or simplifications of the Seed-Idriss method of determining site-specific values for the two cyclic-stress ratios. Most of these modifications stem from three factors. (1) Many of the geotechnical site investigations that are available from the San Bernardino Valley region lack specific information about some of the geotechnical parameters that are essential for the calculation of C_d and C_l; as a result, we had to make generalizations and assumptions about these parameters. (2) Some elements of the Seed-Idriss method are not adapted for lower and higher N_1 values or for the ground-shaking conditions required by the large local earthquakes specified in our analysis. As a result, we had to modify or interpolate some parts of the determinative graphs presented by Seed and Idriss (1982; see figs. 5 and 7 of this report). (3) Regional evaluations such as ours inherently require generalizations and assumptions because the variety of sediment types, overburden pressures, ground-water levels, sediment unit weights, and relative densities would be difficult to address in a specific way for an area as large as the San Bernardino Valley region.

With each assumption and simplification, some confidence in the accuracy of the results is lost and increased generalization of results is necessary. However, because this investigation is regional in character and not site-specific, these factors should not compromise our ability to distinguish between areas where susceptibility to liquefaction is greatest and least.

[2] Seed and others (1985, fig. 6) introduced susceptibility curves that correlate C_l with N_1 for sediment containing 15 percent fines and 35 percent fines. These curves were published after our study was completed and were not incorporated into our analysis. The new curves can be used only when the grain-size distribution of the sediment sampled by the SPT has been determined from mechanical analyses like those presented by Carson and others (1986), and such data are not available for most of the penetration tests performed in the San Bernardino Valley region. A pilot study (table 8 of this report) that we conducted by using the mechanical-analysis data from Carson and others (1986) indicates that, for silty samples, the adjustments to N described in the text yield C_l values that are comparable to those obtained byusing the new curves of Seed and others (1985).

Determination of Susceptibility (*FS*)

The threshold cyclic-stress ratio required for liquefaction (C_l) can be related to the actual cyclic-stress ratio expected to develop during a particular earthquake (C_d) to estimate the ratio *FS* as follows:

$$FS = \frac{C_l}{C_d}. \tag{5}$$

When *FS* is less than 1, the materials tested by the SPT are likely to liquefy during the specified earthquake. Through use of equation 5, we determined liquefaction susceptibility at each of the SPT locations used in this study for each of the scenario earthquakes on the San Andreas (FS_A), San Jacinto (FS_J), and Cucamonga (FS_C) faults:

$$FS = \frac{C_{lA}}{C_{dA}}$$

$$FS = \frac{C_{lJ}}{C_{dJ}}$$

$$FS = \frac{C_{lC}}{C_{dC}}.$$

APPENDIX C

EXAMPLE CALCULATIONS OF C_d, C_l, AND *FS*

This appendix provides an example of how we used data from the geotechnical investigations collected for this study to calculate C_d, C_l, and *FS* at each SPT location. The example includes only minimal explanation; Appendixes A and B provide a more thorough discussion.

The following information is obtained from a hypothetical geotechnical-investigation report:

Distance to the San Andreas Fault = E_A = 6 mi;
Distance to the San Jacinto Fault = E_J = 2 mi;
Distance to the Cucamonga Fault = E_C = 8 mi;
Depth to the SPT = D = 22 ft
Depth to water when the SPT was performed = W_2 = 12 ft
Penetration resistance = N = 15
Median grain size = D_{50} = 0.1 mm

These data allow the determination of C_d, C_l, and *FS* for the three earthquakes evaluated in this study.

Determining C_d developed at the site by an M_s=8.0 earthquake on the San Andreas fault (C_{dA}) requires calculation of A_{maxA}, σ_o, σ_o', and r_d. Once calculated, these factors insert into equation 1 as follows:

$$C_{dA} = 0.65 \cdot \frac{\sigma_o'}{\sigma_{o\,(1)}'} \cdot \frac{A_{maxA}}{g} \cdot r_d \,. \qquad (1)$$

For E_A=6 mi, figures 2 and 3 indicate that

$$A_{maxA} = 0.50\ g \,.$$

For W_1=20 ft, where W_1 corresponds to the nearest ground-water multiple of 10 ft overlying the SPT depth, σ_o and $\sigma_{o\,(1)}'$ are calculated by using equations 2 and 3:

$$\begin{aligned} \sigma_o &= \gamma \cdot z \qquad (2)\\ &= (\gamma_u \cdot W_1) + [\gamma_s \cdot (D - W_1)]\\ &= (105 \cdot 20) + [130\ (22 - 20)]\\ &= 2{,}360\ \text{lb/ft}^2 \end{aligned}$$

and

$$\begin{aligned} \sigma_{o\,(1)}' &= \sigma_o - u \qquad (3)\\ &= \sigma_o - [(D - W_1) \cdot \gamma_w]\\ &= 2{,}360 - [(22 - 20) \cdot 62.43]\\ &= 2{,}235\ \text{lb/ft}^2 \end{aligned}$$

where γ_w equals the unit weight of water.

For D=22 ft, figure 4 indicates that

$$r_d = 0.95.$$

Inserting these values for A_{maxA}, σ_o, σ_o', and r_d into equation 1 yields:

$$C_{dA} = 0.65 \cdot \frac{2{,}360}{2{,}235} \cdot \frac{0.50}{1} \cdot 0.95$$

$$C_{dA} = 0.326.$$

Determining C_d developed at the site by an M_s=7.0 earthquake on the San Jacinto Fault (C_{dJ}) requires solving equation 1, modified as follows:

$$C_{dJ} = 0.65 \cdot \frac{\sigma_o}{\sigma_{o\,(1)}'} \cdot \frac{A_{maxJ}}{g} \cdot r_d$$

where A_{maxJ} equals the maximum acceleration developed at the site by the M_s=7.0 earthquake. Similarly, determining C_d developed at the site by an M_s=6.75 earthquake on the Cucamonga fault (C_{dC}) requires solving equation 1, as follows:

$$C_{dC} = 0.65 \cdot \frac{\sigma_o}{\sigma_{o\,(1)}'} \cdot \frac{A_{maxC}}{g} \cdot r_d$$

where A_{maxC} equals the maximum acceleration developed at the site by the M_s=6.75 earthquake. Calculations of C_{dJ} and C_{dC} use the same values for σ_o, σ_o', and r_d as used for calculating C_{dA}; however, they require different values for A_{max}. For E_J=2 mi, figures 2 and 3 indicate that

$$A_{maxJ} = 0.60\ \text{g}$$

and for E_C=8 mi, figures 2 and 3 indicate that

$$A_{maxC} = 0.35\ \text{g}$$

Substituting these values for A_{maxJ} and A_{maxC} yields:

$$C_{dJ} = 0.65 \cdot \frac{2{,}360}{2{,}235} \cdot \frac{0.60}{1} \cdot 0.95$$

$$C_{dJ} = 0.391$$

$$C_{dC} = 0.65 \cdot \frac{2{,}360}{2{,}235} \cdot \frac{0.35}{1} \cdot 0.95$$

$$C_{dC} = 0.228.$$

Determining C_l developed at the site by each of the three earthquakes requires that figure 5 be used to convert N to N_1 and using this N_1 and figure 6 to find C_l. Before

converting N to N_1, it is sometimes necessary to adjust N to compensate for a loss of driving energy that results at shallow depths from using a short length of rod during the SPT. In this example, D is 10 ft or greater; therefore no adjustment to N is required, and the unadjusted N converts directly to N_1 using equation 4:

$$N_1 = C_N \cdot N \tag{4}$$

with C_N derived from figure 5. Figure 5 requires determination of $\sigma_o'_{(2)}$ for the ground-water conditions occurring when and where the SPT test was performed. Thus, from equation 3,

$$\begin{aligned}\sigma_0'_{(2)} &= \sigma_o - u \\ &= [(\gamma_u \cdot W_2) + (\gamma_s \cdot (D-W_2))] - [(D-W_2) \cdot \gamma_w] \\ &= [(105 \cdot 12) + (130\ (22-12))] - [(22-12)\ 62.43] \\ &= 2.498\ \text{lb/ft}^2.\end{aligned}$$

Assuming that D_r equals 60 percent, for this value of $\sigma_o'_{(2)}$ figure 5 indicates that

$$C_N = 1.0$$

So,

$$\begin{aligned}N_1 &= C_N \cdot N \\ &= 1 \cdot 15 \\ &= 15.\end{aligned}$$

Because D_{50} is less than 0.15 mm, the material tested at this site is considered to be silty sand. Therefore, before using figure 6 to find C_l, N_1 must be increased by 7.5 to enable a more accurate determination of C_l. Thus,

$$N_1 = 22.5.$$

For this value of N_1, figure 6 indicates that the minimum cyclic-stress ratio required for liquefaction to develop at the site during an M_s=8.0 earthquake on the San Andreas fault is

$$C_{lA} = 0.219.$$

Because $\sigma_o'_{(2)}$ does not exceed about 3,380 lb/ft^2, no adjustment for high effective stress is required to C_{lA}.

The N_1 determined above can be used with figure 6 to calculate C_l for other local earthquakes. Thus, the minimum cyclic-stress ratio required for liquefaction to occur at the site during an M_s=7.0 earthquake on the San Jacinto fault is

$$C_{lJ} = 0.255$$

and the minimum cyclic-stress ratio required in order for liquefaction to occur at the site during an M_s=6.75 earthquake on the Cucumonga fault is

$$C_{lC} = 0.266.$$

Neither C_{lJ} or C_{lC} require an adjustment for high effective stress.

The ratio of C_l to C_d for each earthquake determines FS. Where FS is less than 1.0 for a particular earthquake, liquefaction can be expected to develop. In this example, FS at the hypothetical site resulting from an M_s=8.0 earthquake on the San Andreas fault equals:

$$FS_A = \frac{C_{lA}}{C_{dA}}$$

$$FS_A = \frac{0.219}{0.326}$$

$$FS_A = 0.67.$$

FS resulting from an M_s=7.0 earthquake on the San Jacinto fault equals:

$$FS_J = \frac{C_{lJ}}{C_{dJ}}$$

$$FS_J = \frac{0.255}{0.391}$$

$$FS_J = 0.65,$$

and FS resulting from an M_s=6.75 earthquake on the Cucamonga fault equals:

$$FS_C = \frac{C_{lC}}{C_{dC}}$$

$$FS_C = \frac{0.266}{0.228}$$

$$FS_C = 1.17.$$

Thus, for W_1 equal to 20 ft, the materials tested at this hypothetical site would be likely to liquefy during an M_s=8.0 earthquake on the San Andreas fault and an M_s=7.0 earthquake on the San Jacinto fault, but not during an M_s=6.75 earthquake on the Cucamonga fault.

AVAILABILITY OF BOOKS AND MAPS OF THE U.S. GEOLOGICAL SURVEY

Instructions on ordering publications of the U.S. Geological Survey, along with prices of the last offerings, are given in the current-year issues of the monthly catalog "New Publications of the U.S. Geological Survey." Prices of available U.S. Geological Survey publications released prior to the current year are listed in the most recent annual "Price and Availability List." Publications that are listed in various U.S. Geological Survey catalogs (**see back inside cover**) but not listed in the most recent annual "Price and Availability List" are no longer available.

Prices of reports released to the open files are given in the listing "U.S. Geological Survey Open-File Reports," updated monthly, which is for sale in microfiche from the U.S. Geological Survey, Books and Open-File Reports Section, Federal Center, Box 25425, Denver, CO 80225. Reports released through the NTIS may be obtained by writing to the National Technical Information Service, U.S. Department of Commerce, Springfield, VA 22161; please include NTIS report number with inquiry.

Order U.S. Geological Survey publications **by mail** or **over the counter** from the offices given below.

BY MAIL

Books

Professional Papers, Bulletins, Water-Supply Papers, Techniques of Water-Resources Investigations, Circulars, publications of general interest (such as leaflets, pamphlets, booklets), single copies of Earthquakes & Volcanoes, Preliminary Determination of Epicenters, and some miscellaneous reports, including some of the foregoing series that have gone out of print at the Superintendent of Documents, are obtainable by mail from

U.S. Geological Survey, Books and Open-File Reports
Federal Center, Box 25425
Denver, CO 80225

Subscriptions to periodicals (Earthquakes & Volcanoes and Preliminary Determination of Epicenters) can be obtained ONLY from the

Superintendent of Documents
Government Printing Office
Washington, D.C. 20402

(Check or money order must be payable to Superintendent of Documents.)

Maps

For maps, address mail orders to

U.S. Geological Survey, Map Distribution
Federal Center, Box 25286
Denver, CO 80225

Residents of Alaska may order maps from

Alaska Distribution Section, U.S. Geological Survey
New Federal Building - Box 12
101 Twelfth Ave., Fairbanks, AK 99701

OVER THE COUNTER

Books

Books of the U.S. Geological Survey are available over the counter at the following U.S. Geological Survey Public Inquiries Offices, all of which are authorized agents of the Superintendent of Documents:

- **WASHINGTON, D.C.**—Main Interior Bldg., 2600 corridor, 18th and C Sts., NW.
- **DENVER, Colorado**—Federal Bldg., Rm. 169, 1961 Stout St.
- **LOS ANGELES, California**—Federal Bldg., Rm. 7638, 300 N. Los Angeles St.
- **MENLO PARK, California**—Bldg. 3 (Stop 533), Rm. 3128, 345 Middlefield Rd.
- **RESTON, Virginia**—503 National Center, Rm. 1C402, 12201 Sunrise Valley Dr.
- **SALT LAKE CITY, Utah**—Federal Bldg., Rm. 8105, 125 South State St.
- **SAN FRANCISCO, California**—Customhouse, Rm. 504, 555 Battery St.
- **SPOKANE, Washington**—U.S. Courthouse, Rm. 678, West 920 Riverside Ave.
- **ANCHORAGE, Alaska**—Rm. 101, 4230 University Dr.
- **ANCHORAGE, Alaska**—Federal Bldg., Rm. E–146, 701 C St.

Maps

Maps may be purchased over the counter at the U.S. Geological Survey offices where books are sold (all addresses in above list) and at the following U.S. Geological Survey offices:

- **ROLLA, Missouri**—1400 Independence Rd.
- **DENVER, Colorado**—Map Distribution, Bldg. 810, Federal Center
- **FAIRBANKS, Alaska**—New Federal Bldg., 101 Twelfth Ave.